Intertidal wetland sediment carbon budgets along eroding and prograding coasts

Lea Marlene Merle Stolpmann

Submitted in fulfilment of the requirements for the

Degree of Doctor of Philosophy

School of Geographical & Earth Sciences

College of Science and Engineering

University of Glasgow

May 2024

Abstract

Coastal ecosystems are vital in providing ecosystem services such as coastal protection, habitat provision and increasing biodiversity. With increasing global atmospheric CO_2 concentrations and a warming climate, their ability to sequester large amounts of carbon within their biomass and soil, relative to their occupied area, has been of increased interest. The soil carbon salt marshes and mangroves sequestered is however under threat due to anthropogenic impacts and processes changing the formation and development condition of these ecosystems. Insufficient sediment supply and rising sea levels are threatening to drown these systems and turn a healthy ecosystem into an erosional stage. In particular the effect of erosion on soil characteristics and processes has to be understood to determine the emission of carbon to the atmosphere and thus their carbon storage capacity. This thesis aims to determine 1) the effect of geomorphic condition on the soil to atmosphere emission of CO_2 within salt marshes and mangroves, 2) the hydrodynamic influences on soil processes such as soil temperature within salt marshes, 3) the difference between carbon fluxes at salt marsh sites of differing geomorphic conditions. Geomorphic condition was found to significantly influence CO_2 emissions at salt marsh sites, with eroding sites having a greater emission rate. The emission rate of CO_2 was further influenced by the tidal cycle as well as the interaction of groundwater level and soil temperature. The effect of geomorphic condition on CO_2 emissions was also studied within mangrove forests, showing however no significant relationship. Soil processes driving the remineralization of carbon to CO_2, such as soil temperature was found to be influenced by tidal driven hydrodynamics (i.e., current velocity and groundwater levels) and to be seasonal dependent. Geomorphic different coastal ecosystems were further expected to receive carbon sources of different origins. Within the mangrove ecosystems these differences were observed within the soil cores at depth, indicating a change in carbon origin, although with site specific variations. Sediment deposited on a salt marsh flat was however only significantly different between geomorphic conditions in the percentage of inorganic carbon. The results emphasise the connectivity of coastal hydrology and wetland soil processes, not only driving the carbon delivery to the wetlands but also the processes influencing its storage and emission. The conservation and restoration of vegetated coastal habitats does therefore need to address this connectivity in order to maintain and preserve the immense carbon storage capacity of these ecosystems.

Table of Contents

List of Tables

List of Figures

Acknowledgements

I would like to thank my supervisors, Dr Adrian Bass, Dr Thorsten Balke and Dr Alejandra Vovides for their support and approach to science. They showed me that academia can be a space to openly discuss ideas, without the stress and constant pressure. Thank you for the opportunities to adjust the research topic and linking geomorphic and biogeochemical methods. Thanks to the many conference opportunities I had to present my work but also to merely attend. They were inspirational and gave me motivation seeing so many other geoscientists talk about their work.

I would also like to acknowledge and thank the Living Deltas Research Hub scholarship for funding my research. For the opportunities to meet inspiring people and to undertake research in Vietnam once the travel restrictions ceased and the borders opened. With the COVID-19 pandemic in "full-swing" at the start of the PhD, a slight change of topic was necessary, shifting from mangroves to salt marshes.

Massive thanks go to Kenny and Thomas. Driving to Caerlaverock and helping on fieldwork during all weather conditions. We had sunny 25°C and got sunburned, although we also had freezing cold conditions where we had to skid over the mudflat to the most easterly site. Thanks to everyone helping on fieldwork, Ying, Edward, Nasser, Maisie, Nina. Not to forget, thanks to Edward for carrying the found canoe back to the car.

Thanks to the Glasgow PhD community, even during the pandemic they tried to organise events and helped everyone to find a space to meet.

And of course, I want to thank my parents. Thank you for your constant support. Thank you for believing in me and encouraging me to apply and to accept the offer.

Last but definitely not least, thank you, Rick, for your support and being there for me.

Author's Declaration

The thesis presented here is the result of my original work, except where other materials have been cited (e.g., publicly available datasets and figures). The thesis has not been submitted for any other degree at the University of Glasgow or any other institution.

Chapter 2 and 3 in this thesis follow the 'Alternative Format Thesis' guidelines derived from the University Code of Practice. Chapter 2 and 3 have been submitted for publication and are under review at the time of submission. The text, figures, and tables are thus identical to the submitted versions of the manuscripts. The supplementary materials of those chapters have been moved into the Appendix.

I confirm that Chapter 2 was jointly authored with Thorsten Balke (T.B.) and Adrian M. Bass (A.M.B.) where I (L.M.S.) contributed 90% of this work. With the CRediT statement as follows:

Conceptualization: T.B., A.M.B.

Data curation: L.M.S.

Formal analysis: L.M.S.

Funding acquisition: T.B., A.M.B.

Investigation: L.M.S.

Methodology: L.M.S., T.B., A.M.B.

Project Administration: T.B., A.M.B.

Resources: T.B., A.M.B.

Supervision: T.B., A.M.B.

Visualization: L.M.S.

Writing - original draft: L.M.S.

Writing - review & editing: L.M.S., T.B., A.M.B.

I confirm that Chapter 3 was jointly authored with Cai J.T. Ladd (C.J.T.L.), Thorsten Balke (T.B.) and Adrian M. Bass (A.M.B.) where I (L.M.S.) contributed 90% of this work. With the CRediT statement as follows:

Conceptualization: L.M.S., C.J.T.L., T.B., A.M.B.

Funding acquisition: C.J.T.L, T.B., A.M.B.

Investigation: L.M.S., C.J.T.L.

Formal analysis: L.M.S., C.J.T.L.

Visualization: L.M.S.

Writing - original draft preparation: L.M.S.

Writing - review and edition: L.M.S., C.J.T.L., T.B., A.M.B.

Lea Stolpmann

Glasgow, May 2024

Abbreviations

BP	Before present
CH_4	Methane
CO_2	Carbon dioxide
DIC	Dissolved inorganic carbon
DOC	Dissolved organic carbon
DSAS	Digital shore analysis system
GHG	Greenhouse gas
GLMM	Generalised Linear Mixed Effects Model
IC	Inorganic carbon
LMEM	Linear Mixed Effects Model
LMM	Linear Mixed Effects Model
LOI	Loss on ignition
LRR	Linear regression rate
MR	Managed realignment
OC	Organic carbon
PCA	Principal component analysis
PIC	Particulate inorganic carbon
POC	Particulate organic carbon
SGD	Submarine groundwater discharge
SLR	Sea level rise
SSC	Suspended sediment concentration
SST	Sea-surface temperature
UK	United Kingdom
US	United States of America
USGS	United States Geographical Survey
VCE	Vegetated coastal ecosystem
VPDB	Vienna Pee Dee Belemnite

1 Introduction

1.1 Carbon cycle

The global carbon cycle describes the movement of carbon between the atmosphere biosphere, lithosphere, and hydrosphere. In the atmosphere it takes predominantly the form of carbon dioxide (CO_2), which is taken up by plants in their biomass through photosynthesis and accumulates in the associated soils (Shields, 2005). Carbon returns to the atmosphere through multiple mechanisms, i.e., through decomposition and the respiration of organic matter or by combustion of long-term geologic pools, i.e., fossil fuels (Figure 1.1). Atmospheric carbon has increased in concentration and has reached the highest level in the last 2 million years with 410 ppm in 2019 (IPCC, 2023) and reaching 419 ppm in 2023 (Copernicus, 2024).

The increase in CO_2, a greenhouse gas (GHG), in the atmosphere is trapping infrared radiation within the Earth's atmosphere and subsequently increasing global temperatures (by 1.09 °C in 2011-2020 relative to the 1850-1900 average (IPCC, 2023)). The main cause of atmospheric increase in CO_2 is the burning of fossil fuel, which releases the stored carbon (IPCC, 2023). Climate change mitigation strategies include the reduction of anthropogenic released CO_2 and other GHGs as well as the increased capture of atmospheric carbon (IPCC, 2023).

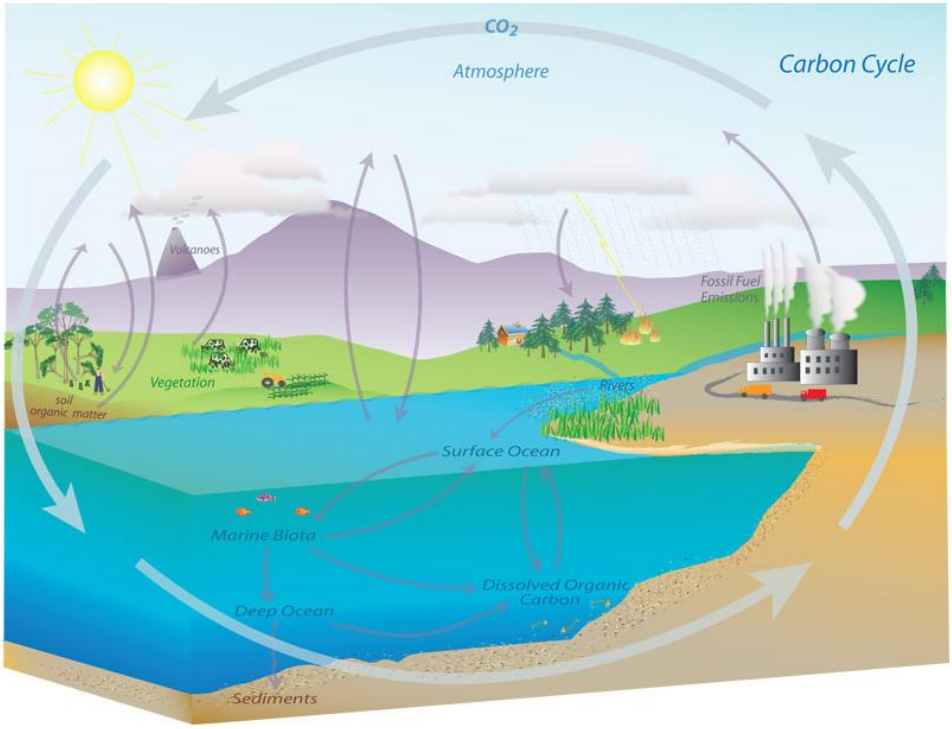

Figure 1.1 Schematic of the global carbon cycle (from: National Oceanic and Atmospheric Administration, 2019).

1.2 Vegetated coastal ecosystems and blue carbon

Vegetated coastal ecosystems (VCE) occur globally at the interface between terrestrial and coastal environments (Duarte, 2017). These systems comprise of habitats such as mangrove forests, tidal marshes, sea grass beds and macroalgae and cover approximately 36 - 185 million hectares (360,000 - 1,850,000 km^2) of coastlines globally (Macreadie et al., 2021). The uncertainty stems from uncertainties in the distribution of sea grass beds and tidal marshes (Bunting et al., 2018; Jayathilake and Costello, 2018; Mcowen et al., 2017).

VCEs are of ecological and commercial importance through the services they provide. They increase biodiversity, providing habitat, specifically nursery habitats, supporting fish production (Jänes et al., 2020; Ley and Rolls, 2018). The vegetation acts further as a wave breaker and buffer zone, protecting the coast (Barbier et al., 2011). Wave and current energy are dissipated through the vegetation and have thus a lower impact on coastal areas (Möller et al., 2014; Zhao et al., 2017). The vegetation also enhances sediment capture helping consolidate the soil, thus reducing coastal erosion (Feagin et al., 2015). The importance of VCEs for coastal protection is increasingly recognised, evident in their inclusion in coastal planning strategies (Temmerman et al., 2013).

The importance of VCEs (mangrove forests, tidal marshes and sea grass beds) in relation to climate change mitigation is due to their ability to capture and store carbon either in their above- and belowground biomass or sequestering it in the soil (Mcleod et al., 2011). Indeed, these ecosystems sequester a greater amount of carbon per unit area of habitat than terrestrial ecosystems such as boreal and tropical forests (Duarte et al., 2005; Mcleod et al., 2011). The importance of these habitats has been recognised globally by naming the sequestered carbon “blue carbon”, a policy term aimed at increasing the political awareness around the importance of these habitats in the global carbon system (Mcleod et al., 2011). This ecosystem service is seen as one important asset in combating and mitigating climate change (Duarte et al., 2013; Lecerf et al., 2021). Indeed, coastal and marine ecosystems have been incorporated by 46 countries in their mitigation solutions to address climate change as part of their Nationally Determined Contributions (Lecerf et al., 2021).

1.2.1 Salt marsh

Saltmarshes are formed along soft sediment coasts in temperate regions (Duarte, 2017). The salt marsh extent ranges from the mudflat towards the boundary with terrestrial vegetation and divided into lower, middle, and upper marsh area (Foster et al., 2013). Where the seaward extent of the marsh zonation is based upon the inundation frequency (Balke et al., 2016). Inundation characteristics further determine the type of salt marsh vegetation. The initial estimates of global saltmarsh area were 20,000 - 38,000 km^2 (Chmura et al., 2003; Woodwell and Pecan, 1973), with a revised estimate of the global saltmarsh area at 54,951 km^2, incorporating both field surveys, remote sensing, and ground-truthing of data (Mcowen et al., 2017).

A total extent of 468.5 – 491.93 km^2 (46,850-49,193 ha) of salt marsh habitat is estimated to be in the UK, encompassing Great Britain and Northern Ireland (Foster et al., 2013). They are distributed around the UK coastline, predominantly located within estuaries, and bays, however also at loch/fjord heads (Adam, 1978; Haynes, 2016; Figure 1.2). Coastal management actions are increasingly recognising the value of salt marsh habitats, mainly for flood prevention and protection (Crooks et al., 2002; Möller et al., 2014).

Salt marshes are however experiencing stresses and are heavily impacted by anthropogenic influences. Salt marshes are lost in the UK because of agricultural and industrial land reclamations (Foster et al., 2013), however also due to erosion and sea-level rise leading to blocked habitat migration further landwards, i.e., coastal squeeze (van der Wal and Pye, 2004; Wolters et al., 2005). Restoration efforts are in place to conserve these important habitats, mainly using managed realignment schemes by breaching tidal defences and reinstating tidal inundations (Adams et al., 2021; Burden et al., 2013). A UK salt marsh code is being developed to investigate the feasibility for carbon credits for managed realignment projects (Burden et al., 2023). Sites are further protected through UK policies such as the Wildlife and Countryside Act 1981 c. 69, Habitats and Species Regulations 2010 and the Biodiversity Action Plan (Foster et al., 2013).

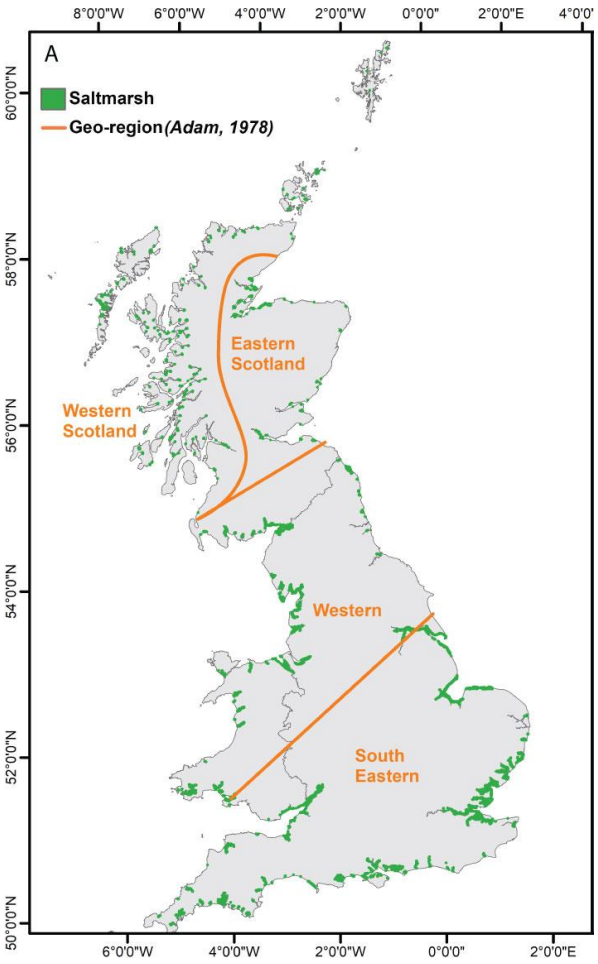

Figure 1.2 Salt marsh extent of Great Britain, has been exaggerated by 1.5 times to increase visibility (from: Smeaton et al., 2022).

1.2.2 Mangroves

Mangroves are a group of plants adapted to diverse coastal habitats. Growing as shrubs, trees, and ferns (Tomlinson, 2016), and distributed along coastlines in soft sediments (Rastogi et al., 2021). They occur primarily in the tropics but are also found in the temperate zones, controlled by temperature related limits (Quisthoudt et al., 2012). Their global range is restricted approximately to latitudes between 32° N and 38° S (Rastogi et al., 2021). They are able to grow in a variety of salinities and inundation regimes, although restricted to sheltered shorelines with lower wave energy (Rastogi et al., 2021), establishing differing geomorphic systems, among others: deltaic, tidal, composite, fringing barriers (Rastogi et al., 2021). The global area estimate for mangrove forests has been estimated at 147,000 km^2 (Leal and Spalding, 2022).

The Mekong River Delta in the south of Vietnam is the third largest delta worldwide (Coleman and Huh, 2004). Mangrove records have been preserved in sediment cores and

date back to 6000 to 5000 years BP (Nguyen et al., 2000). However, large-scale losses of mangrove forests have occurred in the period from 1816 to the 21st century, whereby only 680 km^2 of the once 40,000 km^2 of mangroves remain (Nguyen et al., 2016). Drivers of mangrove loss are different for the period before and after the Vietnamese war, 1954-1975 (Nguyen et al., 2016). The construction of canals and waterways as well as agricultural developments were the primary drivers of mangrove area losses before the Vietnamese war (Nguyen et al., 2016). During the war, clearing and defoliation led to an estimated loss of 270 km^2 within the Mekong Delta (Nguyen et al., 2016; Orians and Pfeiffer, 1970). In the period following the war, mangroves were lost due to timber and charcoal production, and deforestation to construct ponds for shrimp aquaculture (Vo et al., 2013). The construction of canals and dykes further led to changes in inundation regimes and sediment deposition, facilitating shoreline erosion or smothering of mangroves (Anthony et al., 2015; Besset et al., 2019; Fagherazzi et al., 2017).

Charlotte Harbor, west Florida in the United States of America is an estuarine system with an extent of approx. 700 km^2 with mangrove-seagrass shorelines (Poulakis et al., 2003). The areas of mangrove forests and salt marshes are publicly owned or protected (Pierce et al., 2004), with the Charlotte Harbor Preserve State Park covering about 190 km^2 (Charlotte Harbor Preserve State Park, 2024). The region can be categorised as a subtropical climate with wet and dry seasons (US Department of Commerce, n.d.).

1.3 Blue carbon stocks

Coastal vegetated ecosystems, such as salt marshes and mangroves, are referred to as blue carbon ecosystems, as they store organic carbon within their biomass and sediments (Mcleod et al., 2011). Carbon, stored by mangrove and salt marsh systems for sequestration is either allochthonous or autochthonous. Sequestration describes the capacity of an ecosystem to capture and store carbon and is counteracted by the amount of carbon emitted from the system. If the sequestration of carbon is offset by the emission of carbon, the system is classified as a carbon source, the opposite being a carbon sink (Macreadie et al., 2013). Allochthonous carbon is produced outside the system and is transported into the system, i.e., by tides, rivers, or groundwater, with macro- algae and phytoplankton being important sources of organic matter (Xia et al., 2021). Autochthonous carbon is carbon produced in the same system, in the case of mangrove and salt marshes, it is the vegetation itself that provides carbon by litterfall, standing and dead biomass. The relative contribution of organic carbon from different carbon sources to mangrove and salt marsh soils is spatially variable across sites and regions (Bouillon et al., 2003; Middelburg et al., 1997). Primarily influenced by elevation and distance to sediment sources such as tidal creeks and the vegetation seaward edge, controlling the inundation frequency and duration (Fagherazzi et al., 2012). Delineating the carbon origin can be achieved using carbon stable isotope ratios, the relative abundance of heavy (C^{13}) to light (C^{12}) carbon atoms (Mueller et al., 2019; Saintilan et al., 2013). The relative proportions of carbon stable isotopes vary based on the source of carbon and the photosynthetic pathways between plants (Saintilan et al., 2013). The variable origin of autochthonous vs. allochthonous carbon in wetland soils has implications on ecosystem scale carbon budgets, carbon crediting, and effective offsetting of GHGs (Needelman et al., 2018). Deposited organic carbon (OC) in the top-soil of salt marshes is often autochthonous, whereas the long-term storage of OC is of allochthonous origin (Van De Broek et al., 2018). Thus, it has been argued that the sequestering of old allochthonous carbon, which originated outside of the salt marsh, does not contribute to the removal of current atmospheric CO_2 (Komada et al., 2022; Van De Broek et al., 2018), but may help to prevent it returning to the atmosphere. It does however highlight the need for assessments of blue carbon accounting across habitat boundaries as proposed by Krause et al., (2022).

Organic carbon is stored within the ecosystems in the above-ground biomass (wood, rhizomes, leaves), the below-ground biomass (roots), as well as the soil (Alongi, 2020). The average carbon stock of mangrove forest and saltmarshes globally has been estimated to be 738.9 ± 27.9 Mg C_{org} ha^{-1} and 334.4 ± 3.5 Mg C_{org} ha^{-1}, respectively (where 1 Mg equals

1,000,000 g) (Alongi, 2020). The median values and the percentage of total carbon stock stored in each component is summarized from Alongi (2020) in Table 1.1.

Table 1.1 Median C_{org} content in mangrove and saltmarsh habitats. Edited from (Daniel M. Alongi, 2020). Summed median carbon stocks (percentage total storage). Soil depth of 1m.

Ecosystem	**Median carbon stocks in Mg C_{org} ha^{-1} (percentage total storage)**
Mangrove, added components	628.8
Above-ground biomass	94.1 (14.97)
Below-ground biomass	34.2 (5.44)
Soil	500.5 (79.6)
Saltmarsh	294.2
Above-ground biomass	2.4 (0.816)
Below-ground biomass	9.6 (3.26)
Soil	282.2 (95.92)

1.4 Factors influencing soil carbon sequestration

Sequestered carbon is naturally lost from mangrove and salt marsh systems (Table 1.2). The pathways are either directly into the coastal environment as litter, as particulate, or dissolved organic carbon (POC / DOC) (Alongi, 2020; Bouillon et al., 2008; Sippo et al., 2019, 2020), or by remineralization and consequent emission in gaseous form to the atmosphere as either CO_2 or methane (CH_4) (Alongi, 2020; Atwood et al., 2017; Bouillon et al., 2008; Bulmer et al., 2017; Cahoon et al., 2003; Lang'at et al., 2014; Lovelock et al., 2011; Lovelock et al., 2017a; Sidik and Lovelock, 2013). Microbes are consuming organic matter deposited at or near the sediment surface, during which CO_2 is produced as a product of aerobic respiration under the availability of oxygen (Kristensen et al., 2008). Therefore, the storage of carbon within coastal ecosystems, such as salt marshes and mangroves, is particularly efficient, as the soil is often waterlogged and anoxic, preventing aerobic respiration. Although the lack of oxygen may lead to the production of CH_4 through methanogenesis, an anaerobic process (Pendleton et al., 2012).

Table 1.2 Natural carbon fluxes from mangrove forests and salt marshes. Fluxes based on global mangrove area of 86,495 km^2; salt marsh area: 54,951 km^2 (Alongi, 2020).

Habitat	Pathway	Carbon loss	Reference
Mangroves	CO_2 emissions (soil - atmosphere)	53 Tg C a^{-1} 42 ± 31 Tg C a^{-1}	Alongi, 2020 Bouillon et al., 2008
	POC export (soil - water)	190.24 Tg C a^{-1} 21 ± 22 Tg C a^{-1}	Alongi, 2020 Bouillon et al., 2008
Salt marshes	CO_2 emissions (soil – atmosphere)	31 Tg C a^{-1}	Alongi, 2020
	POC export (soil – water)	46.9 Tg C a^{-1}	Alongi, 2020

Natural carbon loss from mangroves and salt marshes is accelerated through the disturbance of these habitats (Pendleton et al., 2012). The loss or degradation of coastal vegetated ecosystems results in the loss of carbon sequestration potential (Chmura et al., 2003; Duarte et al., 2005; Pendleton et al., 2012), and potentially in the remineralization of buried carbon to CO_2 and its atmospheric emission (Lovelock et al., 2017a; Pendleton et al., 2012). The rate of remineralization is dependent on abiotic and biotic factors, primarily driving microbial activity and access to carbon (Lovelock et al., 2017a; Spivak et al., 2019).

For example, soil respiration is influenced by the tidal cycle and groundwater level, regulating the availability of oxygen within the soil (Chen et al., 2022; Cui et al., 2021). Greater and longer inundations and higher groundwater levels can waterlog the system, preventing the exchange with oxygen and thus reducing soil respiration (Chen et al., 2022), alternatively more frequent inundations can contribute to higher particulate and dissolved carbon outwelling (Cai, 2011). Microbial activity and thus the production of GHG is further positively affected by temperature, which in turn can be controlled by inundation and the exchange of porewater with seawater (Jacotot et al., 2019; Kirwan et al., 2014). In this regard, climate change will have a profound impact on CO_2 emissions from coastal ecosystems through changed temperatures and sea-level rise, leading among others to changed inundation regimes (Lovelock et al., 2017b).

Sea-level rise requires coastal wetland systems to build up their elevation by accumulating sediment and organic material to prevent drowning (Fagherazzi et al., 2020). The supply of material and its' importance for elevation gain differs between wetland types (Cahoon et al., 2020). Minerogenic systems are highly reliant on mineral sediment supply, whereas biogenic systems rely on soil organic matter accumulation through autochthonous carbon production

(Cahoon et al., 2020). Consequently, a lack of sufficient sediment supply is leading to wetland destabilization and coastal erosion (Fagherazzi et al., 2017; Ladd et al., 2019).

1.5 Biogeomorphology – Influence of vegetation on geomorphology

1.5.1 Edge erosion

Ecosystem engineering species such as mangroves and salt marshes establish landforms through the feedback between biological and physical processes, this being the concept of bio-geomorphology (Viles, 2020). These are coastal systems, and as such subject to the dynamic coastal environment, where waves, tidal inundations, sediment supply, and sea level rise influence the growth and development of vegetation (Balke et al., 2013, 2016; Bhargava et al., 2021). The establishment and evolution of these landforms is highly dynamic and includes both eroding and expanding phases (Fagherazzi et al., 2013; Gedan et al., 2011).

Vegetation can trap sediment through the decreased flow rate of water through the vegetation, enabling sediment to settle (Mudd et al., 2010; Temmerman et al., 2012). Increased sedimentation can lead to greater vegetation growth, which increases the sediment trapping capacity further (Mudd et al., 2010). With increasing vertical elevation, a consequence of sediment accretion, the salt marsh vegetation changes from a pioneer to an established vegetation, characterized by higher diversity and strengthening of the marsh platform through their root growth (Ford et al., 2016). With growing elevation, the location of the hydrodynamic forcings on the marsh edge change and start undercutting the cliff (Tonelli et al., 2010). With the undercutting of the cliff, the erosion process of the ecosystems is initiated (Brooks et al., 2021)

Salt marsh erosion is a worldwide phenomenon and a major driver of salt marsh area loss (Campbell et al., 2022). The process of marsh edge erosion is initiated through hydrodynamic forcings, i.e., tides, waves, and storm surges (Brooks et al., 2021). Starting with the undercutting of the cliff, after which the substrate fails and topples over (Bendoni et al., 2014; Brooks et al., 2021). Salt marsh edge erosion is complex with direct and indirect drivers (Brooks et al., 2021), being researched through numerical modelling studies

(Bendoni et al., 2019), field studies (Zhao et al., 2017), and laboratory studies (Bendoni et al., 2014; Brooks et al., 2022; Ford et al., 2016). Sediment characteristics, which facilitate salt marsh edge resistance against erosion have been reviewed by Brooks et al., (2021). Sediment particle size (Feagin et al., 2009; Ford et al., 2016; Lo et al., 2017), and different sediment organic content (Ford et al., 2016) are determining factors of marsh erodibility, with erosion resistant sediment characterized by finer cohesive sediment within the clay-silt fraction and higher organic content.

Not only do differential site properties dictate the propensity for erosion, but they are presumably also directly and/or indirectly affecting differential carbon fluxes and carbon sequestration capability (Figure 1.3). Differences in hydrodynamic forcings between eroding and expanding sites determines the sediment supply, with insufficient supply being a cause of erosion (Ladd et al., 2019). Through a differential sediment supply and exchange, the organic matter supply to geomorphologically different marshes is thus also expected to be affected (Roner et al., 2016). Grain size has a direct influence on water drainage (Cao et al., 2021), and therefore also the oxygenation of the sediment. Erosion-prone sites, characterized by coarser grains (Feagin et al., 2009; Ford et al., 2016; Lo et al., 2017) will have a greater drainage capacity (Crooks et al., 2002) and thus a higher oxygenation rate (Mossman et al., 2012), which potentially will affect remineralization rates and thus carbon storage capacities (Alongi, 2020). Furthermore, eroding sites are more likely to have highly productive and mature plant communities, resulting in greater carbon stores through more autochthonous carbon input (Marchand, 2017).

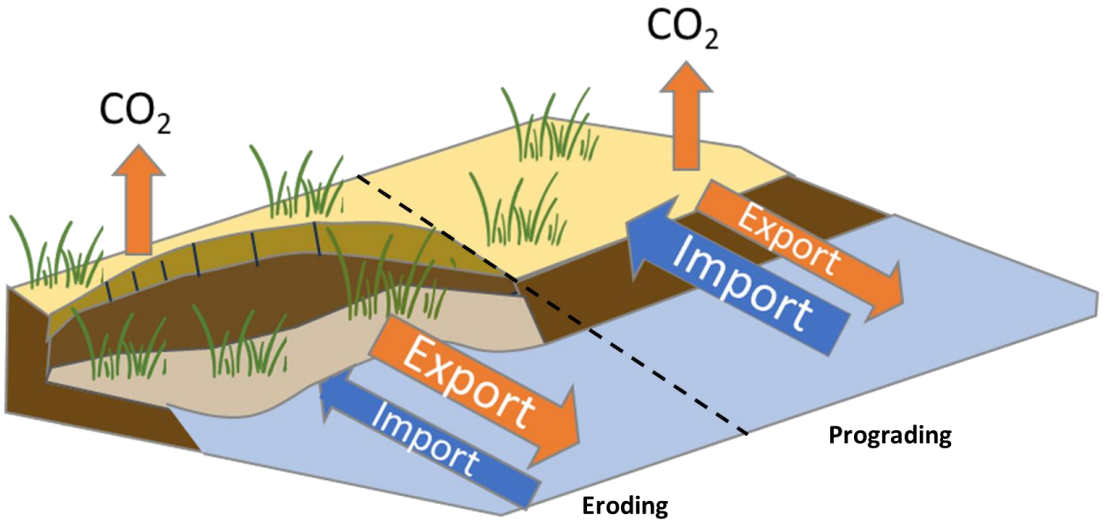

Figure 1.3 Schematic on carbon fluxes at geomorphic different salt marsh sites (left: eroding condition; right: prograding condition). Export/import arrows represent

hypothesised sedimentary carbon fluxes (thinner arrow = lower fluxes, thicker arrow = higher fluxes).

1.6 Aims and research questions

The primary aim of this PhD thesis is to investigate the carbon storage capacity of coastal wetlands under the influence of differing geomorphic conditions (Table 1.3; Figure 1.3), with a focus on how the interaction between vegetation and geomorphic conditions influences the carbon efflux from mangrove and salt marsh habitats. In addition, the study quantifies the influence of erosion and prograding processes on carbon storage and efflux and develops a model that connects biogeomorphological changes to carbon fluxes.

In **Chapter 2**, the sediment to atmosphere CO_2 efflux is quantified from a salt marsh with eroding and prograding sections in Scotland. Further the influencing factors are identified, demonstrating that hydrological and sedimentary conditions inherent to the site are impacting soil to atmosphere CO_2 emissions. Tidal cycle, geomorphic condition, distance to seaward vegetation edge, as well as the interaction between groundwater level and soil temperature showed to have an impact on the CO_2 flux. Whereby eroding sites showed a significantly greater emission of CO_2 than prograding sites, highlighting the importance of geomorphic conditions in influencing soil respiration. It was further hypothesized that soil temperatures are differently affected by hydrodynamic conditions, depending on the site's geomorphology.

Chapter 3 builds on the findings of Chapter 2, further elucidating the relationship between hydrodynamic forcings and soil temperature at geomorphologically different salt marsh sites in Scotland. With the use of "Mini-buoys" (in-situ micro-hydrodynamic sensors), current and wave orbital velocities were measured and using the groundwater level, the influencing factors on soil temperature were determined. Soil temperature at the salt marsh edges were, contrary to our initial hypothesis, not influenced significantly by geomorphic conditions. However, current velocity interacting with groundwater level as well as seasonal influence of groundwater level drove soil temperature.

In **Chapter 4** mangrove forests of differing geomorphic conditions in Florida (US) and the Mekong Delta (Vietnam) are studied. The differences in carbon sources sequestered within the soil as well as the soil to atmosphere CO_2 emissions between eroding and expanding conditions are explored. Using the carbon stable isotope signature to delineate between marine vs. terrestrial carbon, it was found that expanding sites had a greater marine influence than eroding sites. The initial hypothesis that soil CO_2 emissions to the atmosphere are

dependent on the geomorphology was rejected, showing however site-specific results, which could be indicative of the study's limitations.

Chapter 5 examines the geomorphic influence on carbon fluxes through sediment deposition and tidally influenced suspended sediment in a UK salt marsh. Seasonal and spatial differences between carbon sources of deposited and suspended sediment at an eroding and prograding salt marsh site were observed.

Chapter 6 synthesises the body of work presented, considering key findings from the perspective of carbon fluxes and sequestration potential in salt marsh and mangrove ecosystems. Remaining research gaps and potential future research questions are discussed.

Table 1.3 Thesis outline by topics discussed in each chapter.

Chapter	Process	Carbon cycle component	Ecosystem
Chapter 2; Chapter 4	CO_2 respiration between geomorphic different sites	Soil – atmospheric CO_2 emission	Salt marsh; Mangrove
Chapter 3	Hydrodynamic forcing influence on soil temperature	Indirect influence on soil-atmospheric CO_2 emission	Salt marsh
Chapter 4; Chapter 5	Source of carbon sequestered and supplied to geomorphic different sites	Carbon capture and sequestration	Mangrove; Salt marsh

References

Adam, P., 1978. Geographical Variation in British Saltmarsh Vegetation. Journal of Ecology 66, 339–366. https://doi.org/10.2307/2259141

Adams, J.B., Raw, J.L., Riddin, T., Wasserman, J., Van Niekerk, L., 2021. Salt Marsh Restoration for the Provision of Multiple Ecosystem Services. Diversity 13, 680. https://doi.org/10.3390/d13120680

Alongi, D.M., 2020. Carbon Balance in Salt Marsh and Mangrove Ecosystems: A Global Synthesis. J. Mar. Sci. Eng. 8, 767. https://doi.org/10.3390/jmse8100767

Anthony, E.J., Brunier, G., Besset, M., Goichot, M., Dussouillez, P., Nguyen, V.L., 2015. Linking rapid erosion of the Mekong River delta to human activities. Sci Rep 5, 14745. https://doi.org/10.1038/srep14745

Atwood, T.B., Connolly, R.M., Almahasheer, H., Carnell, P.E., 2017. Global patterns in mangrove soil carbon stocks and losses. Nature climate change 7, 523–528. https://doi.org/10.1038/nclimate3326

Balke, T., Stock, M., Jensen, K., Bouma, T.J., Kleyer, M., 2016. A global analysis of the seaward salt marsh extent: The importance of tidal range. Water Resources Research 52, 3775–3786. https://doi.org/10.1002/2015WR018318

Barbier, E.B., Hacker, S.D., Kennedy, C., Koch, E.W., Stier, A.C., Silliman, B.R., 2011. The value of estuarine and coastal ecosystem services. Ecological Monographs 81, 169–193. https://doi.org/10.1890/10-1510.1

Besset, M., Gratiot, N., Anthony, E.J., Bouchette, F., Goichot, M., Marchesiello, P., 2019. Mangroves and shoreline erosion in the Mekong River delta, Viet Nam. Estuarine, Coastal and Shelf Science 226, 106263. https://doi.org/10.1016/j.ecss.2019.106263

Bouillon, S., Borges, A.V., Castañeda-Moya, E., Diele, K., Dittmar, T., Duke, N.C., Kristensen, E., Lee, S.Y., Marchand, C., Middelburg, J.J., Rivera-Monroy, V.H., Smith, T.J., Twilley, R.R., 2008. Mangrove production and carbon sinks: A revision of global budget estimates. Global Biogeochem. Cycles 22. https://doi.org/10.1029/2007GB003052

Bouillon, S., Dahdouh-Guebas, F., Rao, A.V.V.S., Koedam, N., Dehairs, F., 2003. Sources of organic carbon in mangrove sediments: variability and possible ecological implications. Hydrobiologia 495, 33–39. https://doi.org/10.1023/A:1025411506526

Bulmer, R.H., Schwendenmann, L., Lohrer, A.M., Lundquist, C.J., 2017. Sediment carbon and nutrient fluxes from cleared and intact temperate mangrove ecosystems and adjacent sandflats. Science of The Total Environment 599–600, 1874–1884. https://doi.org/10.1016/j.scitotenv.2017.05.139

Bunting, P., Rosenqvist, A., Lucas, R.M., Rebelo, L.-M., Hilarides, L., Thomas, N., Hardy, A., Itoh, T., Shimada, M., Finlayson, C.M., 2018. The Global Mangrove Watch—A New 2010 Global Baseline of Mangrove Extent. Remote Sensing 10, 1669. https://doi.org/10.3390/rs10101669

Burden, A., Austin, W., Fitton, R., Garbutt, A., Gupta, S., Hipkiss, A., Mahon, C., McGrath, T., Pontee, N., Reed, M., 2023. Feasibility study of VCS VM0033 (NEIRF1072 Saltmarsh Carbon Code), Report to the Natural Environment Investment Readiness Fund (NEIRF). UK Centre for Ecology & Hydrology, Bangor.

Burden, A., Garbutt, R.A., Evans, C.D., Jones, D.L., Cooper, D.M., 2013. Carbon sequestration and biogeochemical cycling in a saltmarsh subject to coastal managed realignment. Estuarine, Coastal and Shelf Science 120, 12–20. https://doi.org/10.1016/j.ecss.2013.01.014

Cahoon, D.R., Hensel, P., Rybczyk, J., McKee, K.L., Proffitt, C.E., Perez, B.C., 2003. Mass tree mortality leads to mangrove peat collapse at Bay Islands, Honduras after Hurricane Mitch: *Hurricane-induced mangrove peat collapse*. Journal of Ecology 91, 1093–1105. https://doi.org/10.1046/j.1365-2745.2003.00841.x

Cai, W.-J., 2011. Estuarine and Coastal Ocean Carbon Paradox: CO2 Sinks or Sites of Terrestrial Carbon Incineration? Annu. Rev. Mar. Sci. 3, 123–145. https://doi.org/10.1146/annurev-marine-120709-142723

Charlotte Harbor Preserve State Park | Florida State Parks [WWW Document], 2024. URL https://www.floridastateparks.org/parks-and-trails/charlotte-harbor-preserve-state-park (accessed 9.28.24).

Chen, G., Bai, J., Wang, J., Liu, Z., Cui, B., 2022. Responses of soil respiration to simulated groundwater table and salinity fluctuations in tidal freshwater, brackish and salt marshes. Journal of Hydrology 612, 128215. https://doi.org/10.1016/j.jhydrol.2022.128215

Chmura, G.L., Anisfeld, S.C., Cahoon, D.R., Lynch, J.C., 2003. Global carbon sequestration in tidal, saline wetland soils. Global Biogeochem. Cycles 17, n/a-n/a. https://doi.org/10.1029/2002GB001917

Coleman, J.M., Huh, O.K., 2004. Major deltas of the world: a perspective from space.

Copernicus, 2024. Copernicus: 2023 is the hottest year on record, with global temperatures close to the 1.5°C limit [WWW Document]. URL https://climate.copernicus.eu/copernicus-2023-hottest-year-record (accessed 5.6.24).

Crooks, S., Schutten, J., Sheern, G.D., Pye, K., Davy, A.J., 2002. Drainage and Elevation as Factors in the Restoration of Salt Marsh in Britain. Restoration Ecology 10, 591–602. https://doi.org/10.1046/j.1526-100X.2002.t01-1-02036.x

Cui, H., Bai, J., Du, S., Wang, J., Keculah, G.N., Wang, W., Zhang, G., Jia, J., 2021. Interactive effects of groundwater level and salinity on soil respiration in coastal wetlands of a Chinese delta. Environmental Pollution 286, 117400. https://doi.org/10.1016/j.envpol.2021.117400

Duarte, C.M., 2017. Reviews and syntheses: Hidden forests, the role of vegetated coastal habitats in the ocean carbon budget. Biogeosciences 14, 301–310. https://doi.org/10.5194/bg-14-301-2017

Duarte, C.M., Losada, I.J., Hendriks, I.E., Mazarrasa, I., Marbà, N., 2013. The role of coastal plant communities for climate change mitigation and adaptation. Nature Clim Change 3, 961–968. https://doi.org/10.1038/nclimate1970

Duarte, C.M., Middelburg, J.J., Caraco, N., 2005. Major role of marine vegetation on the oceanic carbon cycle. Biogeosciences 2, 1–8.

Fagherazzi, S., Bryan, K., Nardin, W., 2017. Buried Alive or Washed Away: The Challenging Life of Mangroves in the Mekong Delta. Oceanog. 30, 48–59. https://doi.org/10.5670/oceanog.2017.313

Fagherazzi, S., Kirwan, M.L., Mudd, S.M., Guntenspergen, G.R., Temmerman, S., D'Alpaos, A., van de Koppel, J., Rybczyk, J.M., Reyes, E., Craft, C., Clough, J., 2012. Numerical models of salt marsh evolution: Ecological, geomorphic, and climatic factors. Reviews of Geophysics 50. https://doi.org/10.1029/2011RG000359

Feagin, R.A., Figlus, J., Zinnert, J.C., Sigren, J., Martínez, M.L., Silva, R., Smith, W.K., Cox, D., Young, D.R., Carter, G., 2015. Going with the flow or against the grain? The promise of vegetation for protecting beaches, dunes, and barrier islands from erosion. Frontiers in Ecology and the Environment 13, 203–210. https://doi.org/10.1890/140218

Foster, N.M., Hudson, M.D., Bray, S., Nicholls, R.J., 2013. Intertidal mudflat and saltmarsh conservation and sustainable use in the UK: A review. Journal of Environmental Management 126, 96–104. https://doi.org/10.1016/j.jenvman.2013.04.015

Hamilton, S.E., Casey, D., 2016. Creation of a high spatio-temporal resolution global database of continuous mangrove forest cover for the 21st century (CGMFC-21). Global Ecology and Biogeography 25, 729–738. https://doi.org/10.1111/geb.12449

Haynes, T.A., 2016. Scottish saltmarsh survey national report (No. 786). Scottish Natural Heriate Commissioned Report.

Huu Nguyen, H., Dargusch, P., Moss, P., Tran, D.B., 2016. A review of the drivers of 200 years of wetland degradation in the Mekong Delta of Vietnam. Reg Environ Change 16, 2303–2315. https://doi.org/10.1007/s10113-016-0941-3

IPCC, 2023: Summary for Policymakers (Synthesis Report), 2023. , Climate Change 2023. Intergovernmental Panel on Climate Change (IPCC), Geneva, Switzerland. https://doi.org/10.59327/IPCC/AR6-9789291691647

Jacotot, A., Marchand, C., Allenbach, M., 2019. Biofilm and temperature controls on greenhouse gas (CO2 and CH4) emissions from a Rhizophora mangrove soil (New Caledonia). Science of The Total Environment 650, 1019–1028. https://doi.org/10.1016/j.scitotenv.2018.09.093

Jänes, H., Macreadie, P.I., Zu Ermgassen, P.S.E., Gair, J.R., Treby, S., Reeves, S., Nicholson, E., Ierodiaconou, D., Carnell, P., 2020. Quantifying fisheries enhancement from coastal vegetated ecosystems. Ecosystem Services 43, 101105. https://doi.org/10.1016/j.ecoser.2020.101105

Jayathilake, D.R.M., Costello, M.J., 2018. A modelled global distribution of the seagrass biome. Biological Conservation 226, 120–126. https://doi.org/10.1016/j.biocon.2018.07.009

Kirwan, M.L., Guntenspergen, G.R., Langley, J.A., 2014. Temperature sensitivity of organic-matter decay in tidal marshes. Biogeosciences 11, 4801–4808. https://doi.org/10.5194/bg-11-4801-2014

Komada, T., Bravo, A., Brinkmann, M., Lu, K., Wong, L., Shields, G., 2022. “Slow” and “fast” in blue carbon: Differential turnover of allochthonous and autochthonous organic matter in minerogenic salt marsh sediments. Limnology & Oceanography 67. https://doi.org/10.1002/lno.12090

Krause, J.R., Hinojosa-Corona, A., Gray, A.B., Herguera, J.C., McDonnell, J., Schaefer, M.V., Ying, S.C., Watson, E.B., 2022. Beyond habitat boundaries: Organic matter cycling requires a system-wide approach for accurate blue carbon accounting. Limnology and Oceanography 67, S6–S18. https://doi.org/10.1002/lno.12071

Kristensen, E., Bouillon, S., Dittmar, T., Marchand, C., 2008. Organic carbon dynamics in mangrove ecosystems: A review. Aquatic Botany 89, 201–219. https://doi.org/10.1016/j.aquabot.2007.12.005

Lang’at, J.K.S., Kairo, J.G., Mencuccini, M., Bouillon, S., Skov, M.W., Waldron, S., Huxham, M., 2014. Rapid Losses of Surface Elevation following Tree Girdling and

Cutting in Tropical Mangroves. PLOS ONE 9, e107868. https://doi.org/10.1371/journal.pone.0107868

Leal, M., Spalding, M., 2022. The State of the Worlds Mangroves 2022. Global Mangrove Alliance.

Lecerf, M., Herr, D., Thomas, T., Elverum, C., Delrieu, E., Picourt, L., 2021. Coastal and marine ecosystems as nature-based solutions in new or updated Nationally Determined Contributions. Ocean & Climate Platform, Conservation International, IUCN, GIZ, Rare, The Nature Conservancy and WWF.

Ley, J.A., Rolls, H.J., 2018. Using otolith microchemistry to assess nursery habitat contribution and function at a fine spatial scale. Marine Ecology Progress Series 606, 151–173. https://doi.org/10.3354/meps12765

Lovelock, C.E., Atwood, T., Baldock, J., Duarte, C.M., Hickey, S., Lavery, P.S., Masque, P., Macreadie, P.I., Ricart, A.M., Serrano, O., Steven, A., 2017a. Assessing the risk of carbon dioxide emissions from blue carbon ecosystems. Frontiers in Ecology and the Environment 15, 257–265. https://doi.org/10.1002/fee.1491

Lovelock, C.E., Fourqurean, J.W., Morris, J.T., 2017b. Modeled CO2 Emissions from Coastal Wetland Transitions to Other Land Uses: Tidal Marshes, Mangrove Forests, and Seagrass Beds. Frontiers in Marine Science 4.

Lovelock, C.E., Ruess, R.W., Feller, I.C., 2011. CO2 Efflux from Cleared Mangrove Peat. PLoS ONE 6, e21279. https://doi.org/10.1371/journal.pone.0021279

Macreadie, P.I., Costa, M.D.P., Atwood, T.B., Friess, D.A., Kelleway, J.J., Kennedy, H., Lovelock, C.E., Serrano, O., Duarte, C.M., 2021. Blue carbon as a natural climate solution. Nat Rev Earth Environ 2, 826–839. https://doi.org/10.1038/s43017-021-00224-1

Macreadie, P.I., Hughes, A.R., Kimbro, D.L., 2013. Loss of 'Blue Carbon' from Coastal Salt Marshes Following Habitat Disturbance. PLoS ONE 8, e69244. https://doi.org/10.1371/journal.pone.0069244

Mcleod, E., Chmura, G.L., Bouillon, S., Salm, R., Björk, M., Duarte, C.M., Lovelock, C.E., Schlesinger, W.H., Silliman, B.R., 2011. A blueprint for blue carbon: toward an improved understanding of the role of vegetated coastal habitats in sequestering CO2. Frontiers in Ecology and the Environment 9, 552–560. https://doi.org/10.1890/110004

Mcowen, C., Weatherdon, L., Bochove, J.-W., Sullivan, E., Blyth, S., Zockler, C., Stanwell-Smith, D., Kingston, N., Martin, C., Spalding, M., Fletcher, S., 2017. A

global map of saltmarshes. Biodiversity Data Journal 5, e11764. https://doi.org/10.3897/BDJ.5.e11764

Middelburg, J.J., Nieuwenhuize, J., Lubberts, R.K., van de Plassche, O., 1997. Organic Carbon Isotope Systematics of Coastal Marshes. Estuarine, Coastal and Shelf Science 45, 681–687. https://doi.org/10.1006/ecss.1997.0247

Möller, I., Kudella, M., Rupprecht, F., Spencer, T., Paul, M., van Wesenbeeck, B.K., Wolters, G., Jensen, K., Bouma, T.J., Miranda-Lange, M., Schimmels, S., 2014. Wave attenuation over coastal salt marshes under storm surge conditions. Nature Geosci 7, 727–731. https://doi.org/10.1038/ngeo2251

Mueller, P., Do, H.T., Jensen, K., Nolte, S., 2019. Origin of organic carbon in the topsoil of Wadden Sea salt marshes. Marine Ecology Progress Series 624, 39–50. https://doi.org/10.3354/meps13009

National Oceanic and Atmospheric Administration, 2019. Carbon cycle [WWW Document]. URL https://www.noaa.gov/education/resource-collections/climate/carbon-cycle (accessed 1.19.24).

Needelman, B.A., Emmer, I.M., Emmett-Mattox, S., Crooks, S., Megonigal, J.P., Myers, D., Oreska, M.P.J., McGlathery, K., 2018. The Science and Policy of the Verified Carbon Standard Methodology for Tidal Wetland and Seagrass Restoration. Estuaries and Coasts 41, 2159–2171. https://doi.org/10.1007/s12237-018-0429-0

Nguyen, V.L., Ta, T.K.O., Tateishi, M., 2000. Late Holocene depositional environments and coastal evolution of the Mekong River Delta, Southern Vietnam. Journal of Asian Earth Sciences 18, 427–439. https://doi.org/10.1016/S1367-9120(99)00076-0

Orians, G.H., Pfeiffer, E.W., 1970. Ecological Effects of the War in Vietnam. Science 168, 544–554. https://doi.org/10.1126/science.168.3931.544

Pendleton, L., Donato, D.C., Murray, B.C., Crooks, S., Jenkins, W.A., Sifleet, S., Craft, C., Fourqurean, J.W., Kauffman, J.B., Marbà, N., Megonigal, P., Pidgeon, E., Herr, D., Gordon, D., Baldera, A., 2012. Estimating Global "Blue Carbon" Emissions from Conversion and Degradation of Vegetated Coastal Ecosystems. PLoS ONE 7, e43542. https://doi.org/10.1371/journal.pone.0043542

Pierce, R.H., Wetzel, D.L., Estevez, E.D., 2004. Charlotte Harbor Initiative: Assessing the Ecological Health of Southwest Florida's Charlotte Harbor Estuary. Ecotoxicology 13, 275–284. https://doi.org/10.1023/B:ECTX.0000023571.55816.2c

Poulakis, G., Blewett, D., Mitchell, M., 2003. The Effects of Season and Proximity to Fringing Mangroves on Seagrass-Associated Fish Communities in Charlotte

Harbor, Florida. Gulf of Mexico Science 21. https://doi.org/10.18785/goms.2102.03

Quisthoudt, K., Schmitz, N., Randin, C.F., Dahdouh-Guebas, F., Robert, E.M.R., Koedam, N., 2012. Temperature variation among mangrove latitudinal range limits worldwide. Trees 26, 1919–1931. https://doi.org/10.1007/s00468-012-0760-1

Rastogi, R.P., Phulwaria, M., Gupta, D.K. (Eds.), 2021. Mangroves: Ecology, Biodiversity and Management. Springer Singapore, Singapore. https://doi.org/10.1007/978-981-16-2494-0

Saintilan, N., Rogers, K., Mazumder, D., Woodroffe, C., 2013. Allochthonous and autochthonous contributions to carbon accumulation and carbon store in southeastern Australian coastal wetlands. Estuarine, Coastal and Shelf Science 128, 84–92. https://doi.org/10.1016/j.ecss.2013.05.010

Shields, G.A., 2005. CARBON CYCLE, in: Selley, R.C., Cocks, L.R.M., Plimer, I.R. (Eds.), Encyclopedia of Geology. Elsevier, Oxford, pp. 335–345. https://doi.org/10.1016/B0-12-369396-9/00156-8

Sidik, F., Lovelock, C.E., 2013. CO2 Efflux from Shrimp Ponds in Indonesia. PLoS ONE 8, e66329. https://doi.org/10.1371/journal.pone.0066329

Sippo, J.Z., Maher, D.T., Schulz, K.G., Sanders, C.J., McMahon, A., Tucker, J., Santos, I.R., 2019. Carbon outwelling across the shelf following a massive mangrove dieback in Australia: Insights from radium isotopes. Geochimica et Cosmochimica Acta 253, 142–158. https://doi.org/10.1016/j.gca.2019.03.003

Sippo, J.Z., Sanders, C.J., Santos, I.R., Jeffrey, L.C., Call, M., Harada, Y., Maguire, K., Brown, D., Conrad, S.R., Maher, D.T., 2020. Coastal carbon cycle changes following mangrove loss. Limnol Oceanogr lno.11476. https://doi.org/10.1002/lno.11476

Smeaton, C., Burden, A., Ruranska, P., Ladd, C.J.T., Garbutt, A., Jones, L., McMahon, L., Miller, L.C., Skov, M.W., Austin, W.E.N., 2022. Using citizen science to estimate surficial soil Blue Carbon stocks in Great British saltmarshes. Frontiers in Marine Science 9. https://doi.org/doi.org/10.3389/fmars.2022.959459

Spivak, A.C., Sanderman, J., Bowen, J.L., Canuel, E.A., Hopkinson, C.S., 2019. Global-change controls on soil-carbon accumulation and loss in coastal vegetated ecosystems. Nat. Geosci. 12, 685–692. https://doi.org/10.1038/s41561-019-0435-2

Temmerman, S., Meire, P., Bouma, T.J., Herman, P.M.J., Ysebaert, T., De Vriend, H.J., 2013. Ecosystem-based coastal defence in the face of global change. Nature 504, 79–83. https://doi.org/10.1038/nature12859

Tomlinson, P.B., 2016. The botany of mangroves, Second edition. ed. Cambridge University Press, New York.

US Department of Commerce, N. (n.d.). Tampa Bay Original Climate Page. NOAA's National Weather Service. Retrieved 13 February 2024, from https://www.weather.gov/tbw/tampabayoriginalclimatepage

Van De Broek, M., Vandendriessche, C., Poppelmonde, D., Merckx, R., Temmerman, S., Govers, G., 2018. Long-term organic carbon sequestration in tidal marsh sediments is dominated by old-aged allochthonous inputs in a macrotidal estuary. Global Change Biology 24, 2498–2512. https://doi.org/10.1111/gcb.14089

van der Wal, D., Pye, K., 2004. Patterns, rates and possible causes of saltmarsh erosion in the Greater Thames area (UK). Geomorphology 61, 373–391. https://doi.org/10.1016/j.geomorph.2004.02.005

Vo, Q.T., Oppelt, N., Leinenkugel, P., Kuenzer, C., 2013. Remote Sensing in Mapping Mangrove Ecosystems — An Object-Based Approach. Remote Sensing 5, 183–201. https://doi.org/10.3390/rs5010183

Wolters, M., Bakker, J.P., Bertness, M.D., Jefferies, R.L., Möller, I., 2005. Saltmarsh erosion and restoration in south-east England: squeezing the evidence requires realignment. Journal of Applied Ecology 42, 844–851. https://doi.org/10.1111/j.1365-2664.2005.01080.x

Woodwell, G.M., Pecan, E.V., 1973. Carbon and the Biosphere: Proceedings of the 24th Brookhaven Symposium in Biology, Upton, NY, May 16-18, 1972. Technical Information Center, US Atomic Energy Commission.

Xia, S., Song, Z., Li, Q., Guo, L., Yu, C., Singh, B.P., Fu, X., Chen, C., Wang, Y., Wang, H., 2021. Distribution, sources, and decomposition of soil organic matter along a salinity gradient in estuarine wetlands characterized by C:N ratio, δ13C-δ15N, and lignin biomarker. Global Change Biology 27, 417–434. https://doi.org/10.1111/gcb.15403

Zhao, Y., Yu, Q., Wang, D., Wang, Y.P., Wang, Y., Gao, S., 2017. Rapid formation of marsh-edge cliffs, Jiangsu coast, China. Marine Geology 385, 260–273. https://doi.org/10.1016/j.margeo.2017.02.001

2 Sediment to Atmosphere CO_2 Efflux Increases at Retreating Salt Marsh Edges

The following chapter is a reformatted version of a manuscript submitted to the Journal of: Estuarine, Coastal and Shelf Science by Stolpmann, L.M., Balke, T. & Bass, A.M.

Abstract

Coastal intertidal wetlands are dynamic and biodiverse habitats with carbon-rich waterlogged soils. When the soil gets exposed to oxygen, carbon can be emitted as CO_2 back into the atmosphere. In this study we investigate whether contrasting stepped vs. gradual marsh edge topography, resulting from lateral cliff erosion versus expansion influences the soil-atmosphere CO_2 fluxes. CO_2 fluxes were quantified alongside groundwater level, soil temperature, and local sediment grain size across an estuarine salt marsh with differing seaward edge topography. We found that the CO_2 flux from the marsh soil was on average greater at cliffed-eroding compared to sloped-prograding sites (0.7 ± 0.11 g/m^2 hr^{-1} and 0.26 ± 0.06 g/m^2 hr^{-1}, respectively). Soil respiration varied temporally with tidal cycle, groundwater levels, soil temperature, and spatially with distance to the seaward vegetation edge. Overall, fluxes during a neap cycle were significantly greater compared to spring tidal cycles. Our study thus highlights that soil CO_2 efflux is affected by marsh topography resulting from cliff formation and marsh edge undercutting, leading to carbon losses from the remaining marsh platform. Our findings highlight the spatial and temporal variability of carbon fluxes in a salt marsh environment and the importance of geomorphic form and process in understanding coastal carbon dynamics.

Keywords

Salt marshes

Blue carbon

Erosion

Groundwater dipwell

2.1 Introduction

Coastal intertidal wetlands (i.e., mangroves, salt marshes, seagrass) occupy the transition zone between the terrestrial and marine environment. In addition to their unique biodiversity, they provide a range of ecosystem services (Barbier et al., 2011), such as coastal protection (Ford et al., 2016; Greenberg et al., 2014; Möller et al., 2014; Worm et al., 2006), and carbon storage (Mcleod et al., 2011). Due to their waterlogged saline soils and net sedimentation salt marshes are globally sequestering carbon at a rate of approx. 48-59 Tg C y^{-1} (Wang et al., 2021). Disturbances, such as relative-sea level rise, lack of sediment supply and coastal erosion can significantly threaten salt marsh extent (Campbell et al., 2022). The last two decades showed a net total salt marsh loss of 1,452.84 km^2 globally, (i.e., a rate of 0.28% y^{-1}) and hence the loss of the associated carbon stores and carbon sequestering function of these habitats (Campbell et al., 2022).

When marshes shift from net sedimentation to lateral erosion previously deposited sediments and associated sequestered carbon are mobilized (Braun et al., 2019; Theuerkauf et al., 2015), exporting it either as dissolved/particulate organic carbon (D/POC), and/or dissolved inorganic carbon (DIC) to coastal waters (Cai, 2011; Lovelock et al., 2017a). This leads to an estimated global export from salt marshes to adjacent coastal waters of 0.60 ± 0.11, 5.28 ± 1.21 and 2.55 ± 0.55 Mg C ha^{-1} y^{-1} of POC, DIC and DOC (mean ± SE) respectively (Alongi, 2020). Exposing the remaining sediments and sequestered carbon to oxygen can further lead to the emission of CO_2 to the atmosphere (Lovelock, et al., 2017b), yet this has rarely been quantified in the context of geomorphic form (i.e., topography such as cliffed/undercut marsh edges) and process (i.e. sedimentation and erosion).

Soil processes and conditions, which can differ between marsh topography/geomorphic form and can affect carbon stores, include the retention of groundwater (Van Putte et al., 2020) as well as soil temperature (Bu et al., 2015b; Wang et al., 2007). Physical soil properties like grain size and soil compaction directly interact with geomorphic processes and soil biogeochemistry (Lo et al., 2017; Wang et al., 2017). Tidal inundation durations, depending on marsh elevation, drives the import of allochthonous carbon onto the salt marsh (Xia et al., 2021), soil anaerobic conditions and soil salinity, and thus directly affect aerobic decomposition and thus outgassing of carbon (Cai, 2011).

Most studies estimate carbon loss in salt marsh ecosystems due to disturbances directly from the change of carbon stocks (Bu et al., 2015a; Coverdale et al., 2014; Theuerkauf et al., 2015) or from modelling the decomposition rate of organic matter dependent on the fraction exposed to oxic conditions (Lovelock et al., 2017b). Direct measurements of carbon

decomposition into CO_2 and methane (CH_4) production have been mainly performed through incubation experiments (McTigue et al., 2021). Determining how geomorphic processes leading to differing salt marsh topography affect soil-atmosphere CO_2 effluxes are therefore crucial for accounting carbon budgets.

In this study we answer the question whether marsh topography (i.e., geomorphic form resulting from geomorphic processes of lateral erosion vs. expansion) should be considered when assessing overall carbon efflux from marsh soils in addition to active sediment fluxes in and out of the marsh. We investigate the following research questions: (i) Does the soil-atmosphere CO_2 flux differ between eroding and prograding salt marsh sites?; (ii) How do eroding and prograding salt marsh sites differ in their soil properties, i.e., carbon content, carbon stable isotopes ($\delta^{13}C$), indicating marine vs terrestrial carbon sources, inundation/groundwater level and soil temperature?; (iii) Which soil properties statistically determine CO_2 efflux? We hypothesized a higher soil-atmosphere CO_2 efflux from cliffed-eroding salt marsh sites compared to sloping-prograding sites due to soil exposure associated with cliff retreat. To our knowledge, we provide the first study to systematically contrast soil-atmosphere CO_2 efflux between marsh topographies (geomorphic form) resulting from geomorphic process (i.e., eroding vs. prograding). We believe that understanding the link between geomorphic form and carbon dynamics in coastal wetlands will be of increasing importance in a climate change future.

2.2 Materials and Methods

2.2.1 Study site

Marsh topographic influence on soil-atmosphere CO_2 flux due to geomorphic change was studied at the Caerlaverock salt marsh in the Solway Firth, UK (Figure 2.1). The study site is characterized by temperate climate with a macro-tidal range of over 8m (Cutts and Hemingway, 1996). The salt marsh extends from west to east for approx. 8 km along the north shore of the Solway Firth, with a width of up to 1km at the eastern side (Clyne et al., 2007). The salt marsh has been classified as a sandy and sandy mud type, dominated by grasses (Sghair, 2013).

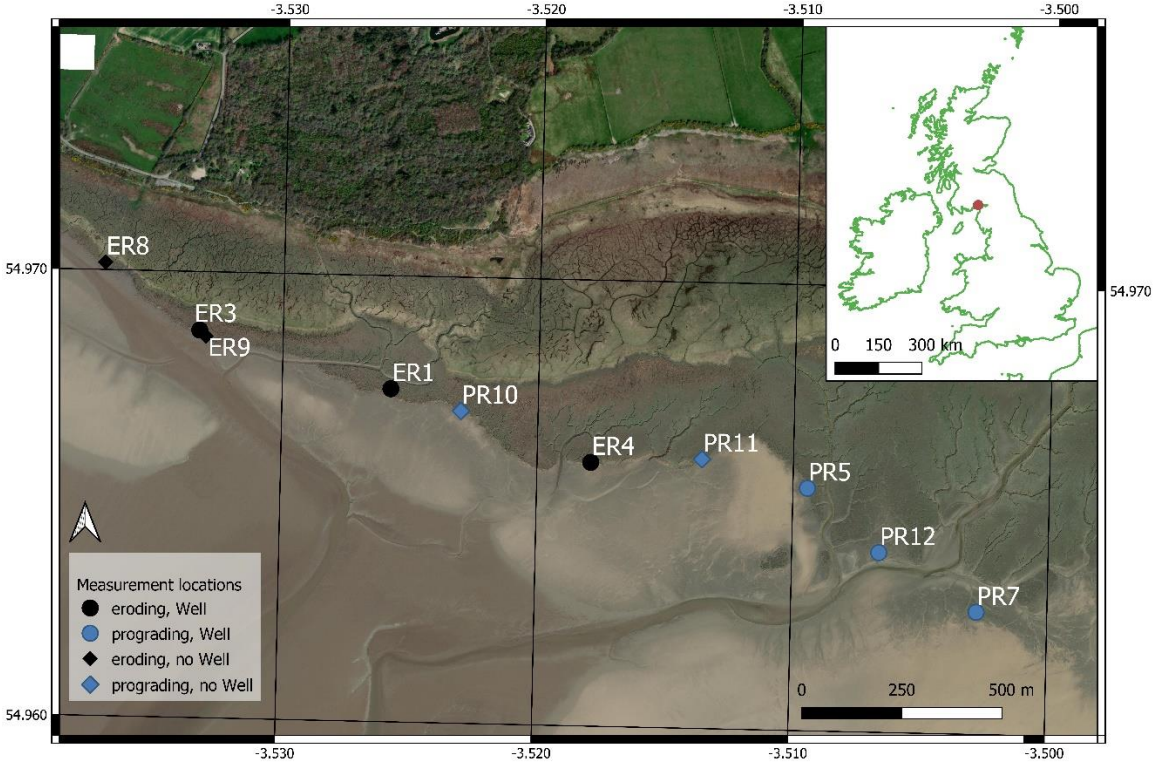

Figure 2.1 Map of study location at Caerlaverock salt marsh, Scotland, UK. The inset map shows the location within the UK. Sites with groundwater wells are marked with a circle, sites without groundwater well are marked with a square. The black fill marks eroding sites, the blue fill marks prograding sites.

The linear retreat rate of the seaward marsh edge was calculated with the digital shoreline analysis ArcGIS tool (DSAS) from the United States Geographical survey USGS (Himmelstoss et al., 2018). The coastline was manually digitized using satellite images from the years 2009, 2014, 2018 and 2019 ("EDINA Aerial Digimap Service," 2018; "EDINA Aerial Digimap Service," 2014). Sites were classified as eroding or prograding, according to the linear regression rate of the closest transect, showing either a cliff edge due to past erosion or are sloping towards the mudflat resulting from the continued growth of the seaward marsh edge (Figure 2.2).

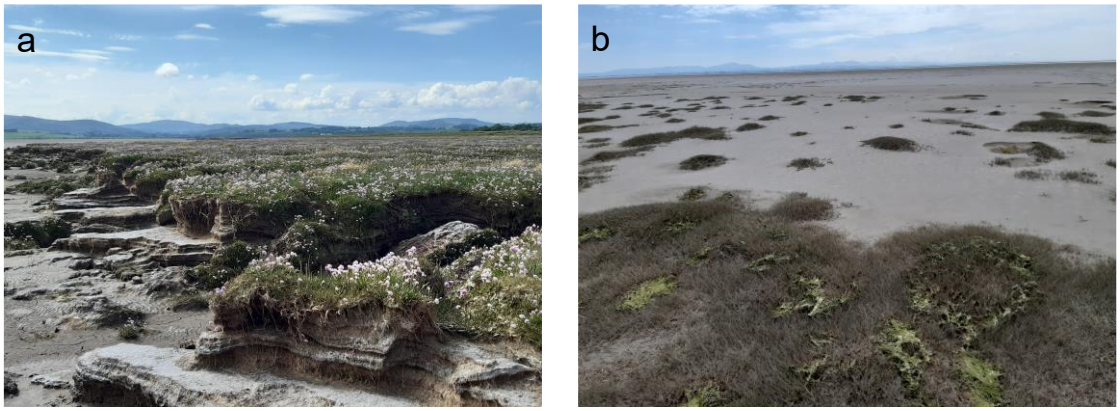

Figure 2.2 Cliffed-eroding salt marsh site (a), and sloping-prograding salt marsh site (b) at Caerlaverock salt marsh within the Solway Firth, Scotland, UK.

2.2.2 Field sampling

Soil-atmosphere CO_2 efflux, groundwater level, groundwater temperature, soil temperature and soil cores were measured and taken at Caerlaverock salt marsh during sampling campaigns from June 2021 to March 2022 (Table A.6).

Five vented groundwater wells of 1m depth were installed along the salt marsh coastline at an initial distance of 3 m to the vegetation edge (Table A.7). Three groundwater wells were installed at eroding (ER1; ER3; ER4) and two at prograding sites (PR5; PR7). The groundwater well at site ER4 failed, with continued high readings following high tides due to sand ingress and was excluded from the analysis. Groundwater wells were constructed following the design by Van Putte et al., (2020), however no infilling with filter sand and bentonite was done, as the salt marsh at Caerlaverock is of sandy sediment. Groundwater well locations were determined with differential global positioning system (DGPS, version) with a horizontal and vertical accuracy of ~2 cm. Non-vented pressure loggers (Rugged

TROLL 100) were installed in the groundwater wells on 1st of July 2021 and readings were taken with a frequency of 10 minutes until 9th of March 2022. Except for the groundwater well at site PR7, where measurements were made from the 21st of October 2021, after a faulty logger was exchanged. Groundwater pressure readings were corrected for atmospheric pressure from local measurements.

Soil temperature loggers (HOBO Pendant® MX Water Temperature Data Logger, MX2201) with an accuracy of 0.1°C were installed in August 2021 at all sites, at the corresponding distance of the groundwater well, at a depth of 10 cm (Figure 2.1). Temperature measurements were taken every 15 minutes.

One sediment core was taken to 1 m depth with an Edelman auger at each site with a groundwater well. Included in the analysis are the cores from sites, which included groundwater well measurements (i.e., ER1, ER3, PR5, PR7). Subsamples of 40 cm^3 were taken every 10 cm on which all following soil analyses were performed (section 2.3).

Soil CO_2 emission was measured in June, August, and November 2021, as well as in January and March 2022 (Table A.7). This monitoring regime was selected to cover temporal variations of CO_2 efflux across seasons, as this study is looking at influences on CO_2 efflux due to the underlying soil conditions rather than through active sediment erosion. Soil-atmosphere CO_2 emissions were measured during low tide at the 10 soil temperature measurement sites (5 groundwater well and soil temperature; 5 soil temperature sites; Figure 2.1). At each site, measurements were performed within the vegetation at three positions going landwards from the seaward vegetation edge at distances of 0.3 m, 1 m, and 3 m (Figure 2.2). Flux was measured with a Licor (LI-850) using the closed-chamber method. Measurements were performed in duplicates with a measuring time of two minutes each, depending on gas accumulation time. A polynomial regression was used to calculate the rate of change of CO_2 concentration, subsequently used to calculate CO_2 flux ($g/m^2\ hr^{-1}$) (Bass et al., 2016; Kutzbach et al., 2007).

$$Gas\ flux = \left(a \times \left(\frac{P}{1013}\right) \times \left(\frac{273}{T+273}\right) \times M\right) \times \left(\frac{V}{A}\right) / 1000 \times 3600 \quad \textbf{Equation 2.1}$$

Where a = initial increase at time t = 0; p = Air pressure within the chamber; T = air temperature in °C; M = molar weight of measurement gas; V = volume of chamber; A = Area of chamber.

2.2.3 Sediment sample processing

The four sediment cores to 1 m depth, were analyzed in 10 cm subsamples. Soil samples were freeze dried for 48h after collection. Following freeze drying, bulk density, loss on ignition (LOI), grain size, carbon content and carbon stable isotopes ($\delta^{13}C$) were determined for every 10 cm subsample taken from the cores (n = 57). Loss on ignition was determined to enable comparisons to a wider range of studies.

Bulk density was calculated by dividing the dry sediment weight by the subsampled volume (Mobilian and Craft, 2021).

Grain size analysis was performed on approx. 5 g of the 10 cm subsamples with the use of hydrogen peroxide (100 volumes > 30%) added to the samples and left for two hours to react before more hydrogen peroxide was added and left to evaporate overnight (Gray et al., 2010). Samples were then slowly heated from 80 °C to 100 °C until a clear layer of supernatant formed, and the reaction ceased. They were transferred into centrifugal tubes and centrifuged for 30 minutes at 2500 rpm then dried for 24 h at 90 °C. The grain size distribution was performed with a Coulter Fluid module (LS230) for 3 runs of 90 seconds. To prevent clogging, 25 ml of water and 5 ml of Calgon were added to the samples, placed for 3 minutes into an ultrasonic bath before the sample was pipetted into the coulter module.

Isotopic carbon analysis of $\delta^{13}C$ and total carbon concentration measurements (mg/mg) were performed on the freeze-dried 10 cm subsamples with a Picarro Cavity Ring-down Spectrometer (G2201-*i*) coupled to a combustion module (A0201). For this analysis, approx. 5 mg of the subsamples were placed into weighted tin capsules. Inorganic carbon was removed from freeze-dried subsamples with hydrochloric acid (1 M) and left to react overnight until reaction ceased. Samples were washed to neutral pH before drying at 60°C. Subsamples of approx. 20 mg were placed into weighted tin capsules and analysed for organic carbon content and $\delta^{13}C_{org}$ with the Picarro Cavity Ring-down Spectrometer (G2201-*i*) coupled to a combustion module (A0201). Values of $\delta^{13}C$ and $\delta^{13}C_{org}$ are presented in standard delta notation (‰) relative to the Vienna Pee Dee Belemnite (VPDB) standard, with an accuracy of 0.2 to 0.3‰ (Picarro, 2019). Carbon stable isotopic ratios are indicative of the source of organic matter as well as its decomposition status (Lamb et al., 2007).

2.2.4 Statistical analyses

All statistical analyses were performed using R (4.1.1; R Core Team, 2021). Groundwater level data for the analyses was taken from four sites (two eroding and two prograding). Groundwater level was expressed as distance to the sediment surface (m). Groundwater well inundation duration above the soil surface was calculated for the entire continuous measurement period from October 2021 to March 2022 for all four groundwater wells using the R *VulnToolkit* package (1.1.4; Hill, 2021). Spring low tide groundwater levels were averaged over the continuous measurement period from October 2021 to March 2022.

Inorganic carbon percentage was calculated by subtracting the organic carbon percentage from the total carbon percentage. Negative values of inorganic carbon percentages were regarded as 0% inorganic carbon (Mueller et al., 2023).

Differences in groundwater level characteristics between sites were analyzed with Kruskal-Wallis tests and Wilcoxon signed rank pairwise tests.

A series of Pearson's correlations were performed between 1) inundation duration and well elevation, 2) spring tidal low tide groundwater levels and well elevation, 3) spring tidal low tide groundwater levels and inundation duration, as well as between 4) surface (0-50 cm) sediment clay percentage (<4 µm) and average spring low tide groundwater levels.

2.2.4.1 Mixed Effects Models

To determine the relationship between tidal cycle, erosion conditions, distance to cliff, groundwater level, soil temperature and CO_2 efflux, a Generalized Linear Mixed Effects Model (GLMM) and a Linear Mixed Effects Model (LMM) were selected. These models were chosen due to the study design, making it possible to include repeated measurements as random effects in the models. The most parsimonious models for both the GLMM and the LMM were determined using likelihood ratio tests and AIC scores (Zuur et al., 2009).

Model 1 – Generalized Linear Mixed Effects Model

The influence of erosion status, tidal cycle, and distance to seaward marsh edge on soil-atmosphere CO_2 efflux was analyzed using data from all sites (Figure 2.1, Table A.6), including a total of 148 CO_2 efflux measurements. A Generalized Linear Mixed Effects Model (GLMM) from the *lme4* R-package (1.1.28; Bates et al., 2015) was applied, as the residuals were not normally distributed using a Linear Mixed Effects Model.

Model 2 – Linear Mixed Effects Model

The effect of soil temperature, groundwater level and tidal cycle on CO_2 flux was analyzed with a Linear Mixed Effects Model (LMM). The response variable of CO_2 flux did not meet the assumption of normality and was transformed using the cube root transformation, after testing for normality following log and square root transformation. For the LMM, a subset of measurements was used, taken at groundwater well sites, at the 3 m distance from the seaward vegetation edge, in line with the groundwater well location and soil temperature logger. A total of 32 CO_2 efflux measurements were included. Soil temperature and groundwater level were both averaged over a 24-hour period prior to the CO_2 flux measurement.

Model 3 – Mixed Effects Models

The effect of erosion conditions on sediment characteristics were analyzed with Linear Mixed Effects Models (LMM) or Generalized Linear Mixed Effects Models (GLMM) when the response variable could not meet the assumption of normal distribution of residuals following transformations. Model assumptions were analyzed using the *DHARMa* R-package (Hartig and Lohse, 2022).

2.2.4.2 Time Series Analyses

Data from October 2021 to March 2022 was used to test the relationship between continuous soil, groundwater, and air temperature as well as continuous groundwater level to different marsh topographies resulting from geomorphic change. The difference in soil temperature between site ER1 and site PR5 was calculated and a moving average with a period of 7 days applied to smooth the data, calculated using the R-package *zoo* (Zeileis et al., 2023). Changes in soil temperature were analyzed for site ER1 and site PR5. Site ER1 was chosen, as it is the only eroding site with a groundwater well, from which a soil temperature logger was safely retrieved in March 2022. Site PR5 was chosen as a contrast, as it can be regarded as stable (i.e., no high eroding/prograding linear regression rate) to be able to observe any potential changes in temperature due to cliff formation. By analyzing the difference in soil temperature, the influence of air temperature was removed, as both sites are assumed to be similarly influenced by the local ambient air temperature.

A different trend in soil temperature difference was observed from January 2022 onwards, motivating the comparison of average soil temperature differences between the two periods,

October to December 2021, and January to March 2022. Separate cross-correlations analyses were applied for 2021 and 2022 between 1) groundwater level and soil temperature difference; and 2) difference of air to groundwater temperature and soil temperature difference.

2.3 Results

2.3.1 CO_2 efflux at prograding and eroding marsh edges

Sediment-atmosphere CO_2 efflux was compared between all measured salt marsh sites, containing soil temperature loggers and/or groundwater wells. Soil CO_2 efflux was significantly greater at eroding than prograding sites during the spring tidal cycle, 0.7 ± 0.11 $g/m^2\ hr^{-1}$ vs. 0.26 ± 0.06 $g/m^2\ hr^{-1}$, respectively (mean ± SE; Figure 2.3, Figure 2.4, Table A.2).

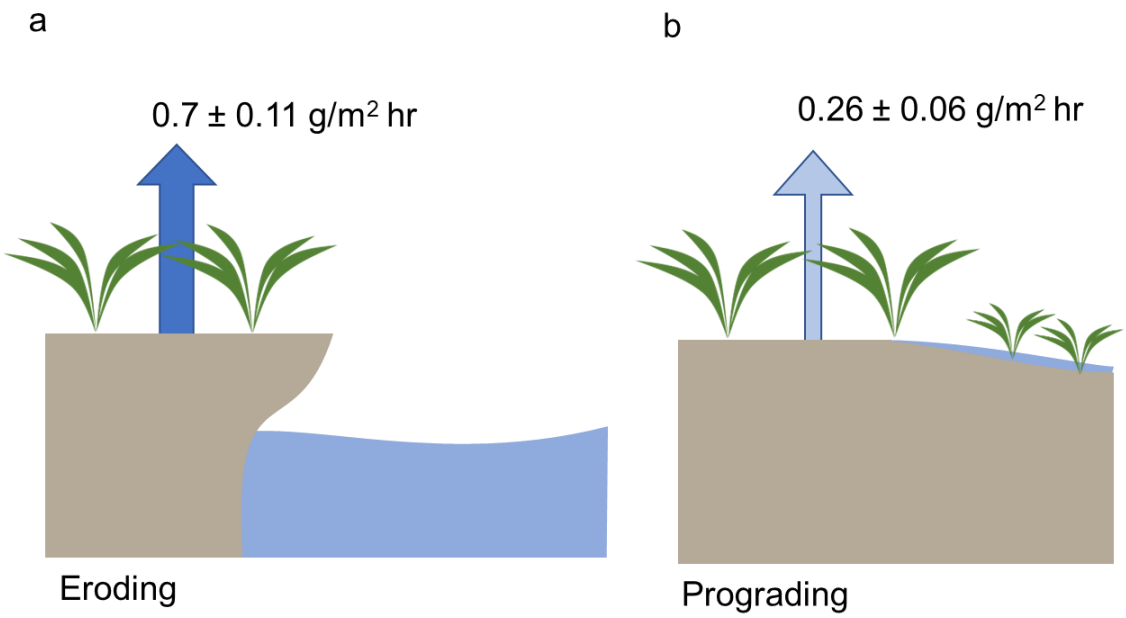

Figure 2.3 Schematic drawing of soil-atmosphere CO_2 flux ($g/m^2\ hr^{-1}$) ± SE from (a) eroding, and (b) prograding salt marsh edges during spring tidal cycles.

2.3.2 Drivers of CO_2 flux

Tidal cycle and measurement distance to the vegetation edge significantly influenced the CO_2 flux (Figure 2.4, Table S1). During the neap tidal cycle CO_2 flux showed significant variation, independent of the distance to the vegetation edge. However, during the spring

tidal cycle the CO_2 flux increased with distance to the vegetation edge. During the spring tidal cycle, CO_2 flux difference between eroding and prograding sites was amplified. The effect of soil temperature, groundwater level and tidal cycle on CO_2 efflux was modelled with a LMM using Site and Date as random effects. The interaction of soil temperature and groundwater level had a significant effect on the CO_2 efflux (Figure 2.5, Table A.3, Figure A.1). The relationship between soil temperature and CO_2 efflux depended on the groundwater level. The efflux of CO_2 was lower at lower soil temperatures and higher groundwater levels, whereas it was greater when groundwater levels dropped.

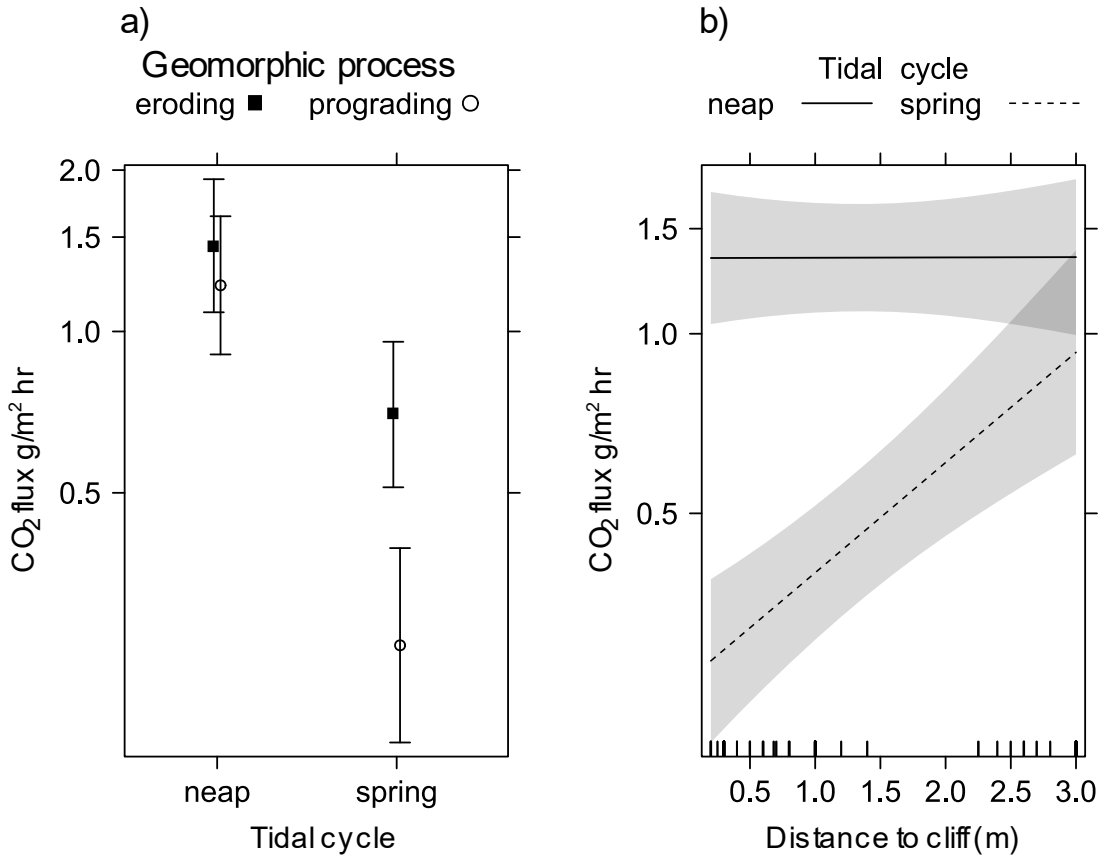

Figure 2.4 Relationship between CO_2 flux (g/m^2 hr) and a) Interaction of tidal cycle (neap vs. spring) and geomorphic process (eroding vs. prograding); b) Interaction of measurement distance to cliff/seaward vegetation edge (m) and tidal cycle (neap vs. spring). Lines represent model fit through data as identified from a GLMM with "Site" as a random intercept (Table S1), confidence bands and error bars represent 95% confidence intervals. Tick marks along plot shows deciles of distribution of predictor variable.

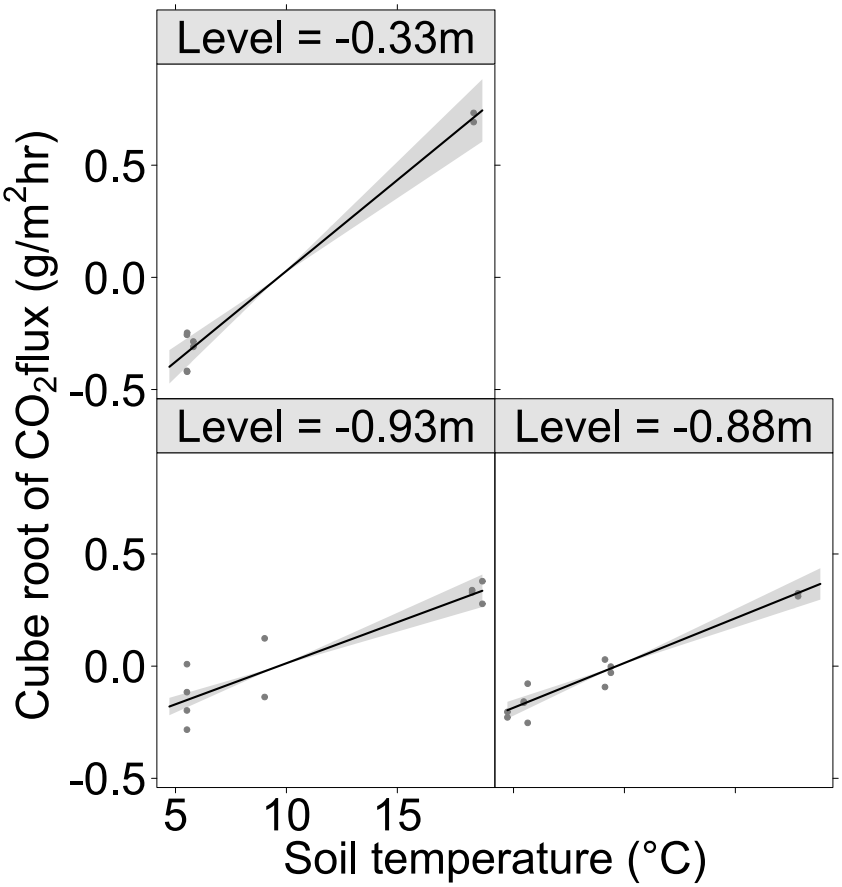

Figure 2.5 Effect of interaction between soil temperature and groundwater level (m) on cube root transformed soil-atmosphere CO_2 efflux (g/m2 hr^{-1}) across eroding and prograding sites identified from a LMM with "Site" as random intercept and "Visit" as random slope (Table S2). Lines represent model fit through the data, with the confidence bands representing the 95% confidence intervals. Data points are distribution of standardized partial residuals.

The measured differences in low-tide groundwater levels among sites for spring tidal cycles from November 2021 to March 2022 were significant among sites as well as within sites (Table A.4, Table A.5). Sites showed fluctuations of low tide average groundwater levels during spring tidal cycles, except for site PR7, where a decreasing trend in groundwater level was apparent. Average groundwater level at low tides was lowest at ER1 and highest at PR7. ER3 and PR5 showed the highest similarity (Figure 2.6).

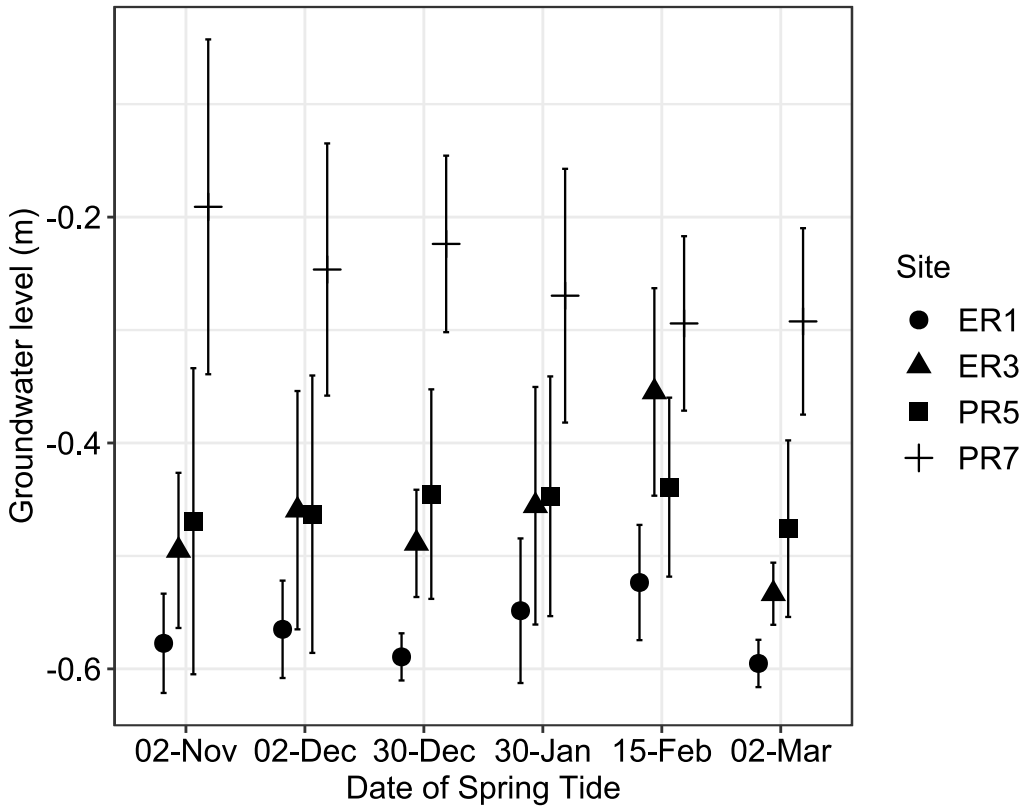

Figure 2.6 Average groundwater level (m) at low tide during spring tidal cycles from November 2021 to March 2022 for sites ER1, ER3, PR5, PR7. Error bars represent ± 1 SD.

Inundation frequency (duration) above the marsh surface of groundwater wells was highest at site PR7 with 4.79% (159. 9 h), followed by site ER1 (3.29%; 109.9 h); ER3 (2.73%; 91.2 h) and lowest at site PR5 (2.48%; 82.9 h; Table A.6). There was a significant negative correlation between inundation duration and well elevation ($r = -0.99$, p-value < 0.05). Inundation duration however, was not significantly correlated to groundwater level ($r = 0.75$, p-value = 0.25). Furthermore, groundwater level was not significantly correlated to site elevation ($r = -0.82$, p-value = 0.18).

Changes in soil temperature were analyzed for site ER1 and site PR5. The difference in soil temperature between ER1 and PR5 changed throughout the measurement period. Whereas the moving average of the calculated difference did not show a trend from October to December 2021, it was apparent for January to March 2022 (Figure 2.7). The average difference in soil temperature in these periods was -0.26℃, October to December 2021, and 0.02℃ between January and March 2022. During the period from October to December 2021 the soil temperature at site ER1 was greater than PR5 9.4% of the time, whereas it was greater than PR5 64.5% of the time in the period from January to March 2022. The difference between air temperature and groundwater temperature at site ER1 was on average -1.34℃ in 2021 and 0.01℃ in 2022. During October to December 2021 the air temperature was

14.5% of the time greater than the groundwater temperature at site ER1, in the period from January to March 2022 it was 57% of the time.

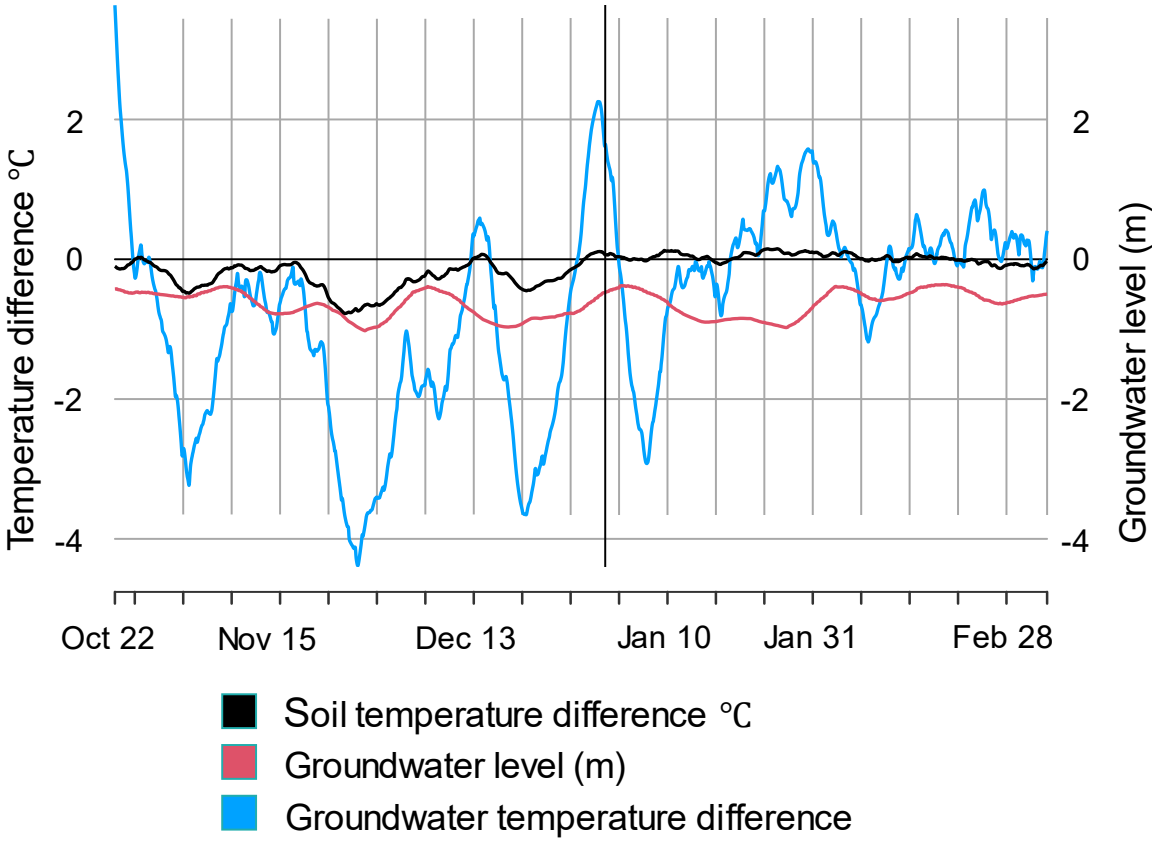

Figure 2.7 Moving average applied over 7 days on: Difference in soil temperature between site ER1 and PR5 (black), groundwater level at site ER1 (red); difference between air temperature and groundwater temperature at site ER1 (blue). Vertical line shows January 2022. Horizontal line at y = 0 shows no difference in soil temperature between site ER1 and PR5 and positive values show higher temperatures at the eroding site ER1 than prograding site PR5 (red), and higher air temperature than groundwater temperature at site ER1 (blue).

Cross-correlation analysis between groundwater level at site ER1 and soil temperature difference between ER1 to PR5 for October to December 2021 showed that an increase in groundwater level was associated with increased soil temperature differences after 0-7 hours (lag = 0; r^2 = 0.41; Figure A.2). Whereas from January to March the cross-correlation analysis showed a negative and weaker correlation between groundwater level and soil temperature difference (lag = -28; r^2 = -0.3; Figure A.3). Here, increased groundwater levels were associated with lower soil temperature differences up to 28 hours later. The cross-correlation analysis of groundwater temperature difference to soil temperature is showing a positive lag of 29 hours during up to the end of December (lag = 29; r^2 = 0.27; Figure A.4), but a negative lag and correlation after January 2022 (lag = -21; r^2 = -0.14; Figure A.5). The

differences in the air and groundwater temperature difference are lagging soil temperature differences during the measurement period in the first half but leading during the second half of the monitoring period.

2.3.3 Soil characteristics

Percentage clay (<4 µm) and organic carbon percentage were significantly different among sites (Figure 2.8, Table A.7). Prograding site PR5 had a lower clay percentage than all other sites (3.48 ± 1.78 %, Figure 2.8) and at depth 140 cm 0 % clay. Site ER3 showed outliers at depth 60 cm and 80 cm with 10.71 % and 12.51 %, respectively. The percentage of silt was different between eroding and prograding conditions (Figure 2.8). Prograding site PR5 showed the lowest percentage silt with 25.61 ± 7.16 %, followed by site PR7 (31.35 ± 10.71 %). Sand percentage was greater at prograding sites than at eroding sites (PR5: 70.92 ± 8.87 %; PR7: 62.76 ± 13.10 %).

Prograding site PR5 had the highest $\delta^{13}C_{org}$ signature with -22.89 ± 3.68 ‰ and was significantly different from both eroding sites ER1 and ER3, -26.48 ± 1.2 ‰ and -25.81 ± 1.86 ‰, respectively (Figure 2.8). Site PR7 was significantly different to the $\delta^{13}C_{org}$ signatures of the eroding site ER1 (-24.7 ± 1.95 ‰) (Figure 2.8). Organic carbon concentrations was significantly different between sites but not between eroding and prograding conditions (Figure 2.8). Site PR5 had the lowest organic carbon percentage with 0.15 ± 0.06 % and site PR7 the highest with 0.31 ± 0.23 %. There was no significant difference between the inorganic carbon percentages between sites with prograding site PR7 having the highest percentage with 0.55 ± 0.45 %, followed by ER1 (0.39 ± 0.39 %), ER3 (0.33 ± 0.4 %), and PR5 (0.24 ± 0.33 %).

Surface (0-50 cm) sediment clay percentage (<4 µm) was correlated with the average groundwater level at low tides during spring tidal cycles, although not significantly ($r(2) = 0.93$, p-value = 0.072).

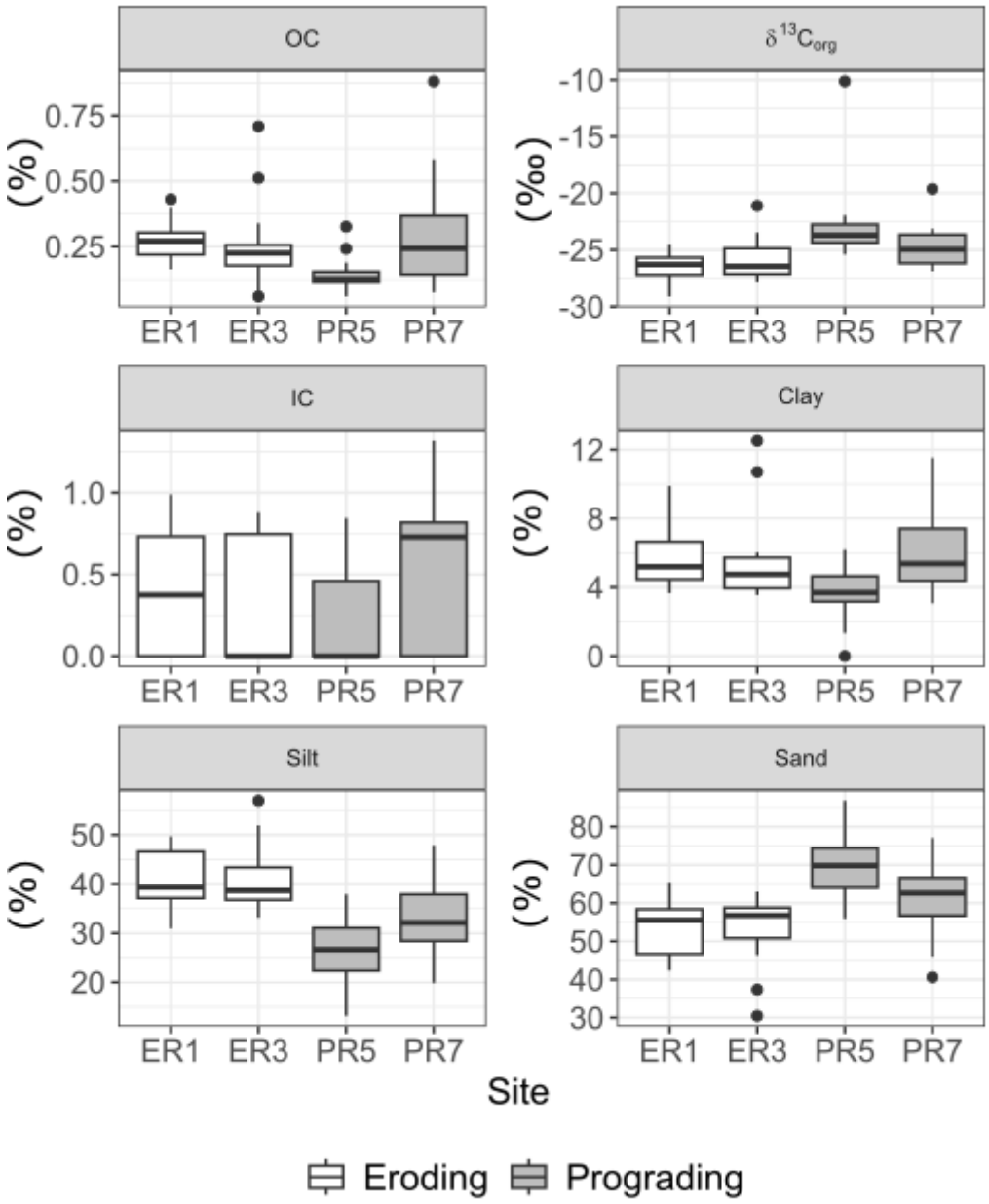

Figure 2.8 Boxplot of sediment analyses of 1 m soil cores taken at two eroding (white) and two prograding (grey) sites (ER1; ER3; PR5; PR7). OC= Organic carbon (percentage), $\delta^{13}C_{org}$ (‰), IC= Inorganic carbon (percentage), clay (<4 µm), silt (4-63 µm), and sand (63-2000 µm) percentages. Standard deviation showing variation with depth per core (ER1 n = 14; ER3 n = 14; PR5 n = 15; PR7 n = 14).

2.4 Discussion

2.4.1 CO_2 efflux at prograding and eroding marsh edges

The results confirm our initial hypothesis that cliffed-eroding sites showed a significantly higher average soil-atmosphere CO_2 efflux than sloped-prograding sites and that this was driven by altered soil conditions. This shows that the geomorphic form resulting from natural geomorphic processes can have similar affects compared to direct anthropogenic disturbances, such as soil extraction for embankments, increasing soil to atmosphere fluxes due to oxygenation and temperature increase of the soil (e.g. (Lovelock et al., 2017a; McTigue et al., 2021). Direct sediment removal from salt marshes due to coastal erosion leads to the loss of 10.1 Mg CO_2 ha^{-1} y^{-1} or 4.3% of the stored carbon, assuming that 50% of the OM will be oxidised over a time span of 30 years after erosion (Lovelock et al., 2017b). Our study shows that soil to atmosphere losses of carbon at eroding marsh edges within the remaining marsh platform need to be added to these calculations, and that even when erosion has ceased, the altered geomorphic form (i.e., marsh cliff formation) continues to lead to carbon losses.

Our measured CO_2 emissions at cliffed-eroding sites during spring and neap tides (700 ± 110 mg m^{-2} hr^{-1}, 1445 ± 209 mg m^{-2} hr^{-1}, mean ± SE, respectively) were approx. 2 - 2.5-times higher than the emission measured by Bu et al., (2015a). The site characteristics following reclamation resemble the site conditions at our studied cliffed-eroding sites, where changes to marsh topography let to higher CO_2 emissions (Bu et al., 2015a). The overall average soil respiration rate reported in our study is comparatively high in relation to other wetland respiration rates (Cui et al., 2021). However, the CO_2 efflux is still well within the range of 100-10,000 g m^{-2} yr^{-1} for tidal salt marsh systems (Cao et al., 2020; Magenheimer et al., 1996; Seyfferth et al., 2020). We suggest that soil to atmosphere losses of carbon over longer timescales will need to include the rates of erosion and the difference between labile vs. recalcitrant carbon pools in the soil (Lovelock et al., 2017b). A knowledge gap also remains in determining the fate of any eroded particulate carbon. It is estimated that the majority of sequestered carbon is mineralized after erosion and emitted as CO_2 to the atmosphere, with about 25-50% of carbon subsequently being buried in ocean sediments (Cai, 2011).

2.4.2 Soil conditions resulting from geomorphic form

Eroding and prograding sites differed in their characteristics, i.e., groundwater level, groundwater temperature, soil temperature, and sediment characteristics. Eroding marshes were characterized by decreased groundwater levels, increased soil temperature and greater silt percentage.

Our results, however, did not always show the hypothesized differences but displayed a strong dependency on inundation. The studied salt marsh was only inundated during spring tides. During neap tides there was no significant difference in CO_2 efflux between eroding and prograding sites. However, during spring tides, tidal inundation influenced groundwater levels and resulted in differing retentions of groundwater. Eroding sites showed a lower groundwater retention following spring high tides than prograding sites. Higher soil moisture during spring than neap tidal cycles has also been shown to decrease CO_2 efflux in other tidal salt marshes (Bu et al., 2015b). Spring and neap tidal cycles are acting on a regular, semi-lunar cycle. The impact of lower soil moisture on CO_2 emission was further shown on a longer timescale following land reclamation after dike construction (Bu et al., 2015a). Even nine years after reclamation, the disturbed land emitted 3-times more CO_2 (0.73 Mg ha^{-1} yr^{-1} CO_2) than the undisturbed salt marsh on Chongming Island with the Yangtze Estuary (Bu et al., 2015a).

Soil temperature was higher at eroding sites in comparison to prograding sites and had a positive effect on CO_2 efflux. Again, our findings indicate that geomorphic form and process mediate soil conditions, being primary drivers of carbon fluxes, which have previously been studied mainly for direct anthropogenic disturbances (Cui et al., 2021, Pendall et al., 2004). Soil temperature has been shown to be influenced by the tidal hydrology (Wang et al., 2007), though such a direct correlation was only observed at one of our sample sites, possibly due to their relatively high elevation within the tidal frame. Increased groundwater levels at eroding site ER1 corresponded to higher soil temperature and thus a smaller difference in soil temperature between sites (ER1 to PR5). This relationship between soil temperature difference and groundwater level was again very time-dependent and only true for the measurement period until the end of December 2021 but does not hold true from January 2022 until March 2022. Our cross-season monitoring did highlight seasonal variability of tides on groundwater saturation yet might need to be expanded to longer periods to fully assess interdependencies and lag effects (e.g., of winter saturation) over time. The fact that soil moisture dampens any change in soil temperature through groundwater due to higher

heat capacity of water in comparison to soil (Seybold et al., 2002), complicates our observations.

We did however show that lower groundwater levels together with higher soil temperature resulted in higher soil respiration rates. This is in agreement with findings by Cui et al., (2021) from coastal wetlands in China, where the temperature sensitivity value of soil respiration differed between wetlands with varying groundwater levels. This variable effect of soil moisture has also been found in other ecosystems (i.e., temperate croplands, forests; tropical rainforests), where the temperature sensitivity of soil respiration changed with moisture level, depending on ecosystem type (Goodrick et al., 2016; Meyer et al., 2018).

Our study thus evidenced that geomorphic form of intertidal marshes, corresponding with differing groundwater levels and soil temperature, indirectly affects carbon fluxes.

The soil properties, in particular soil carbon percentages (OC and IC) are not the deciding factors impacting differences in soil-atmosphere CO_2 emissions between geomorphic conditions. Organic carbon percentages were significantly different between sites of prograding conditions and the inorganic carbon percentage shows no significant difference between sites. Both can thus be regarded as minor importance on the emission of CO_2. Our carbon stable isotope analyses further corroborates the potential importance of assessing lability of carbon as this can refer to carbon origin as well as decomposition status (Lamb et al., 2007). Greater $\delta^{13}C_{org}$ values indicate marine carbon input, particularly evident within the study area at prograding sites PR5 and PR7 (Xia et al., 2021). On the other hand, $\delta^{13}C_{org}$ values are also increasing with decomposition status and age of the carbon pool. Difference in sediment characteristics, such as grain size, carbon concentration and carbon stable isotope ratios will indirectly impact resistance to surface or lateral erosion (Brooks et al., 2021; Lo et al., 2017) and should be further investigated in this context.

2.4.3 Limitations and considerations

Our study site is a minerogenic salt marsh and soil to atmosphere emissions of CO_2 might differ to biogenic marshes or mangroves (Balke and Friess, 2016). However, biogenic marshes also experience cliff formation and undercutting leading to exposure of the deeper soil layers with lateral erosion. Furthermore, not every aspect of soil biology has been assessed, the relationship between soil temperature and soil microbial activity has been inferred based on previous studies (Cui et al., 2021). Although our study is limited in comparing eroding and prograding conditions at a single site, our results are within the range of published carbon stocks and CO_2 emissions (Mason et al., 2022). Experimental excavation

of marsh cliff edges could yield further mechanistic insight beyond our study describing natural geomorphic conditions.

2.4.4 Future implications for Blue Carbon

In view of accelerated sea level rise (Fagherazzi et al., 2020), increased storminess (Pannozzo et al., 2023), and the restriction of riverine sediment input to the coastal system (Fagherazzi et al., 2013), there is a clear need to better quantify the effects that coastal erosion will have on wetland carbon storage in the future. Our study showed that salt marsh edge erosion is not only impacting the direct erosion of soil carbon stock (Coverdale et al., 2014; Lovelock et al., 2017b; McTigue et al., 2021) but also the emission of CO_2 to the atmosphere by changes to the geomorphic form/topography of the system. Salt marshes with a seaward scarp (whether still eroding or currently stable) provide lower carbon sequestration potential compared to marshes with a gradual transition to the mudflat. This has important implications for management and highlights that protecting marshes from further lateral erosion using breakwaters or coir rolls will not stop the continued loss of carbon from marsh soils where a cliff has already formed. Salt marsh conservation and restoration does need to start before marshes are subject to erosion and cliff formation by ensuring the continued supply of sediment to the coastline. Studies to assess future carbon storage and emissions at eroding intertidal wetland edges, particularly marshes and mangroves, should include future wetland width along the coast (Braun et al., 2019; Theuerkauf et al., 2015), rates of erosion (Braun et al., 2019; Coverdale et al., 2014; Pendleton et al., 2012) and the changes to marsh topography and groundwater levels (this study).

2.5 Conclusions

Our study demonstrated that within a single marsh area, geomorphic form (i.e., sloped vs. cliffed) resulting from geomorphic process (i.e., progradation vs. lateral erosion) affects soil conditions and hence soil to atmosphere carbon fluxes. Cliffed-eroding sites showed a significantly higher CO_2 efflux from the soil compared to sloped-prograding marsh edges. This should be understood as additional loss of carbon to the active loss of organic matter removal due to erosion. Enhanced soil to air carbon flux was predominantly driven by differing groundwater levels and soil temperature. This could potentially improve our ability to accurately assess the carbon storage potential of geomorphologically active salt marshes due to topographic differences in addition to sediment flux due to erosion and deposition alone. This may have important implications for coastal management and shows that cliffed marsh edges increase soil carbon efflux even when erosion might have been halted. It is thus crucial that sediment supply is maintained, and anthropogenic disturbance and pollution are controlled to allow salt marshes to prograde where possible and to function as carbon sinks into the future.

Acknowledgments

Research was funded by the United Kingdom Research and Innovation Global Challenges Research Fund (Living Deltas Research Hub) (Grant No. NE/S008926/1). We would like to thank NatureScot for permitting work at Caerlaverock; and T. Prentice, K. Roberts, and Y. Zheng for field assistance.

Open Research

Data is available via University of Glasgow's Research Repository https://researchdata.gla.ac.uk/1377/

References

Alongi, D.M., 2020. Carbon Balance in Salt Marsh and Mangrove Ecosystems: A Global Synthesis. J. Mar. Sci. Eng. 8, 767. https://doi.org/10.3390/jmse8100767

Balke, T., Friess, D.A., 2016. Geomorphic knowledge for mangrove restoration: a pan-tropical categorization. Earth Surface Processes and Landforms 41, 231–239. https://doi.org/10.1002/esp.3841

Barbier, E.B., Hacker, S.D., Kennedy, C., Koch, E.W., Stier, A.C., Silliman, B.R., 2011. The value of estuarine and coastal ecosystem services. Ecological Monographs 81, 169–193. https://doi.org/10.1890/10-1510.1

Bass, A.M., Bird, M.I., Kay, G., Muirhead, B., 2016. Soil properties, greenhouse gas emissions and crop yield under compost, biochar and co-composted biochar in two tropical agronomic systems. Science of The Total Environment 550, 459–470. https://doi.org/10.1016/j.scitotenv.2016.01.143

Bates, D., Mächler, M., Bolker, B., Walker, S., 2015. Fitting Linear Mixed-Effects Models Using lme4. Journal of Statistical Software 67, 1–48. https://doi.org/10.18637/jss.v067.i01

Braun, K.N., Theuerkauf, E.J., Masterson, A.L., Curry, B.B., Horton, D.E., 2019. Modeling organic carbon loss from a rapidly eroding freshwater coastal wetland. Scientific Reports 9, 4204. https://doi.org/10.1038/s41598-019-40855-5

Brooks, H., Möller, I., Carr, S., Chirol, C., Christie, E., Evans, B., Spencer, K.L., Spencer, T., Royse, K., 2021. Resistance of salt marsh substrates to near-instantaneous hydrodynamic forcing. Earth Surf Processes Landf 46, 67–88. https://doi.org/10.1002/esp.4912

Bu, N.-S., Qu, J.-F., Li, G., Zhao, B., Zhang, R.-J., Fang, C.-M., 2015a. Reclamation of coastal salt marshes promoted carbon loss from previously-sequestered soil carbon pool. Ecological Engineering 81, 335–339. https://doi.org/10.1016/j.ecoleng.2015.04.051

Bu, N.-S., Qu, J.-F., Zhao, H., Yan, Q.-W., Zhao, B., Fan, J.-L., Fang, C.-M., Li, G., 2015b. Effects of semi-lunar tidal cycling on soil CO2 and CH4 emissions: a case study in the Yangtze River estuary, China. Wetlands Ecol Manage 23, 727–736. https://doi.org/10.1007/s11273-015-9415-5

Cai, W.-J., 2011. Estuarine and Coastal Ocean Carbon Paradox: CO2 Sinks or Sites of Terrestrial Carbon Incineration? Annu. Rev. Mar. Sci. 3, 123–145. https://doi.org/10.1146/annurev-marine-120709-142723

Campbell, A.D., Fatoyinbo, L., Goldberg, L., Lagomasino, D., 2022. Global hotspots of salt marsh change and carbon emissions. Nature 1–6. https://doi.org/10.1038/s41586-022-05355-z

Cao, L., Zhou, Z., Xu, X., Shi, F., 2020. Spatial and temporal variations of the greenhouse gas emissions in coastal saline wetlands in southeastern China. Environ Sci Pollut Res 27, 1118–1130. https://doi.org/10.1007/s11356-019-06951-9

Clyne, F.J., Garrod, C.J., Tipple, J.R., Jeffs, T.M., 2007. Radiological Habits Survey: Dumfries and Galloway Coast (Environment Report No. Final report RL 08/11).

Coupé, C., 2018. Modeling Linguistic Variables With Regression Models: Addressing Non-Gaussian Distributions, Non-independent Observations, and Non-linear Predictors With Random Effects and Generalized Additive Models for Location, Scale, and Shape. Front. Psychol. 9, 513. https://doi.org/10.3389/fpsyg.2018.00513

Coverdale, T.C., Brisson, C.P., Young, E.W., Yin, S.F., Donnelly, J.P., Bertness, M.D., 2014. Indirect Human Impacts Reverse Centuries of Carbon Sequestration and Salt Marsh Accretion. PLOS ONE 9, e93296. https://doi.org/10.1371/journal.pone.0093296

Cui, H., Bai, J., Du, S., Wang, J., Keculah, G.N., Wang, W., Zhang, G., Jia, J., 2021. Interactive effects of groundwater level and salinity on soil respiration in coastal wetlands of a Chinese delta. Environmental Pollution 286, 117400. https://doi.org/10.1016/j.envpol.2021.117400

Cutts, N., Hemingway, K., 1996. The Solway Firth - broad scale habitat mapping (Scottish Natural Heritage Research, Survey and Monitoring Report No. 46).

EDINA Aerial Digimap Service, 2018.

EDINA Aerial Digimap Service, 2014.

Fagherazzi, S., Mariotti, G., Leonardi, N., Canestrelli, A., Nardin, W., Kearney, W.S., 2020. Salt Marsh Dynamics in a Period of Accelerated Sea Level Rise. JGR Earth Surface 125. https://doi.org/10.1029/2019JF005200

Fagherazzi, S., Mariotti, G., Wiberg, P., McGlathery, K., 2013. Marsh Collapse Does Not Require Sea Level Rise. oceanog 26, 70–77. https://doi.org/10.5670/oceanog.2013.47

Ford, H., Garbutt, A., Ladd, C., Malarkey, J., Skov, M.W., 2016. Soil stabilization linked to plant diversity and environmental context in coastal wetlands. J Veg Sci 27, 259–268. https://doi.org/10.1111/jvs.12367

Goodrick, I., Connor, S., Bird, M.I., Nelson, P.N., Goodrick, I., Connor, S., Bird, M.I., Nelson, P.N., 2016. Emission of CO2 from tropical riparian forest soil is controlled

by soil temperature, soil water content and depth to water table. Soil Res. 54, 311–320. https://doi.org/10.1071/SR15040

Gray, A.B., Pasternack, G.B., Watson, E.B., 2010. Hydrogen peroxide treatment effects on the particle size distribution of alluvial and marsh sediments. The Holocene 20, 293–301. https://doi.org/10.1177/0959683609350390

Greenberg, R., Cardoni, A., Ens, B.J., Gan, X., Isacch, J.P., Koffijberg, K., Loyn, R., 2014. The distribution and conservation of birds of coastal salt marshes. Coastal conservation 19, 180.

Hartig, F., Lohse, L., 2022. DHARMa: Residual Diagnostics for Hierarchical (Multi-Level / Mixed) Regression Models.

Hill, T., 2021. troyhill/VulnToolkit: Littoral. https://doi.org/10.5281/ZENODO.4598510

Himmelstoss, E.A., Farris, A.S., Henderson, R.E., Kratzmann, M.G., Ergul Ayhan Zhang Ouya, J.L., Thieler, E.R., 2018. Digital Shoreline Analysis System (DSAS).

Kutzbach, L., Schneider, J., Sachs, T., Giebels, M., Nykanen, H., Shurpali, N.J., Martikainen, P.J., Alm, J., Wilmking, M., 2007. CO2 flux determination by closed-chamber methods can be seriously biased by inappropriate application of linear regression 21.

Lamb, A.L., Vane, C.H., Wilson, G.P., Rees, J.G., Moss-Hayes, V.L., 2007. Assessing δ13C and C/N ratios from organic material in archived cores as Holocene sea level and palaeoenvironmental indicators in the Humber Estuary, UK. Marine Geology 244, 109–128. https://doi.org/10.1016/j.margeo.2007.06.012

Lo, V.B., Bouma, T.J., van Belzen, J., Van Colen, C., Airoldi, L., 2017. Interactive effects of vegetation and sediment properties on erosion of salt marshes in the Northern Adriatic Sea. Marine Environmental Research 131, 32–42. https://doi.org/10.1016/j.marenvres.2017.09.006

Lovelock, C.E., Atwood, T., Baldock, J., Duarte, C.M., Hickey, S., Lavery, P.S., Masque, P., Macreadie, P.I., Ricart, A.M., Serrano, O., Steven, A., 2017a. Assessing the risk of carbon dioxide emissions from blue carbon ecosystems. Frontiers in Ecology and the Environment 15, 257–265. https://doi.org/10.1002/fee.1491

Lovelock, C.E., Fourqurean, J.W., Morris, J.T., 2017b. Modeled CO2 Emissions from Coastal Wetland Transitions to Other Land Uses: Tidal Marshes, Mangrove Forests, and Seagrass Beds. Frontiers in Marine Science 4.

Magenheimer, J.F., Moore, T.R., Chmura, G.L., Daoust, R.J., 1996. Methane and carbon dioxide flux from a macrotidal salt marsh, Bay of Fundy, New Brunswick. Estuaries 19, 139–145. https://doi.org/10.2307/1352658

Mason, V.G., Wood, K.A., Jupe, L.L., Burden, A., Skov, M.W., 2022. Saltmarsh Blue Carbon in UK and NW Europe - evidence synthesis for a UK Saltmarsh Carbon Code (No. NEIRF1072). UK Centre for Ecology & Hydrology.

Mcleod, E., Chmura, G.L., Bouillon, S., Salm, R., Björk, M., Duarte, C.M., Lovelock, C.E., Schlesinger, W.H., Silliman, B.R., 2011. A blueprint for blue carbon: toward an improved understanding of the role of vegetated coastal habitats in sequestering CO2. Frontiers in Ecology and the Environment 9, 552–560. https://doi.org/10.1890/110004

McTigue, N.D., Walker, Q.A., Currin, C.A., 2021. Refining Estimates of Greenhouse Gas Emissions From Salt Marsh "Blue Carbon" Erosion and Decomposition. Frontiers in Marine Science 8.

Meyer, N., Welp, G., Amelung, W., 2018. The Temperature Sensitivity (Q10) of Soil Respiration: Controlling Factors and Spatial Prediction at Regional Scale Based on Environmental Soil Classes. Global Biogeochemical Cycles 32, 306–323. https://doi.org/10.1002/2017GB005644

Mobilian, C., Craft, C.B., 2021. Wetland Soils: Physical and Chemical Properties and Biogeochemical Processes, in: Reference Module in Earth Systems and Environmental Sciences. Elsevier. https://doi.org/10.1016/B978-0-12-819166-8.00049-9

Möller, I., Kudella, M., Rupprecht, F., Spencer, T., Paul, M., van Wesenbeeck, B.K., Wolters, G., Jensen, K., Bouma, T.J., Miranda-Lange, M., Schimmels, S., 2014. Wave attenuation over coastal salt marshes under storm surge conditions. Nature Geosci 7, 727–731. https://doi.org/10.1038/ngeo2251

Mueller, P., Kutzbach, L., Mozdzer, T.J., Jespersen, E., Barber, D.C., Eller, F., 2023. Minerogenic salt marshes can function as important inorganic carbon stores. Limnology & Oceanography 68, 942–952. https://doi.org/10.1002/lno.12322

Pannozzo, N., Leonardi, N., Carnacina, I., Smedley, R.K., 2023. Storm sediment contribution to salt marsh accretion and expansion. Geomorphology 430, 108670. https://doi.org/10.1016/j.geomorph.2023.108670

Pendleton, L., Donato, D.C., Murray, B.C., Crooks, S., Jenkins, W.A., Sifleet, S., Craft, C., Fourqurean, J.W., Kauffman, J.B., Marbà, N., Megonigal, P., Pidgeon, E., Herr, D., Gordon, D., Baldera, A., 2012. Estimating Global "Blue Carbon" Emissions from Conversion and Degradation of Vegetated Coastal Ecosystems. PLoS ONE 7, e43542. https://doi.org/10.1371/journal.pone.0043542

Picarro, 2019. δ13C for Carbon Dioxide (CO2) CM-CRDS System.

Seybold, C.A., Mersie, W., Huang, J., McNamee, C., 2002. SOIL REDOX, pH, TEMPERATURE, AND WATER-TABLE PATTERNS OF A FRESHWATER TIDAL WETLAND. wetl 22, 149–158. https://doi.org/10.1672/0277-5212(2002)022[0149:SRPTAW]2.0.CO;2

Seyfferth, A.L., Bothfeld, F., Vargas, R., Stuckey, J.W., Wang, J., Kearns, K., Michael, H.A., Guimond, J., Yu, X., Sparks, D.L., 2020. Spatial and temporal heterogeneity of geochemical controls on carbon cycling in a tidal salt marsh. Geochimica et Cosmochimica Acta 282, 1–18. https://doi.org/10.1016/j.gca.2020.05.013

Sghair, F.G.A., 2013. Remote Sensing and GIS for Wetland Vegetation Study. University of Glasgow.

Theuerkauf, E.J., Stephens, J.D., Ridge, J.T., Fodrie, F.J., Rodriguez, A.B., 2015. Carbon export from fringing saltmarsh shoreline erosion overwhelms carbon storage across a critical width threshold. Estuarine, Coastal and Shelf Science 164, 367–378. https://doi.org/10.1016/j.ecss.2015.08.001

Van Putte, N., Temmerman, S., Verreydt, G., Seuntjens, P., Maris, T., Heyndrickx, M., Boone, M., Joris, I., Meire, P., 2020. Groundwater dynamics in a restored tidal marsh are limited by historical soil compaction. Estuarine, Coastal and Shelf Science 244, 106101. https://doi.org/10.1016/j.ecss.2019.02.006

Wang, F., Sanders, C.J., Santos, I.R., Tang, J., Schuerch, M., Kirwan, M.L., Kopp, R.E., Zhu, K., Li, X., Yuan, J., Liu, W., Li, Z., 2021. Global blue carbon accumulation in tidal wetlands increases with climate change. National Science Review 8, nwaa296. https://doi.org/10.1093/nsr/nwaa296

Wang, H., Hsieh, Y.P., Harwell, M.A., Huang, W., 2007. Modeling soil salinity distribution along topographic gradients in tidal salt marshes in Atlantic and Gulf coastal regions. Ecological Modelling 201, 429–439. https://doi.org/10.1016/j.ecolmodel.2006.10.013

Wang, H., van der Wal, D., Li, X., van Belzen, J., Herman, P.M.J., Hu, Z., Ge, Z., Zhang, L., Bouma, T.J., 2017. Zooming in and out: Scale dependence of extrinsic and intrinsic factors affecting salt marsh erosion: Factors on Salt Marsh Edge Erosion. J. Geophys. Res. Earth Surf. 122, 1455–1470. https://doi.org/10.1002/2016JF004193

Worm, B., Barbier, E.B., Beaumont, N., Duffy, J.E., Folke, C., Halpern, B.S., Jackson, J.B.C., Lotze, H.K., Micheli, F., Palumbi, S.R., Sala, E., Selkoe, K.A., Stachowicz, J.J., Watson, R., 2006. Impacts of Biodiversity Loss on Ocean Ecosystem Services. Science 314, 787–790. https://doi.org/10.1126/science.1132294

Xia, S., Song, Z., Li, Q., Guo, L., Yu, C., Singh, B.P., Fu, X., Chen, C., Wang, Y., Wang, H., 2021. Distribution, sources, and decomposition of soil organic matter along a salinity gradient in estuarine wetlands characterized by C:N ratio, δ13C-δ15N, and lignin biomarker. Global Change Biology 27, 417–434. https://doi.org/10.1111/gcb.15403

Zeileis, A., Grothendieck, G., Ryan, J.A., Ulrich, J.M., Andrews, F., 2023. zoo: S3 Infrastructure for Regular and Irregular Time Series (Z's Ordered Observations).

Zuur, A.F., Ieno, E.N., Walker, N., Saveliev, A.A., Smith, G.M., 2009. Mixed effects models and extensions in ecology with R, Statistics for Biology and Health. Springer New York, New York, NY. https://doi.org/10.1007/978-0-387-87458-6

3 Interactive Effects of Groundwater Level and Tidal Current Velocity Influence Salt Marsh Soil Temperature

The following chapter is a reformatted version of a manuscript submitted to the Journal of: Limnology & Oceanography by Stolpmann, L.M., Ladd, C.J.T., Balke, T. & Bass, A.M.

Abstract

Salt marshes are globally recognized as carbon storage hotspots. Microbial decomposition of labile organic carbon is regulated by soil temperature. Yet, the role of morphological, atmospheric, and tidal hydrology in moderating saltmarsh soil temperatures, and hence carbon decomposition rates, has been hitherto overlooked. We examined the influence of groundwater level (determined by rainfall, tidal inundation, and hydrostatic pressure), tidal currents, and wave forcing on soil temperatures at eroding and expanding salt marsh edges continuously for 9 months. High groundwater levels cooled soils in summer whereas warmed them in winter. When groundwater levels were high, higher current velocities lowered soil temperatures irrespective of the season. Higher levels of groundwater are further insulating the soil from evaporation. We attribute this to greater seawater circulation within the soil, increasing heat transfer between seawater, groundwater, and soil. Hydrodynamic effects on soil temperature did not vary between sloping and cliffed salt marsh edges. Soil temperatures followed air surface temperatures when groundwater levels were low. Accounting for groundwater level and tidal current velocity effects on soil temperature is especially important when considering the carbon storage capacity of salt marshes.

Plain Language Summary

Salt marshes are at the intersection of the coastal and terrestrial environment and are ecosystems that store large amounts of carbon within their soil. The amount of carbon stored is impacted by the loss of carbon through temperature dependent respiration (i.e., CO_2 degassing). However the relationship hydrological processes have on the soil temperature is not clear. We determined the impact of tidal current velocity and groundwater level on soil temperature over two contrasting seasons (summer vs winter). We find that the influence groundwater level has on soil temperature is season dependent. Higher levels are cooling the soils in summer, whereas warming them in winter. However when tidal current velocities are high, the soils were cooled, irrespective of the season, attributed to the circulation of seawater within the soil and greater potential of heat transfer. These findings are important to include in calculations for salt marsh carbon budgets.

3.1 Introduction

Salt marshes play an important role in climate regulation by sequestering and storing large amounts of organic carbon below the ground (Mcleod et al., 2011). Across Great Britain, salt marshes are found to store on average 11.55 ± 1.56 kg C m^{-2} (Smeaton et al., 2023). The role of marshes as carbon sequesters is under threat from drivers such as climate change, land reclamation, and sea level rise (SLR; Fagherazzi et al., 2020). Globally, salt marsh habitat is being lost at a rate of 0.28% per year (Campbell et al., 2022). The loss of habitat equates to direct losses in sequestered carbon (Macreadie et al., 2013) and may indirectly affect carbon stocks by altering the morphology and hydrodynamics of salt marshes (Zhao et al., 2017). The latter effects on carbon flux have been poorly studied to date. Identifying the controls of carbon stock gains and losses is key in understanding the climate regulation role of salt marshes.

Soil temperature is key in regulating saltmarsh carbon cycling (Kirwan et al., 2014; Schutte et al., 2020). Higher soil temperatures drive microbially-mediated organic matter decomposition (Tang et al., 2023), resulting in higher CO_2 emissions (Cui et al., 2021; Kirwan et al., 2014). Soil temperature in salt marshes is influenced by temperature differences associated with air, tidal and groundwater sources (Moffett et al., 2008; Xin et al., 2023).

Sediment-atmosphere exchange of heat, water vapour, and CO_2 is influenced by tidal inundation (Moffett et al., 2010). Seawater infiltrates coastal aquifers through the upper intertidal zone during the rising tide and exfiltrates through the lower intertidal zone with the falling tide (Kuan et al., 2019). The extent of the seawater recirculation below-ground is determined in part by the onshore pressure produced by wave forcing (Santos et al., 2012; Xin et al., 2010). Groundwater level is therefore determined by differential infiltration and exfiltration rates of seawater during flood and ebb tides (i.e., wave set-up). Higher time-averaged onshore groundwater tables are reached from faster seawater infiltration during flood tides compared to exfiltration during ebb tides. Seawater circulation within the aquifer leads to 1) density-driven circulation; and 2) tide-induced circulation (Kuan et al., 2019). The tide-induced circulation depends on pressure gradients, where higher tidal current velocities and wave orbital velocities exert a greater pressure on the aquifer, inducing a greater circulation of seawater (Kuan et al., 2019; Yu et al., 2022). When lower groundwater levels coincide with higher soil temperatures, the CO_2 emissions are expected to increase (Schultz et al., 2023; Stolpmann et al., under review).

The connection between hydrological influences (porewater exchange and submarine groundwater discharge) on soil temperature and potential differences between geomorphic

conditions have been proposed in relation to carbon budgets (Guimond and Tamborski, 2021). Yet, seasonal variation in the interaction between meteorological, geomorphic, and hydrological drivers on salt marsh soil temperature has hitherto been overlooked.

We hypothesise that (i) soil temperature is influenced by groundwater temperature and level; (ii) eroding sites have a lower groundwater level and thus a greater influence of other factors, mainly air temperature; (iii) during summer groundwater level will have a cooling effect and temperature changes are not as strong, whereas during winter the groundwater will have an insulating effect, keeping the soil at higher temperatures; (iv) Groundwater levels are influenced by tidal hydrodynamic factors (current and wave orbital velocity). With stronger tidal currents, the groundwater levels are rising faster.

3.2 Materials and Methods

3.2.1 Study site

The study was conducted at the Caerlaverock salt marsh in the Solway Firth, Scotland, UK (Fig. 1). The salt marsh is situated in a meso-tidal setting, experiencing alternating spring and neap tides (Cutts and Hemingway, 1996). Caerlaverock has an extent of 8 km from east to west (Clyne et al., 2007). The salt marsh has experienced erosion in the west and accretion in the east over the last century (Hansom, 2003). With south-west of Caerlaverock Castle the erosion rate has been calculated as 38.1 m yr-1 (Hansom, 2003). The grain size of the study location study site is characterised as sandy loam, i.e., between 53.6 and 70.9 % sand and 25.6 and 41.7 % silt (Stolpmann et al., under review).

3.2.2 Field measurements

Measurements were performed from June 2021 to March 2022. Four groundwater wells were deployed along the seaward salt marsh edge: two (ER1, ER3) at eroding edges, and two (PR5, PR7) at prograding edges (Table 1). Erosion/progradation rate was determined using linear regression of cross shore lateral marsh change (Stolpmann et al., under review). The groundwater wells were 1m deep and positioned 3 m from the seaward edge. A pressure data logger (Rugged TROLL 100) was installed inside of the groundwater well at 1m depth, to measure water level and temperature every 10 minutes. Soil temperature was measured with a temperature logger (HOBO Pendant® MX Water Temperature Data Logger, MX2201) adjacent to the groundwater wells at a soil depth of 10 cm. Temperature was logged every

15 minutes. Mini buoys (i.e., acceleration sensors inside bottom mounted floats; Balke et al., 2021, Ladd et al., 2024) were deployed on the tidal flat 2-3 m from the marsh edge in front of the groundwater well sites to record intertidal hydrodynamics. Current and wave orbital velocities were extracted for 1 minute time steps from 1Hz acceleration data (Ladd et al., 2024).

Groundwater levels and tidal hydrodynamics were subsequently averaged over 15 minutes to compare with soil temperature readings.

Table 3.1 Study site characteristics.

Site	Marsh Surface Elevation (m OD)	Mini Buoy Elevation (m OD)	Latitude (°)	Longitude (°)
ER1	4.495	3.564	54.967452	-3.525752
ER3	4.549	3.375	54.969085	-3.534593
PR5	4.62	4.186	54.965221	-3.509359
PR7	4.123	3.919	54.962923	-3.504087

Figure 3.1 Study area within the Caerlaverock salt marsh, red triangles marking eroding and blue circles marking prograding sites. Inset showing location of study area in the UK (black circle).

3.2.3 Data collation

Sea-surface temperature (SST) was extracted from satellite data with 1/36 degrees horizontal resolution representing the study area (approx. 2km offshore at 54.94595, -3.51515; Copernicus Marine Service Information (CMEMS), 2019), available in daily intervals. Air temperature data was taken from Met Office, with hourly measurement from station 1023 Eskdalemuir (55.31184, -3.20545; Met Office, 2006). The station was selected based on availability of air temperature throughout the period of the field measurements. Air temperature as well as SST were interpolated to the measurement frequency of 15 minutes.

3.2.4 Statistical analysis

Statistical analyses were performed in R (4.1.1). Linear Mixed Effect Models (LMEMs) were performed to test the influence of scaled hydrological variables on soil temperature. Spatial and temporal dependency was accounted for by selecting the random effects using the AIC score and p-value (Zuur et al., 2009). Site (i.e., ID) was set as random intercept. Highly correlated variables (VIF > 3) were removed from the analyses (Zuur et al., 2010). The model was performed on data from periods during full inundation (as detected by the groundwater logger) and filtered for the months of August and February. These months were selected to represent soil temperature differences between summer and winter. Two LMEMs were performed to test 1) all locations and 2) expanding and eroding marsh edges separately on the overall interaction of groundwater level, current velocity, and season on soil temperature. Model variables were dropped from the full model using an iterative approach, where variables were removed based on the AIC score and p-value (Zuur et al., 2009). Predicted model results of soil temperature were descaled to make visual interpretation easier.

Cross-correlation analyses were conducted to determine relationship between variables excluded from the LMEMs and soil temperature for both August and February. Data was further divided into rising and falling tides and 20 cm increments in groundwater level (i.e., -1m to 0.8m, -0.8 to -0.6m, and so on).

Differences in mean temperature (air, groundwater, soil, and SST) during August and February were examined using a Kruskal-Wallis rank sum test appropriate for non-parametric data.

3.3 Results

3.3.1 Relationship between hydrodynamics and temperature

Throughout August, soil and air temperature showed a sinusoidal relationship with maxima during the day and minima during the night (), with soil temperature being consistently ~3.96°C greater than air temperature. A difference in soil temperature minima and maxima can further be seen during spring tides between sites (). Soil temperature between sites showed slightly greater maxima at site PR5 (10th August 2021) in comparison to the other sites (). No data was available for site PR7 for August 2021. Sea surface temperature remained stable, with slight decreases later in the month. Sea surface temperatures were ~2.38°C higher than groundwater temperatures. Groundwater temperature remained stable, at temperatures between those measured in the air and soil. Groundwater level showed a semi-diurnal tidal signal with clear neap and spring tidal cycles. Groundwater levels showed a similar pattern between sites, with levels at site PR5 decreasing at a slower rate during low tide in comparison to sites ER1 and ER3. Air, soil, groundwater, and sea surface temperatures were significantly different from each other during August ($H(3) = 18718$; p-value < 0.0001;).

Throughout February, no diurnal pattern of soil and air temperature changes were evident (). Air temperature over this period showed high standard deviation (). Soil temperature was greater than air temperature and SST by ~1.24°C and 0.91°C, respectively. Groundwater temperatures were higher still, reaching temperatures of 6.25°C. Groundwater levels exhibited semi-diurnal tides and spring-neap cycles, which were less evident for site PR5 (). Temperature differences between air, soil, groundwater, and sea surface was significant during February ($H(3) = 8524.4$; p-value < 0.0001;).

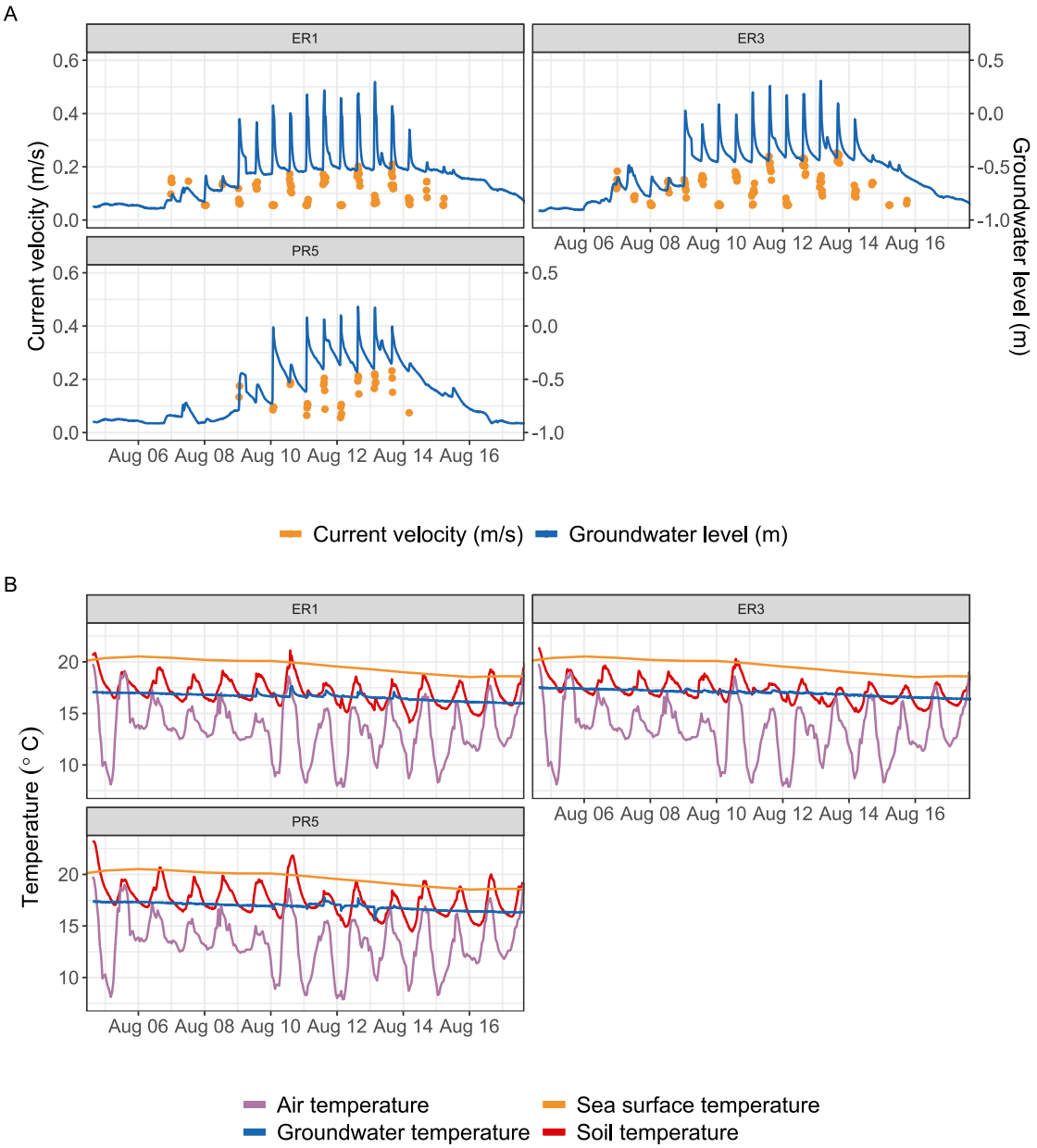

Figure 3.2 A: current velocity (yellow) and groundwater level (blue) for August 2021 study period; B: soil temperature (red) and groundwater temperature (blue) change over time per site throughout August. Air temperature (purple) and sea surface temperature (yellow) are shown for entire coastline and region.

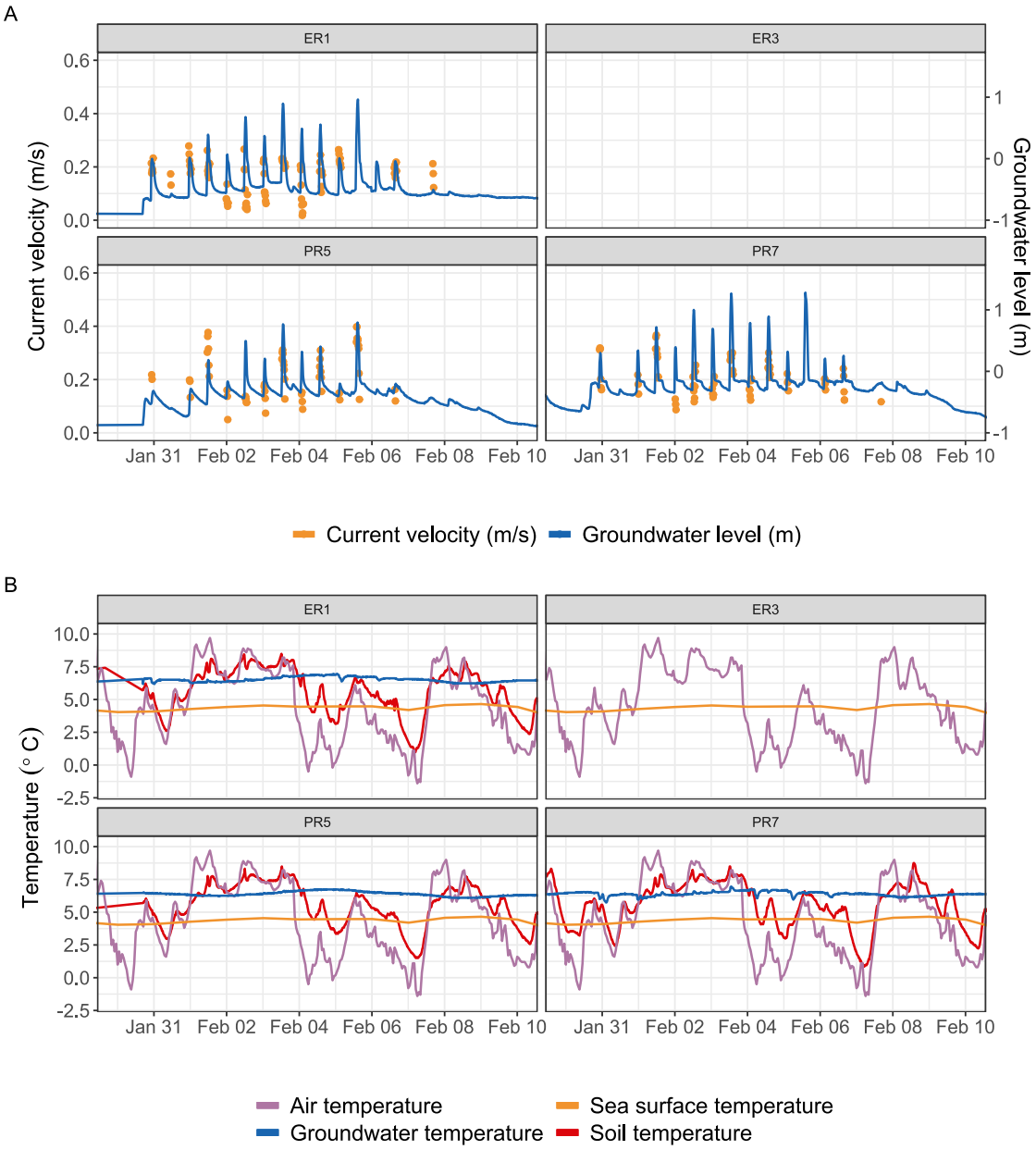

Figure 3.3 A: current velocity (blue) and groundwater level (yellow) for February 2022 study period; B: soil temperature (red) and groundwater temperature (blue) change over time per site. Air temperature (purple) and sea surface temperature (yellow) are shown for entire coastline and region.

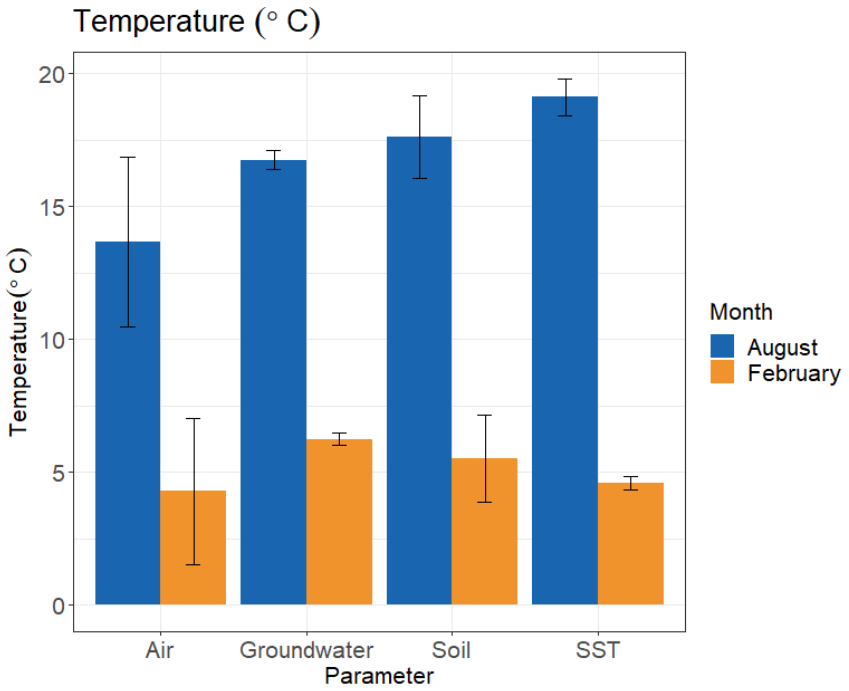

Figure 3.4 Air, groundwater, soil and sea-surface temperature for August 2021 and February 2022 (Mean ± standard deviation).

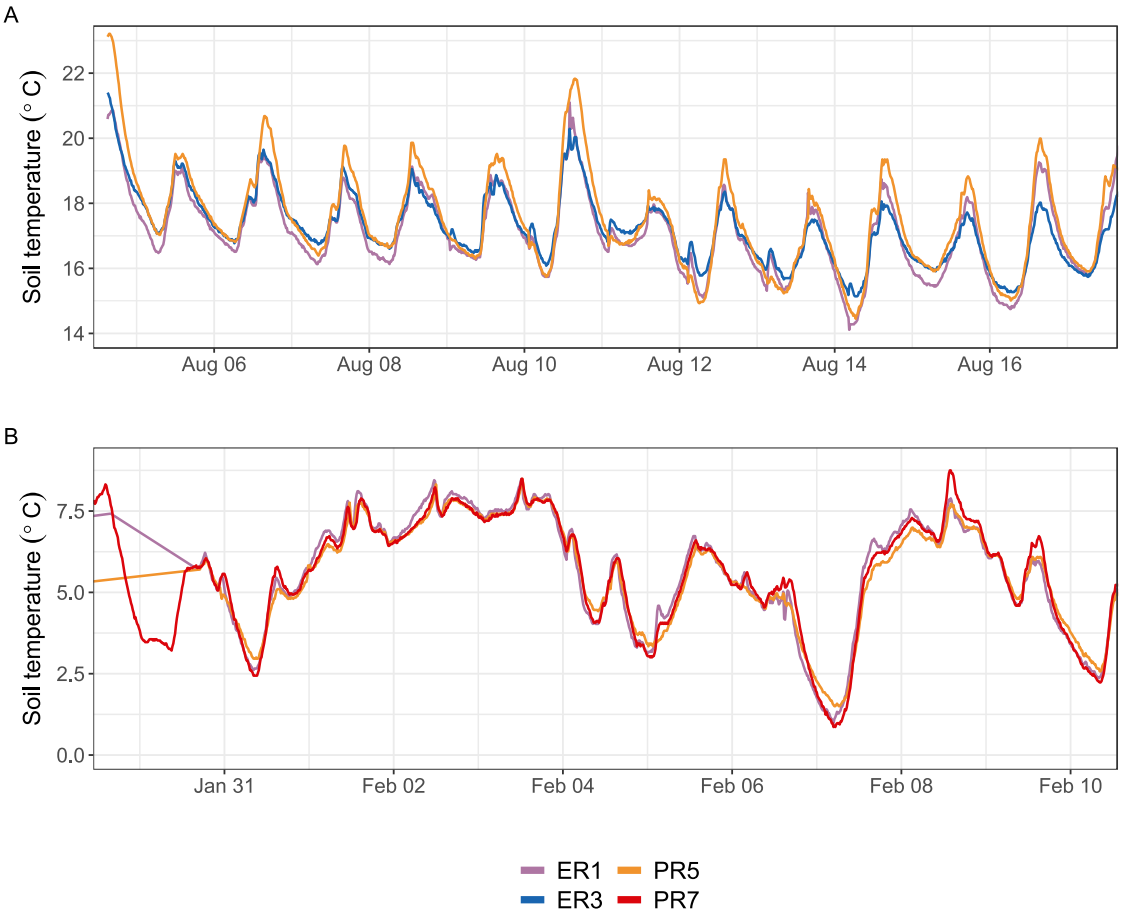

Figure 3.5 Soil temperature (°C) between eroding (ER1, ER3) and prograding (PR5, PR7) sites for August 2021 (A) and February 2022 (B).

3.3.2 Influence of hydrodynamics on soil temperature

Cross-correlation between variables excluded from the Linear Mixed Effects model to avoid collinearity (Zuur et al., 2010), revealed that the highest correlation to soil temperature was from air temperature during August, for falling, rising, and combined tidal cycles (ccf = 0.71, 0.66, 0.7, respectively). During February air temperature also had the largest cross-correlation for falling and rising tides (ccf = 0.87, 0.90), but for the overall tidal cycle it was groundwater temperature (ccf = 0.09).

Table 3.2 Cross correlation between temperature (air and groundwater) and soil temperature for August 2021 and February 2022.

Tidal cycle	Groundwater level (m)	Variables	Ccf at lag = 0 (August)	Ccf at lag = 0 (February)
Rising & Falling tide	Overall	Air – Soil	0.699	0.016 (not sig.)
Rising & Falling tide	Overall	Ground – Soil	0.162	0.09
Rising tide only	Overall	Air – Soil	0.659	0.904
Falling tide only	Overall	Air – Soil	0.711	0.865

With increasing groundwater levels, the influence of air temperature on soil temperature reduced from a maximum at -0.4 to -0.2m (ccf = 0.903) to a correlation coefficient of 0.658 at 0 to 0.2m. The groundwater temperature to soil temperature correlation coefficient increased during the increase in groundwater level from 0.259 at -1m to -0.8m to 0.502 at -0.2 to 0m. Throughout February, the correlation between air temperature to soil temperature remained high during high groundwater levels. The correlation between groundwater temperature and soil temperature reduced to non-significant levels after approximately 5 hours (lag = 20).

Groundwater temperature is significantly cross correlated with soil temperature and vice versa (Figure 3.6). The highest cross-correlation between groundwater temperature and soil temperature during August is reached at positive lags, i.e., soil temperature had a greater cross-correlation with groundwater temperature than the other way around. During February, the reverse was observed – groundwater temperature led soil temperature (i.e., groundwater temperature had a greater cross-correlation with soil temperature).

Air temperature and soil temperature showed high cross-correlation depending on the month (Figure 3.6). Throughout August, the highest cross-correlation was two hours (lag = -8)

where soil temperature was lagging air temperature. Throughout February, significant cross-correlation coefficients were at positive lags, indicating that soil temperature was leading air temperature.

Sea-surface temperature is significantly cross correlated with soil temperature and vice versa (Figure 3.7). The highest cross-correlation between sea-surface temperature and soil temperature during August is reached at positive lags, i.e., soil temperature had a greater cross-correlation with sea-surface temperature than the other way around. During February, the reverse was observed – sea-surface temperature led soil temperature (i.e., sea-surface temperature had a greater cross-correlation with soil temperature).

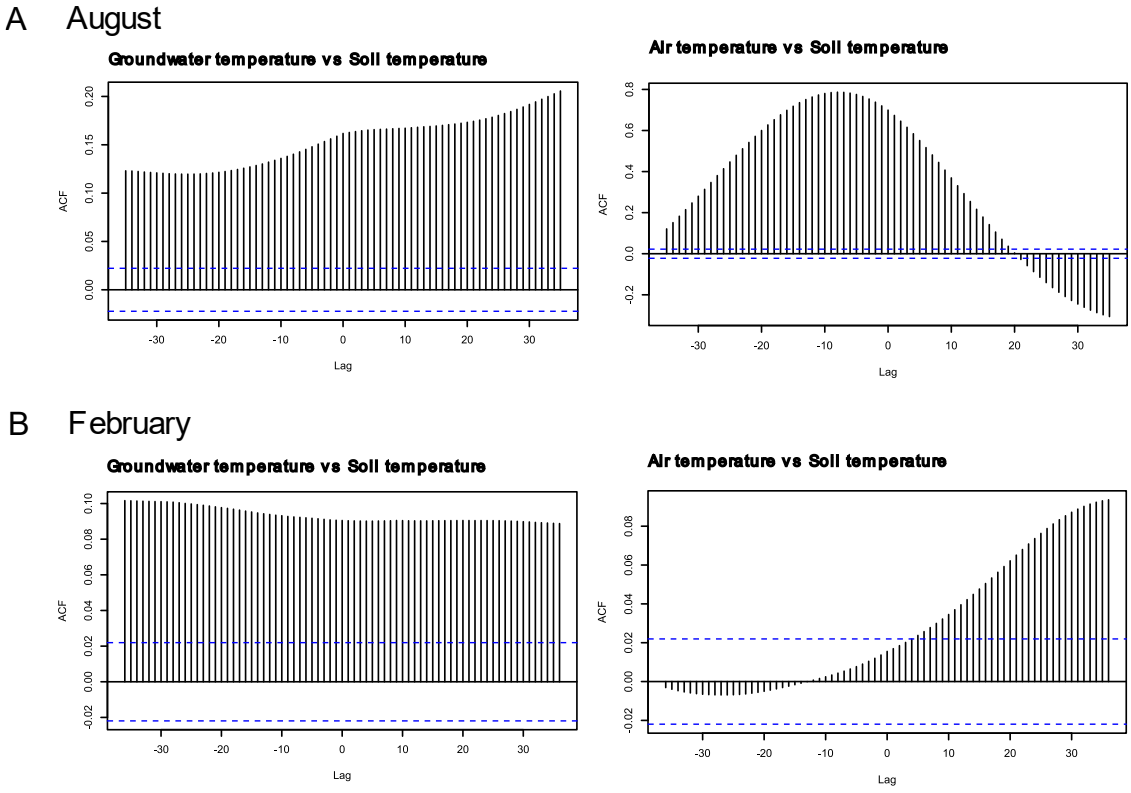

Figure 3.6 Cross correlations for August 2021 (A) and February 2022 (B) between groundwater and soil temperature, and between air and soil temperature. ACF = Autocorrelation function between variables; blue dotted line represents the confidence interval.

A August

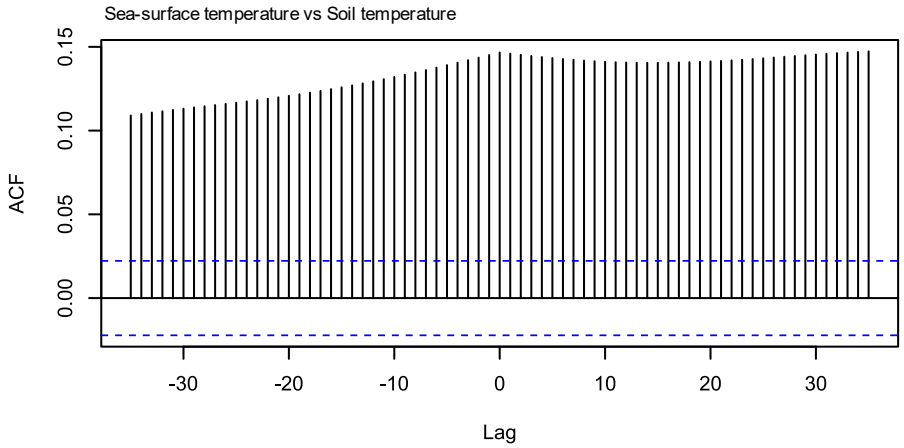

B February

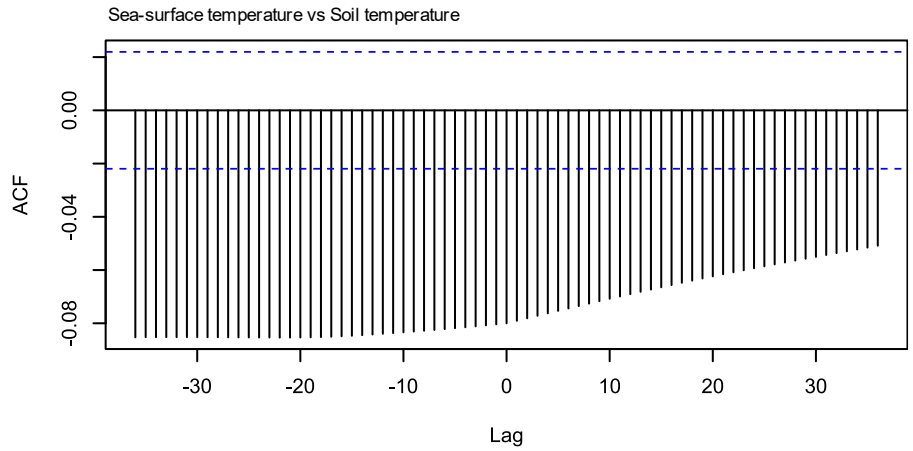

Figure 3.7 Cross correlations for August 2021 (A) and February 2022 (B) between sea-surface and soil temperature. ACF = Autocorrelation function between variables; blue dotted line represents the confidence interval.

3.3.3 Hydrodynamic influence on soil temperature

Soil temperature was significantly influenced by the interaction between groundwater level and tidal current velocity (Table 3.3; Figure 3.9). The effect of groundwater level on soil temperature was significantly different between August and February (Table 3.3). The three-way interaction between groundwater level, tidal current velocity and month was marginally insignificant (p-value = 0.08). Higher groundwater levels during August resulted in lower soil temperatures, whereas soil temperatures increased with increasing groundwater levels throughout February (Figure 3.8). Descaled soil temperatures showed a temperature difference of ~3.33℃ for changing groundwater levels from -0.9 m to 1 m during high tidal current velocities of 0.5 m s^{-1}.

Geomorphic condition was not a significant factor in influencing soil temperature during groundwater logger inundation periods and was excluded from the optimal LMEM.

Table 3.3 LMEM of variables influencing soil temperature with ID as random intercept. X denotes on interaction effect.

	Temperature		
Predictors	*Estimates*	*CI*	*p*
Groundwater level	-0.03	-0.05 – -0.01	**0.007**
Current velocity	0.05	0.02 – 0.09	**0.003**
Month (February)	-2.02	-2.09 – -1.95	**<0.001**
Groundwater level × Current velocity	-0.02	-0.04 – -0.01	**0.001**
Groundwater level × Month (February)	0.08	0.04 – 0.11	**<0.001**

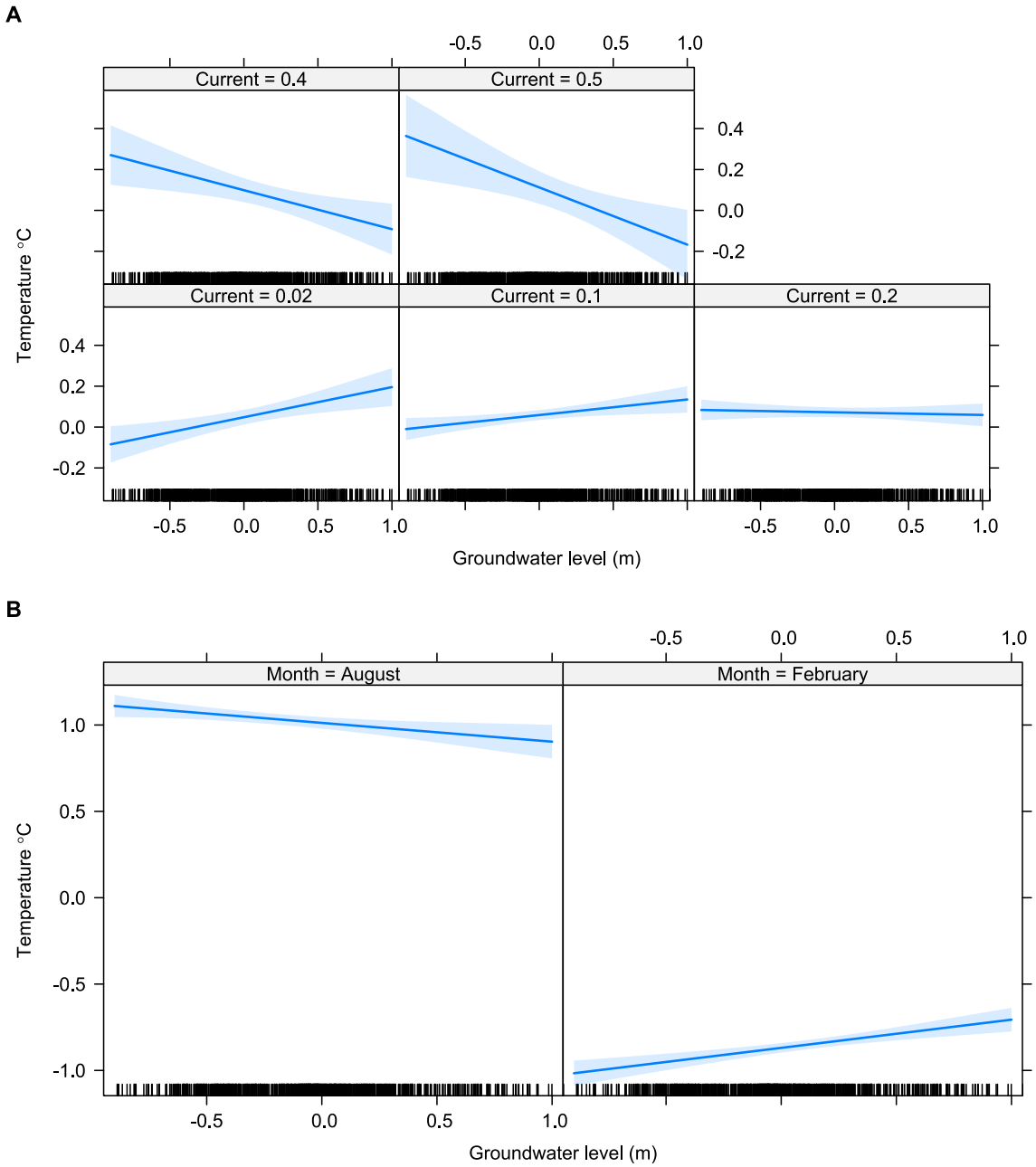

Figure 3.8 Linear Mixed Effects Model (LMEM) on soil temperature (°C) influence by hydrodynamic variables and months. A: Interaction between current velocity (m s^{-1}) and groundwater level (m); B: Interaction between month (August, February) and groundwater level (m).

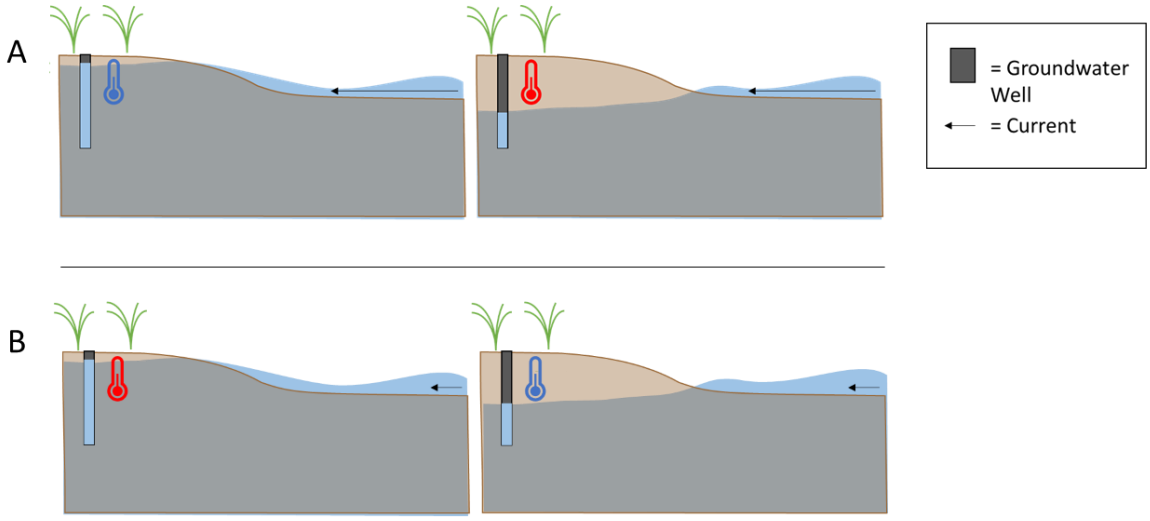

Figure 3.9 Schematic of linear mixed effects model results of groundwater level and tidal current velocity influence on soil temperature at salt marsh edges. Arrow length represents current velocity; long = high, short = low. A: High tidal current velocity lowers soil temperature during high groundwater levels (left) and increases soil temperature during low groundwater levels (right). B: Low tidal current velocity increases soil temperature during high groundwater levels (left) and lower soil temperature during low groundwater levels (right).

3.4 Discussion

The objectives of the study were to determine the groundwater and tidal hydrological influence on soil temperature at salt marsh sites with differing geomorphic conditions. We find that the temperature of marsh edge soils follows air and sea surface temperature, which are moderated by seasonally dependent cooling or warming effect from groundwater level and tidal current velocity. Our work identifies the important and hitherto overlooked role of hydrodynamic influence on temperature-dependent salt marsh processes such as carbon sequestration. Moderation of soil temperature by high groundwater level was dependent on the season. The relatively stable groundwater temperatures warmed the marsh surface during winter and cooled it during summer. Higher groundwater levels provided a thermal buffering capacity, insulating the soil from temperature changes through the export of latent heat to the atmosphere (Befus et al., 2013). The effect of tidal inundations during warm seasons has also been observed to lower the soil temperature during high tides and increase soil temperature during low tides (Huang et al., 2019).

Tidal inundation might have a different effect on the carbon storage capabilities of salt marshes depending on their geographic location. Thus, in areas with colder seawater temperatures, tidal inundations might stabilise and reduce soil respiration, by decreasing soil temperatures. Although the effect of flooding might override any changes to soil temperature, i.e., systems experiencing tidal flooding had greater CO_2 emissions than non-tidal systems as soil temperatures warmed (Krauss et al., 2012; Wang et al., 2019). Combined effects of SLR and ocean warming might lead to increased soil respiration rates and higher emissions of CO_2 if wetlands are periodically flooded and experience insufficient vertical accretion.

Stronger tidal currents were also found to lower soil temperatures regardless of season. Tidal currents circulate seawater within the soil, fuelling porewater exchange and submarine groundwater discharge (SGD) at a scale of (<m) and (>m), respectively (Taniguchi et al., 2019). Higher tidal current velocities can increase seawater circulation within the soil (Befus et al., 2013; Wilson and Morris, 2012). Greater circulation of relatively colder seawater within the soil during larger currents and higher groundwater levels led to lower soil temperatures. Such conditions could also occur during storm surges, along with potential changes in salinity having an effect on GHG emissions (Capooci et al., 2019). The decrease in soil temperature might lead to lower soil respiration. Field measurements of soil-atmosphere CO_2 emission have been shown to decrease during storm surge conditions (Diefenderfer et al., 2018), whereas experimental storm surge reconstruction of decreased porewater salinity was found to increase GHG emissions. (Capooci et al., 2019).

The implications of tidal hydrodynamic influence on soil temperature of microtidal marshes will likely be different. Although their greater organic matter content (Allen, 2000; Bartholdy et al., 2014) might be leading to increased soil respiration, their more frequent tidal inundations might lower soil oxygenation rate and reduce the influence of air temperature on soil temperature. Such contrary processes and influencing factors indicate the need for future work, especially in relation with groundwater and tidal hydrodynamic influences on soil temperature.

Research on the effects of hydrodynamics on coastal wetland temperatures has been limited. Xin et al., (2023) found, investigating soil temperature distributions and influences of groundwater along a creek-marsh section, that increased porewater circulations led to greater heat loss from salt marsh soils. Based on the results, the marsh-creek cross section was characterised into distinct zones according to the soil temperature influences. Soil temperature within the high marsh was influenced by meteorological fluctuations; the near-creek zone by tide-induced porewater circulation; and the low-elevation by reduced sediment-atmosphere heat exchange (Xin et al., 2023). Following this zonation, the soil temperature influence at our study site can be classified as tide-induced porewater circulation, experiencing significant changes due to meteorological factors during non-inundation periods.

Groundwater levels have an important, but previously overlooked buffering effect on salt marsh edge soil temperature. With a predicted soil temperature difference of up to 3.33 ℃ during changing groundwater levels, the implications are particularly relevant for projects aiming to restore wetlands to increase blue carbon storage (McMahon et al., 2023). The main restoration method in the UK and Europe is the managed realignment (MR), the breaching of tidal barrier (French, 2006). Resulting in marshes that are often characterized by reduced groundwater dynamics, higher average groundwater levels, and a lower number of tidal creeks (Lawrence et al., 2018; Spencer et al., 2017; Van Putte et al., 2020). Enhancing groundwater drainage and lowering the average groundwater level of the marsh can be achieved with the creation of small tidal creeks (Lawrence et al., 2022; Van Putte et al., 2020; Wolters et al., 2005). Consequently, considering our findings, a greater channel network will also increase the carbon storage value of restored sites, as the increased circulation of seawater within the sediment will lower the soil temperatures and inhibit the remineralization of deposited organic matter (Cui et al., 2021).

Unlike groundwater level and current velocity, geomorphic conditions (sloped vs. cliffed marsh edge) didn’t lead to significantly different soil temperatures, and no significant interactions of hydrodynamic variables on soil temperature during conditions inundating the

groundwater logger. This was unexpected as soil temperature changed between sites with different geomorphic conditions, i.e., cliffed-eroding (ER1) and sloping-prograding (PR5) sites during the measurement period October-December 2021 compared to January-March 2022 (Stolpmann et al., under review). Differential soil temperatures between geomorphic conditions could be due to the inclusion of all measurement time periods, also incorporating neap tidal cycles. The significantly different groundwater retention at sloping-prograding sites following spring tidal cycles (Stolpmann et al., under review) could lower the soil temperature due to the evaporative cooling effect (Moffett et al., 2010). Thus, the carbon storage value of sloping-prograding sites would improve in comparison to cliffed-eroding sites, supporting arguments for salt marsh restoration from a blue carbon storage perspective (McMahon et al., 2023).

Soil temperature has previously been found to be driven predominantly by marsh elevation, rather than flooding by tidal waters (Alber and O'Connell, 2019). Linear models showed that an increase in elevation of 0.5m, led to an increase in soil temperature by 0.9 to 1.7°C, irrespective of tidal flooding (Alber and O'Connell, 2019). This disagrees with our results, where flooding was the main driver of soil temperature changes. However, marsh elevation change also leads to a change in groundwater level, as higher marshes are flooded less frequently, and groundwater levels are lower than at low elevation marshes. Thus, the negative relationship between soil temperature and elevation found by Alber and O'Connell (2019) could be explained by the positive relationship between soil temperature and groundwater level found by our study.

3.5 Conclusions

This study set out to determine the influence of groundwater and tidal hydrological variables on soil temperature. The research showed that soil temperature is significantly influenced by the interaction of groundwater level and tidal current velocity, as well as by groundwater level and season. The influence of hydrological factors on soil temperature is however not dependent on the geomorphology of the site (i.e., sloping vs cliffed). Salt marsh soil temperature is however expected to increase due to rising ocean temperatures and higher air temperatures and with it, soil respiration and CO_2 emissions. Higher groundwater levels and lower tidal current velocities leading to lower oxygenation of the soil can lower the soil CO_2 emissions. This could for example be achieved at gently sloping salt marsh sites, particularly due to lower groundwater drainage during spring tidal cycles.

Acknowledgments
Research was funded by the United Kingdom Research and Innovation Global Challenges Research Fund (Living Deltas Research Hub) (Grant No. NE/S008926/1). We would like to thank NatureScot for permitting work at Caerlaverock; and T. Prentice, K. Roberts, and Y. Zheng for field assistance.

Open Research

Data is available via University of Glasgow's Research Repository https://researchdata.gla.ac.uk/1377/

This study has been conducted using E.U. Copernicus Marine Service Information; https://doi.org/10.48670/moi-00054

References

Alber, M., O'Connell, J.L., 2019. Elevation Drives Gradients in Surface Soil Temperature Within Salt Marshes. Geophys. Res. Lett. 46, 5313–5322. https://doi.org/10.1029/2019GL082374

Allen, J.R.L., 2000. Morphodynamics of Holocene salt marshes: a review sketch from the Atlantic and Southern North Sea coasts of Europe. Quaternary Science Reviews 19, 1155–1231. https://doi.org/10.1016/S0277-3791(99)00034-7

Balke, T., Vovides, A., Schwarz, C., Chmura, G.L., Ladd, C., Basyuni, M., 2021. Monitoring tidal hydrology in coastal wetlands with the "Mini Buoy": applications for mangrove restoration. Hydrology and Earth System Sciences 25, 1229–1244. https://doi.org/10.5194/hess-25-1229-2021

Bartholdy, J., Bartholdy, A.T., Kim, D., Pedersen, J.B.T., 2014. On autochthonous organic production and its implication for the consolidation of temperate salt marshes. Marine Geology 351, 53–57. https://doi.org/10.1016/j.margeo.2014.03.015

Befus, K.M., Cardenas, M.B., Erler, D.V., Santos, I.R., Eyre, B.D., 2013. Heat transport dynamics at a sandy intertidal zone: Heat transport dynamics at a sandy intertidal zone. Water Resour. Res. 49, 3770–3786. https://doi.org/10.1002/wrcr.20325

Campbell, A.D., Fatoyinbo, L., Goldberg, L., Lagomasino, D., 2022. Global hotspots of salt marsh change and carbon emissions. Nature 1–6. https://doi.org/10.1038/s41586-022-05355-z

Capooci, M., Barba, J., Seyfferth, A.L., Vargas, R., 2019. Experimental influence of storm-surge salinity on soil greenhouse gas emissions from a tidal salt marsh. Science of The Total Environment 686, 1164–1172. https://doi.org/10.1016/j.scitotenv.2019.06.032

Clyne, F.J., Garrod, C.J., Tipple, J.R., Jeffs, T.M., 2007. Radiological Habits Survey: Dumfries and Galloway Coast (Environment Report No. Final report RL 08/11).

Copernicus Marine Service Information (CMEMS), 2019. Atlantic - European North West Shelf - Ocean Physics Analysis and Forecast. https://doi.org/10.48670/moi-00054

Cui, H., Bai, J., Du, S., Wang, J., Keculah, G.N., Wang, W., Zhang, G., Jia, J., 2021. Interactive effects of groundwater level and salinity on soil respiration in coastal wetlands of a Chinese delta. Environmental Pollution 286, 117400. https://doi.org/10.1016/j.envpol.2021.117400

Cutts, N., Hemingway, K., 1996. The Solway Firth - broad scale habitat mapping (Scottish Natural Heritage Research, Survey and Monitoring Report No. 46).

Diefenderfer, H.L., Cullinan, V.I., Borde, A.B., Gunn, C.M., Thom, R.M., 2018. High-frequency greenhouse gas flux measurement system detects winter storm surge effects on salt marsh. Global Change Biology 24, 5961–5971. https://doi.org/10.1111/gcb.14430

Fagherazzi, S., Mariotti, G., Leonardi, N., Canestrelli, A., Nardin, W., Kearney, W.S., 2020. Salt Marsh Dynamics in a Period of Accelerated Sea Level Rise. JGR Earth Surface 125. https://doi.org/10.1029/2019JF005200

French, P.W., 2006. Managed realignment – The developing story of a comparatively new approach to soft engineering. Estuarine, Coastal and Shelf Science 67, 409–423. https://doi.org/10.1016/j.ecss.2005.11.035

Guimond, J., Tamborski, J., 2021. Salt Marsh Hydrogeology: A Review. Water 13, 543. https://doi.org/10.3390/w13040543

Hansom, J.D., 2003. Solway Firth (North Shore), in: Coastal Geomorphology of Great Britain, Geological Conservation Review Series. Joint Nature Conservation Committee: Peterborough, pp. 541–548.

Huang, Y., Guo, H., Chen, X., Chen, Z., Van Der Tol, C., Zhou, Y., Tang, J., 2019. Meteorological controls on evapotranspiration over a coastal salt marsh ecosystem under tidal influence. Agricultural and Forest Meteorology 279, 107755. https://doi.org/10.1016/j.agrformet.2019.107755

Kirwan, M.L., Guntenspergen, G.R., Langley, J.A., 2014. Temperature sensitivity of organic-matter decay in tidal marshes. Biogeosciences 11, 4801–4808. https://doi.org/10.5194/bg-11-4801-2014

Krauss, K.W., Whitbeck, J.L., Howard, R.J., 2012. On the relative roles of hydrology, salinity, temperature, and root productivity in controlling soil respiration from coastal swamps (freshwater). Plant Soil 358, 265–274. https://doi.org/10.1007/s11104-012-1182-y

Kuan, W.K., Xin, P., Jin, G., Robinson, C.E., Gibbes, B., Li, L., 2019. Combined Effect of Tides and Varying Inland Groundwater Input on Flow and Salinity Distribution in Unconfined Coastal Aquifers. Water Resources Research 55, 8864–8880. https://doi.org/10.1029/2018WR024492

Ladd, C.J.T., Vovides, A.G., Wimmler, M.-C., Schwarz, C., Balke, T., 2024. Monitoring tides, currents, and waves along coastal habitats using the Mini Buoy. Limnology and Oceanography: Methods 22, 619–633. https://doi.org/10.1002/lom3.10631

Lawrence, P.J., Smith, G.R., Sullivan, M.J.P., Mossman, H.L., 2018. Restored saltmarshes lack the topographic diversity found in natural habitat. Ecological Engineering 115, 58–66. https://doi.org/10.1016/j.ecoleng.2018.02.007

Lawrence, P.J., Sullivan, M.J.P., Mossman, H.L., 2022. Restored saltmarshes have low beta diversity due to limited topographic variation, but this can be countered by management. Journal of Applied Ecology 59, 1709–1720. https://doi.org/10.1111/1365-2664.14179

Macreadie, P.I., Hughes, A.R., Kimbro, D.L., 2013. Loss of 'Blue Carbon' from Coastal Salt Marshes Following Habitat Disturbance. PLoS ONE 8, e69244. https://doi.org/10.1371/journal.pone.0069244

Mcleod, E., Chmura, G.L., Bouillon, S., Salm, R., Björk, M., Duarte, C.M., Lovelock, C.E., Schlesinger, W.H., Silliman, B.R., 2011. A blueprint for blue carbon: toward an improved understanding of the role of vegetated coastal habitats in sequestering

CO2. Frontiers in Ecology and the Environment 9, 552–560. https://doi.org/10.1890/110004

McMahon, L., Ladd, C.J.T., Burden, A., Garrett, E., Redeker, K.R., Lawrence, P., Gehrels, R., 2023. Maximizing blue carbon stocks through saltmarsh restoration. Frontiers in Marine Science 10.

Met Office, 2006. MIDAS: UK Hourly Weather Observation Data.

Moffett, K.B., Tyler, S.W., Torgersen, T., Menon, M., Selker, J.S., Gorelick, S.M., 2008. Processes Controlling the Thermal Regime of Saltmarsh Channel Beds. Environ. Sci. Technol. 42, 671–676. https://doi.org/10.1021/es071309m

Moffett, K.B., Wolf, A., Berry, J.A., Gorelick, S.M., 2010. Salt marsh–atmosphere exchange of energy, water vapor, and carbon dioxide: Effects of tidal flooding and biophysical controls. Water Resour. Res. 46, 2009WR009041. https://doi.org/10.1029/2009WR009041

Santos, I.R., Eyre, B.D., Huettel, M., 2012. The driving forces of porewater and groundwater flow in permeable coastal sediments: A review. Estuarine, Coastal and Shelf Science 98, 1–15. https://doi.org/10.1016/j.ecss.2011.10.024

Schultz, M.A., Janousek, C.N., Brophy, L.S., Schmitt, J., Bridgham, S.D., 2023. How management interacts with environmental drivers to control greenhouse gas fluxes from Pacific Northwest coastal wetlands. Biogeochemistry 165, 165–190. https://doi.org/10.1007/s10533-023-01071-6

Schutte, C.A., Moore, W.S., Wilson, A.M., Joye, S.B., 2020. Groundwater-Driven Methane Export Reduces Salt Marsh Blue Carbon Potential. Global Biogeochemical Cycles 34, e2020GB006587. https://doi.org/10.1029/2020GB006587

Smeaton, C., Ladd, C.J.T., Miller, L.C., McMahon, L., Garrett, E., Barlow, N.L.M., Gehrels, W.R., Skov, M.W., Austin, W.E.N., 2023. Organic carbon stocks of Great

British saltmarshes. Front. Mar. Sci. 10, 1229486. https://doi.org/10.3389/fmars.2023.1229486

Spencer, K.L., Carr, S.J., Diggens, L.M., Tempest, J.A., Morris, M.A., Harvey, G.L., 2017. The impact of pre-restoration land-use and disturbance on sediment structure, hydrology and the sediment geochemical environment in restored saltmarshes. Science of The Total Environment 587–588, 47–58. https://doi.org/10.1016/j.scitotenv.2016.11.032

Stolpmann, L.M., Balke, T., & Bass, T. (under review) Sediment to Atmosphere CO2 Efflux Increases at Retreating Salt Marsh Edges. Estuarine, Coastal and Shelf Sciences.

Tang, H., Nolte, S., Jensen, K., Rich, R., Mittmann-Goetsch, J., Mueller, P., 2023. Warming accelerates belowground litter turnover in salt marshes – insights from a Tea Bag Index study. Biogeosciences 20, 1925–1935. https://doi.org/10.5194/bg-20-1925-2023

Taniguchi, M., Dulai, H., Burnett, K.M., Santos, I.R., Sugimoto, R., Stieglitz, T., Kim, G., Moosdorf, N., Burnett, W.C., 2019. Submarine Groundwater Discharge: Updates on Its Measurement Techniques, Geophysical Drivers, Magnitudes, and Effects. Frontiers in Environmental Science 7.

Van Putte, N., Temmerman, S., Verreydt, G., Seuntjens, P., Maris, T., Heyndrickx, M., Boone, M., Joris, I., Meire, P., 2020. Groundwater dynamics in a restored tidal marsh are limited by historical soil compaction. Estuarine, Coastal and Shelf Science 244, 106101. https://doi.org/10.1016/j.ecss.2019.02.006

Wang, F., Kroeger, K.D., Gonneea, M.E., Pohlman, J.W., Tang, J., 2019. Water salinity and inundation control soil carbon decomposition during salt marsh restoration: An incubation experiment. Ecol. Evol. 9, 1911–1921. https://doi.org/10.1002/ece3.4884

Wilson, A.M., Morris, J.T., 2012. The influence of tidal forcing on groundwater flow and nutrient exchange in a salt marsh-dominated estuary. Biogeochemistry 108, 27–38. https://doi.org/10.1007/s10533-010-9570-y

Wolters, M., Bakker, J.P., Bertness, M.D., Jefferies, R.L., Möller, I., 2005. Saltmarsh erosion and restoration in south-east England: squeezing the evidence requires realignment. Journal of Applied Ecology 42, 844–851. https://doi.org/10.1111/j.1365-2664.2005.01080.x

Xin, P., Robinson, C., Li, L., Barry, D.A., Bakhtyar, R., 2010. Effects of wave forcing on a subterranean estuary. Water Resources Research 46. https://doi.org/10.1029/2010WR009632

Xin, P., Yu, X., Zhan, L., Cheng, H., Yuan, S., 2023. Surface water-groundwater interaction affects soil temperature distributions and variations in salt marshes. Advances in Water Resources 172, 104366. https://doi.org/10.1016/j.advwatres.2023.104366

Yu, S., Wang, C., Li, H., Zhang, X., Wang, X., Qu, W., 2022. Field and Numerical Investigations of Wave Effects on Groundwater Flow and Salt Transport in a Sandy Beach. Water Resources Research 58, e2022WR032077. https://doi.org/10.1029/2022WR032077

Zhao, Y., Yu, Q., Wang, D., Wang, Y.P., Wang, Y., Gao, S., 2017. Rapid formation of marsh-edge cliffs, Jiangsu coast, China. Marine Geology 385, 260–273. https://doi.org/10.1016/j.margeo.2017.02.001

Zuur, A.F., Ieno, E.N., Elphick, C.S., 2010. A protocol for data exploration to avoid common statistical problems. Methods in Ecology and Evolution 1, 3–14. https://doi.org/10.1111/j.2041-210X.2009.00001.x

Zuur, A.F., Ieno, E.N., Walker, N., Saveliev, A.A., Smith, G.M., 2009. Mixed effects models and extensions in ecology with R, Statistics for Biology and Health. Springer New York, New York, NY. https://doi.org/10.1007/978-0-387-87458-6

4 Differing soil carbon source depending on geomorphic condition at mangrove coastlines

Abstract

Mangrove forests provide essential ecosystems services to coastal areas, such as coastal protection and carbon sequestration. Increasing anthropogenic and hydrodynamic pressure on these systems are leading to coastal erosion and habitat loss, affecting not only the carbon already stored within the soil but also their future carbon storage potential. This study aimed to elucidate if geomorphologically different mangrove systems (eroding vs expanding) have different carbon storage capacities, utilising the Mekong Delta in Vietnam and Charlotte Harbor Preserve State Park in the U.S. as case studies. Sediment cores were taken and sediment to atmosphere CO_2 emissions were measured at varying distances to the seaward vegetation edge. Eroding and expanding sites only differed significantly in soil samples in Florida for grain size percentage as well as loss on ignition percentages. Soil characteristics were site-specific for samples from Vietnam. The carbon stable isotope ratio ($\delta^{13}C$) was not significantly different between geomorphic conditions, showed however differences between depths, reflecting differential organic carbon sources. At expanding systems, it is primarily marine derived vs. terrestrial in the eroding. Finally, we discuss the applications of sediment carbon isotope measurements for coastal biogeomorphology.

4.1 Introduction

Mangrove forests are vital in providing essential ecosystem services, for instance coastal protection and carbon sequestration (Barbier et al., 2011; Mcleod et al., 2011). Due to anthropogenic pressures and climate change, mangrove ecosystems are experiencing global losses and disturbances, primarily by deforestation (Richards and Friess, 2016). Future carbon sequestration potential as well as already sequestered carbon is thereby lost (Arias-Ortiz et al., 2020).

The soil carbon storage potential of mangrove forests depends on age, structure and other geomorphic factors (Chen et al., 2018; Cinco-Castro et al., 2022; He et al., 2018; Marchand, 2017; Yang et al., 2014). For example, younger stands have a greater potential for capturing tidally introduced sediment and have a faster carbon accumulation rate within their biomass than the soil (Chen et al., 2021), however the soil carbon sequestration increases in efficiency with increasing mangrove age (Alongi et al., 2004). However, it takes longer for created adult trees to reach the equivalent peat layer compared to a natural mangrove forests, approx. 55 years opposed to <15 years in younger stands (Osland et al., 2020). This has been attributed to the faster development of vegetation than the soil properties to sequester carbon (Osland et al., 2012). The carbon storage of mangroves is offset by the loss of carbon from the systems, which is dependent on biogeochemical and geomorphic conditions, influencing the decomposition rate as well as the outwelling of carbon (Spivak et al., 2019).

Incorporating stable carbon isotope analyses ($\delta^{13}C$ signature) into sediment organic matter source analysis has been used to determine the relative contribution of local (autochthonous) vs external (allochthonous) organic matter to the system (S. Bouillon et al., 2008; Tue et al., 2011). Higher values of $\delta^{13}C$, thus a higher ratio of C_{13} to C_{12} isotopes, are indicative of a marine origin, i.e., -19 ‰ and lower signatures, i.e., -26 ‰, of a terrestrial origin (Barber et al., 2017). The carbon origin between mangrove forests of differing geomorphic conditions can determine their carbon storage potential, which has been studied for mangroves of different ages and positions within the tidal frame (Marchand 2017). Although it has not been used to differentiate between mangrove systems of varying erosion conditions.

The aim of this study was to determine the geomorphic influence on sediment carbon source and soil to atmosphere CO_2 emissions from mangrove forests of differing minerogenic types, due to inherently different soil carbon percentages. For this purpose, eroding and expanding mangrove sites within the Mekong Delta and the west coast of Florida, US were sampled. It was hypothesized that eroding and expanding sites differed in their predominant carbon source with expanding sites having a greater allochthonous carbon, and eroding sites a

greater autochthonous carbon supply. It was further hypothesized that eroding sites had a greater CO_2 efflux than expanding sites as this mechanism was previously found at geomorphically contrasting salt marsh sites (Chapter 2).

4.2 Materials & Methods

This study was performed within mangrove forests in Florida, US and the Mekong delta in Vietnam in August and August/September 2022, respectively (Figure 4.1, Figure 4.2). In Florida the study was conducted in Charlotte Harbor, an estuarine system comprising of mangrove-seagrass shorelines (Poulakis et al., 2003). The climate is subtropical, seasons are divided into wet, June – October, and dry season, November – May (Table 4.1). In Vietnam, the study was conducted within the Mekong Delta at three sites, Ca Mau, Kien Giang, and Soc Trang with both eroding and expanding conditions (Figure 4.2, Table 4.1). The climate is tropical, with dry and wet season.

Table 4.1 Climate characteristics at study sites. Florida: summer (June/July/Aug); Vietnam: wet (May to November), dry (December to April). Data from: Florida (1991 - 2020; US Department of Commerce, n.d.); Vietnam (Hong et al., 2019).

Variable	**Florida, US**	**Mekong Delta, Vietnam**
Annual precipitation (mm)	1345.438	2000
Seasonal precipitation (mm)	Summer: 670.814 Winter:172.21	Wet: 1800 Dry: 200
Average temperature (°C)	Summer: 28.2 Winter: 18.2	Wet: 30 Dry: 20

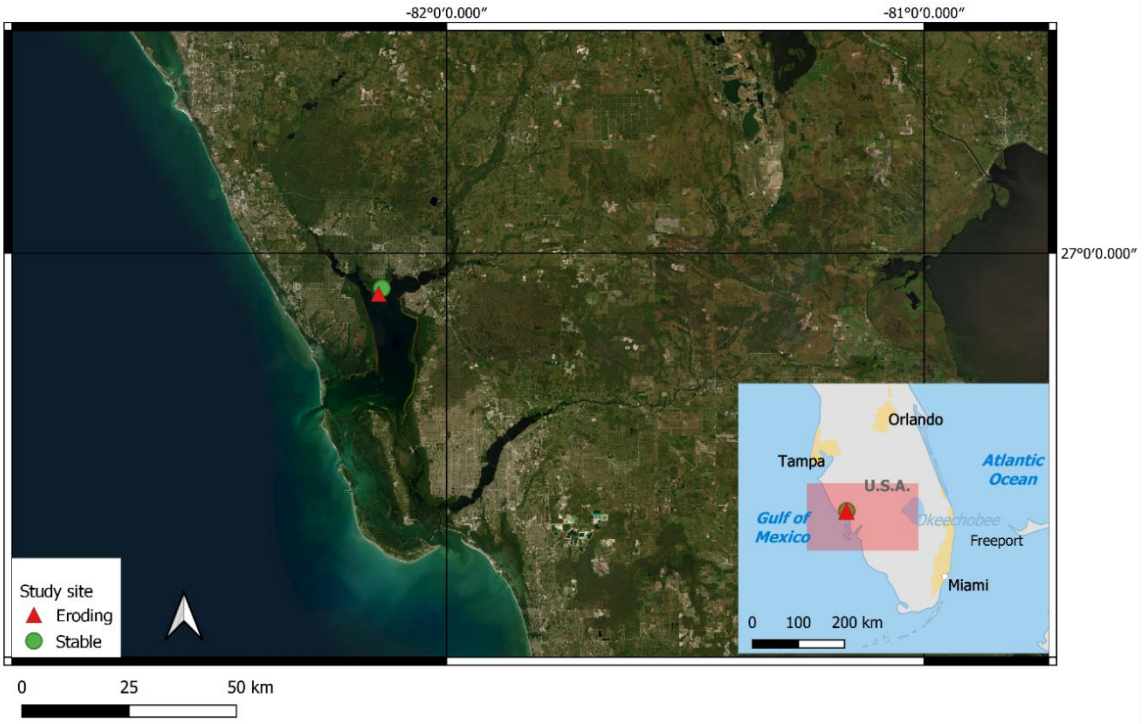

Figure 4.1 Map of study site in Charlotte Harbor, Florida. Eroding sites marked with red triangle and stable site marked with green circle. Made with Natural Earth (2009).

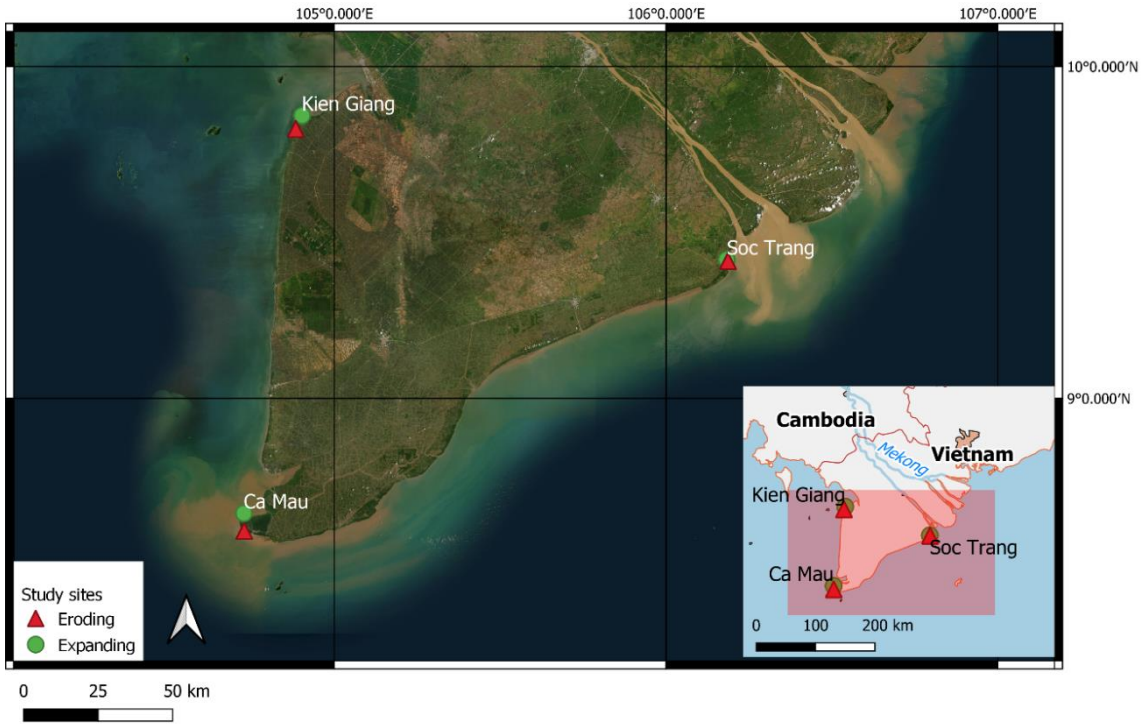

Figure 4.2 Map of study site in Mekong Delta in Vietnam. Eroding sites marked with red triangle and expanding site with green circle. Made with Natural Earth 2009).

4.2.1 Field sampling

Soil cores were taken in Vietnam and Florida from all sites and conditions, i.e., eroding and expanding Table 4.2. Sediment samples were taken at low tide. Soil cores were taken at 10 m from the seaward vegetation edge to a depth of 0.6 m in Vietnam, and to a depth of 1 m in Florida. Soil cores were subsampled into 10 cm parts. No reference isotopic samples were collected, however, for the purpose of this study, the relative differences between the eroding and expanding mangrove forests are of interest.

CO_2 flux was measured with a Licor gas analyser (LI-850) with chamber equilibration method using black PVC sediment chambers (diameter of 8.5 cm with a varying headspace from 624.2 cm^3 to 1,588.86 cm^3, Table 4.2). Care was taken to not include rhizomes and other vegetation when placing the chamber. Flux measurements were done in duplicates with 2 minutes per measurement. The final CO_2 flux (g m^{-2} hr^{-1}) was calculated with a polynomial regression, which was fitted to the initial increase in CO_2 concentration at time t = 0, as outlined in Bass et al., (2016). Fluxes were calculated using the following equation:

$$\text{Gas flux} = \left(a \times \left(\frac{P}{1013}\right) \times \left(\frac{273}{T+273}\right) \times M\right) \times \left(\frac{V}{A}\right) / 1000 \times 3600 \qquad \textbf{Equation 4.1}$$

Where gas flux is measured in g/m^2 hr; a = initial increase in CO_2 concentration at time t=0; p = air pressure within the chamber [mb]; T = air temperature [°C]; M = molar weight of measurement gas; V = volume of chamber [m^3]; A = Area of chamber [m^2].

Table 4.2 Sampling structure at study sites with number of transects for measurements taken.

Country	Location(s)	Sites	Transect soil cores	Transect CO2 flux
Vietnam	Ca Mau	Eroding	1	2
		Expanding	1	2
	Kien Giang	Eroding	1	2
		Expanding	1	0
	Soc Trang	Eroding	2	5
		Expanding	2	2
Florida	Charlotte Harbor	Eroding	1	1
		Expanding	1	1

4.2.2 Sample processing

Sediment samples were freeze dried for 36 hours to allow for further processing. After freeze drying, samples were processed for loss on ignition (LOI), grain size, carbon content and carbon stable isotopes ($\delta^{13}C$) analyses. The loss on ignition technique (LOI) was used to determine total organic matter content, by placing a subsample at 550°C for the duration of four hours and quantifying the weight differential.

Grain size was analysed with Bettersize 2600 particle size analyser on a subsample of 5 g. Organic matter was removed with the use of hydrogen peroxide (100 volumes > 30%). Hydrogen peroxide was added to the samples and after two hours added again, before left to evaporate overnight. Samples were slowly heated from 80°C to 100°C, until a clear layer of supernatant formed, and the reaction stopped. Following this, the samples were centrifuged at 2500rpm for 30 minutes and dried at 90°C for 24 h.

A Picarro Cavity Ring-down Spectrometer (G2201-*i*), coupled to a combustion module (A0201) was used to perform the isotopic carbon analysis of $\delta^{13}C$, presented in standard delta notation (‰) relative to VPDB standard, as well as carbon concentration measurements (mg/mg) and carbon percentage (% per sample weight) on the freeze-dried subsamples. The sampling accuracy for $\delta^{13}C$ in carbon dioxide is between 0.2 to 0.3‰ (Picarro, 2019). Subsamples were placed into weighted tin capsules.

4.2.3 Statistical analysis

Shoreline change was calculated using DSAS v5.1 from the U.S. Geological Society (Himmelstoss et al., 2021). With shorelines digitised using Google Earth Pro ("Google Earth Pro," 2024) satellite images between 2010 and 2022. Images were used where no cloud cover was present. The Linear Regression Rate (LRR) was calculated and presented as m yr^{-1}. Negative values represent a loss of shoreline (erosion) and positive values a gain of shoreline (expansion/progradation).

Data was analysed with R (RStudio 2022.12.0+353). A detailed list of analyses performed on the data is provided in (Appendix C). Soil to atmosphere CO_2 flux measurements as well as soil characteristics were analysed using Linear Mixed Effects Models, incorporating random factors to account for the nested study designs. Logarithmic, logit and arcsine transformation were applied if residuals were not normally distributed. Correlations between soil characteristics has been determined for the combination of both eroding and expanding conditions.

A principal component analysis (PCA) was conducted on sediment properties from all sites (Vietnam and Florida) to characterize the soil properties. The PCA was performed on scaled data using the R package prcomp (R Core Team, 2017).

Relative contribution of C_3 terrestrial plants to organic carbon in mangrove sediment cores was calculated using Equation 4.2 as calculated by Tue et al., (2011) and analysed using the Wilcoxon rank sum test and t-test.

$$f_t(\%) = \frac{\delta^{13}C_{sed} - \delta^{13}C_m}{\delta^{13}C_t - \delta^{13}C_m} \times 100 \qquad \textbf{Equation 4.2}$$

The relative contribution of C_3 terrestrial plant sources (%) is f_t; where $\delta^{13}C_{sed}$, $\delta^{13}C_t$, $\delta^{13}C_m$ are carbon stable isotope values of sediment, C_3 terrestrial plants and marine phytoplankton, respectively. This study used a value of -22.1‰ for $\delta^{13}C_m$, as it was reported for marine phytoplankton from the South China Sea (Liu et al., 2007). A value of -29.4‰ was used for $\delta^{13}C_t$, being the lower range limit of $\delta^{13}C$ signatures from mangrove leaves (Bouillon et al., 2008). Isotopic reference signatures were used for the analysis of samples from Florida and Vietnam.

4.3 Results

4.3.1 Sediment characteristics

All soil characteristics at sites in Vietnam were not significantly different between eroding and expanding conditions, but showed site specific variations (Table C.1, Figure C.1, Figure 4.3). With eroding and expanding conditions at Ca Mau, Vietnam showing greater differences in soil characteristics. The eroding and expanding site in Florida showed significant differences in clay, silt and percentages, as well as median grain size (D50) and the loss on ignition percentage (LOI; Table C.1).

All eroding sites sampled in Vietnam showed a lower $\delta^{13}C$ signature throughout the core than the expanding sites (Figure 4.4). These differences between eroding and expanding conditions are significant until the depth of 20 cm (Table C.2

Country	Variable ~ Condition [expanding]	Transformation	Estimate	t-value	p-value
Vietnam	Carbon concentration (mg)	Square root	-0.055	-0.706	0.553
	Carbon percentage	Arcsine	-0.016	-0.65	0.582
	Clay percentage	NA	-0.623	-0.065	0.954
	Silt percentage	NA	7.346	1.717	0.093
	Sand percentage	Logarithmic	0.306	0.612	0.604
	Carbon isotope ratio ($\delta^{13}C$)	Square root	0.788	1.834	0.142
	Median grain size (D50)	Reciprocal	-0.048	-0.453	0.695
	Loss on ignition percentage (LOI)	NA	-1.007	-0.366	0.75
Florida (US)	Carbon concentration (mg)	NA	-0.136	-2.056	0.056
	Carbon percentage	NA	-2.929	-1.661	0.115
	Clay percentage	**Logit**	**-0.43**	**-2.739**	**0.024**
	Silt percentage	**NA**	**-13.848**	**-2.947**	**0.017**
	Sand percentage	**NA**	**18.538**	**3.15**	**0.012**
	Carbon isotope ratio ($\delta^{13}C$)	NA	0.526	1.154	0.265
	Median grain size (D50)	**Square root**	**2.311**	**2.766**	**0.034**
	Loss on ignition percentage (LOI)	**NA**	**-7.214**	**-2.601**	**0.019**

). Carbon stable isotope signatures between the surface (0 cm) and at 50 cm depth were significantly different at expanding sites in Vietnam (Table C.3). Further it was noted that the surface $\delta^{13}C$ value was greater at the eroding site than the expanding site in Florida (Figure 4.4). Carbon percentage was greater for samples from Florida than from Vietnam, 8.69 ± 4.02 % and 1.7 ± 1.44 %, respectively (Figure 4.3

Country	Variable ~ Condition [expanding]	Transformation	Estimate	t-value	p-value
Vietnam	Carbon concentration (mg)	Square root	-0.055	-0.706	0.553
	Carbon percentage	Arcsine	-0.016	-0.65	0.582
	Clay percentage	NA	-0.623	-0.065	0.954
	Silt percentage	NA	7.346	1.717	0.093
	Sand percentage	Logarithmic	0.306	0.612	0.604
	Carbon isotope ratio ($\delta^{13}C$)	Square root	0.788	1.834	0.142
	Median grain size (D50)	Reciprocal	-0.048	-0.453	0.695
	Loss on ignition percentage (LOI)	NA	-1.007	-0.366	0.75
Florida (US)	Carbon concentration (mg)	NA	-0.136	-2.056	0.056
	Carbon percentage	NA	-2.929	-1.661	0.115
	Clay percentage	**Logit**	**-0.43**	**-2.739**	**0.024**
	Silt percentage	**NA**	**-13.848**	**-2.947**	**0.017**
	Sand percentage	**NA**	**18.538**	**3.15**	**0.012**
	Carbon isotope ratio ($\delta^{13}C$)	NA	0.526	1.154	0.265
	Median grain size (D50)	**Square root**	**2.311**	**2.766**	**0.034**
	Loss on ignition percentage (LOI)	**NA**	**-7.214**	**-2.601**	**0.019**

). Carbon percentage was greater at eroding sites for both Vietnam (2.05 ± 1.89 % vs 1.36 ± 0.7 %) and Florida (10.23 ± 4.85 % vs 7.3 ± 2.62 %), however not significantly (Figure 4.3, Table C.1

Country	Variable ~ Condition [expanding]	Transformation	Estimate	t-value	p-value
Vietnam	Carbon concentration (mg)	Square root	-0.055	-0.706	0.553
	Carbon percentage	Arcsine	-0.016	-0.65	0.582
	Clay percentage	NA	-0.623	-0.065	0.954
	Silt percentage	NA	7.346	1.717	0.093
	Sand percentage	Logarithmic	0.306	0.612	0.604
	Carbon isotope ratio ($\delta^{13}C$)	Square root	0.788	1.834	0.142
	Median grain size (D50)	Reciprocal	-0.048	-0.453	0.695
	Loss on ignition percentage (LOI)	NA	-1.007	-0.366	0.75
Florida (US)	Carbon concentration (mg)	NA	-0.136	-2.056	0.056
	Carbon percentage	NA	-2.929	-1.661	0.115
	Clay percentage	**Logit**	**-0.43**	**-2.739**	**0.024**
	Silt percentage	**NA**	**-13.848**	**-2.947**	**0.017**
	Sand percentage	**NA**	**18.538**	**3.15**	**0.012**
	Carbon isotope ratio ($\delta^{13}C$)	NA	0.526	1.154	0.265
	Median grain size (D50)	**Square root**	**2.311**	**2.766**	**0.034**
	Loss on ignition percentage (LOI)	**NA**	**-7.214**	**-2.601**	**0.019**

). The LOI percentage was greater at sites in Florida than Vietnam. Also showing significantly greater values at eroding (21.41 ± 8.35 %) than expanding (14.19 ± 2.61 %) sites in Florida. Whereas in Vietnam the eroding site had a LOI percentage of 7.12 ± 3.99 %, and the expanding site of 6.54 ± 3.2 %.

Clay percentages were greater at the Vietnamese study site compared to the Florida sites, but not different between eroding and expanding sites in Vietnam (28.22 ± 18.53 % vs 28.47 ± 11.86 %). Whereas in Florida the difference was significant (9.56 ± 6.46 % vs 4.69 ± 3.26 %). Silt percentages were significantly greater at eroding sites than expanding sites in Florida (34.41 ± 17.57 % vs 20.11 ± 6.98 %). Whereas in Vietnam the silt percentage was slightly greater at expanding sites than eroding sites (46.08 ± 22.01 % vs 38.73 ± 21.44 %). Sand percentages showed greater values for Florida than Vietnam. With significantly greater sand percentages at the expanding site than the eroding site in Florida (75.2 ± 9.72 % vs 56.04 ± 23.75 %), and similar values in Vietnam (eroding: 30.77 ± 35.96 %; expanding: 27.73 ± 29.9 %).

Table 4.3 Summary of lateral change of mangrove seaward edge (Linear Regression rate LRR; m yr^{-1}) of sampling transects in Florida (Charlotte Harbor) and Vietnam (Ca Mau, Kien Giang, Soc Trang).

Site	Condition	Transect	LRR (m yr^{-1})	Soil texture
Charlotte Harbor	Eroding	1	-0.955	Sandy Loam

	Expanding/Stable	1	-0.065	Loamy Sand
Ca Mau	Eroding	1	-7.49	Silty Clay
	Expanding	1	50.41	Silty Clay Loam
Kien Giang	Eroding	1	-0.845	Silty Clay
	Expanding	1	32	Silty Clay
Soc Trang	Eroding	1	-5.83	Loamy Sand
		4	-6.34	Sandy Clay Loam
	Expanding	1	24.95	Clay Loam
		2	24.95	Sandy Clay Loam

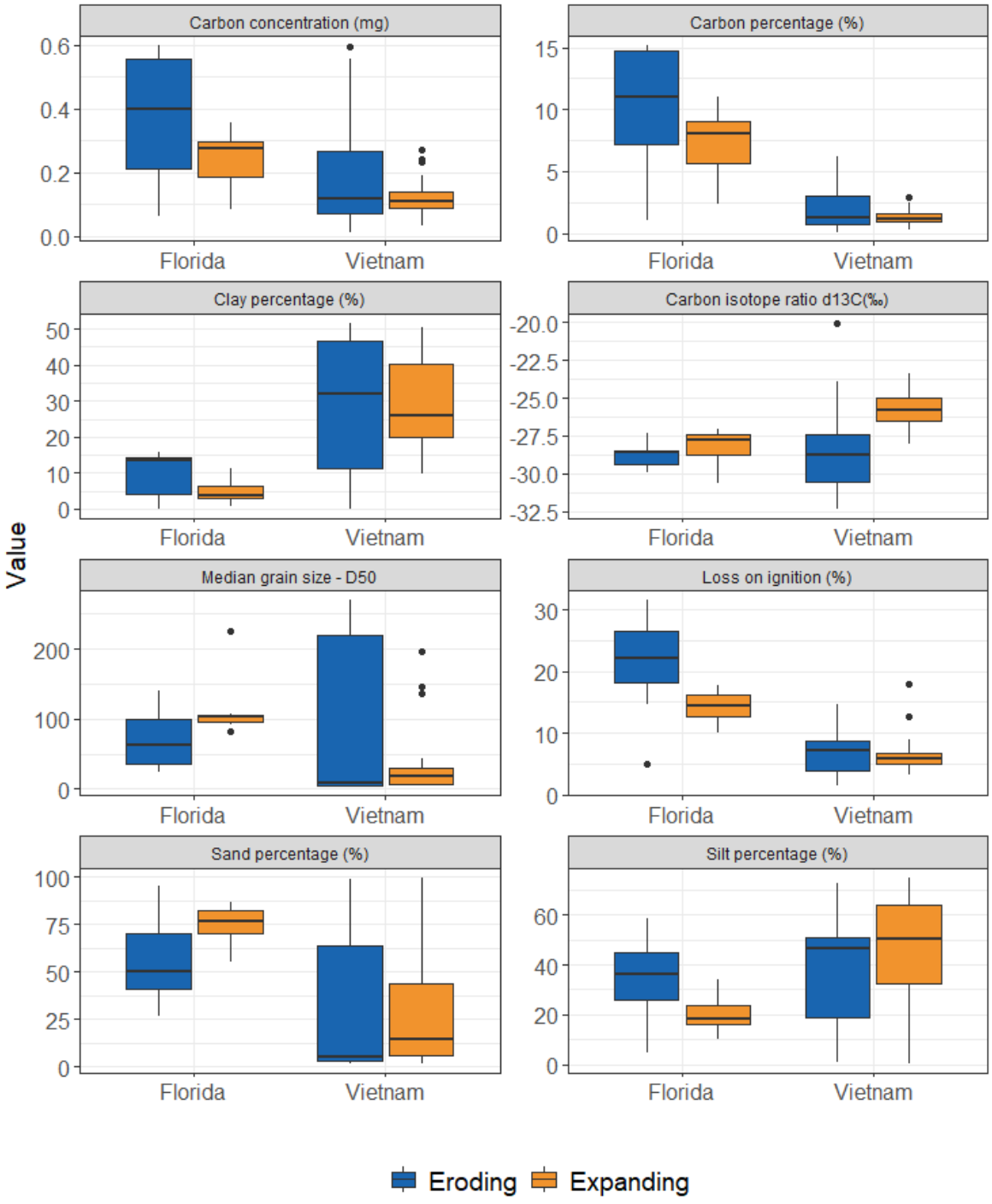

Figure 4.3 Sediment characteristics between geomorphic conditions, eroding = blue, expanding = orange. Sample size: Florida (Eroding n=1; Expanding n=1); Vietnam (Eroding n=4; Expanding n=4).

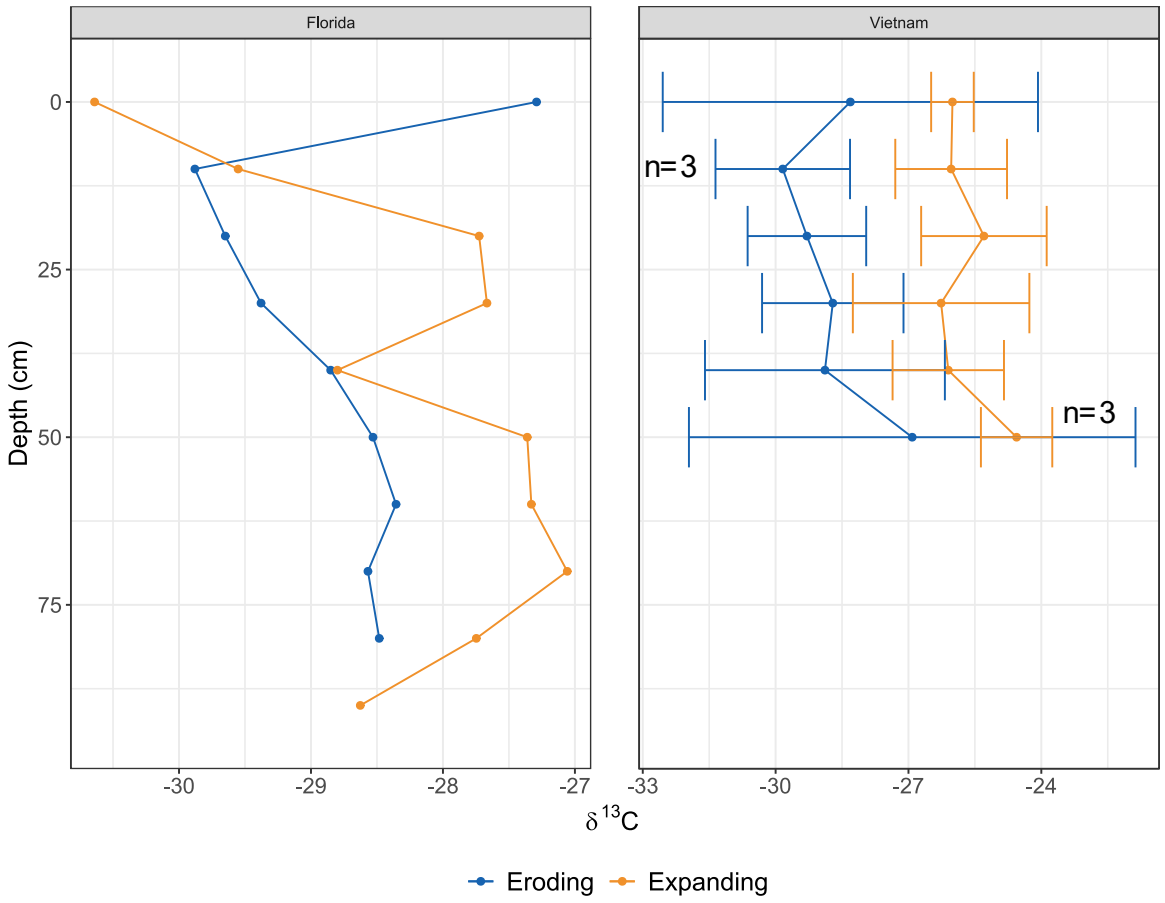

Figure 4.4 Stable carbon isotope signature ($\delta^{13}C$) by depth for geomorphic different (eroding = blue; expanding = orange) mangrove forests in Florida (left; n = 1) and Vietnam (right; n = 4; except where shown). Error bars represent standard deviation between sampling sites (Ca Mau, Kien Giang, Soc Trang).

4.3.2 Relative contribution of C_3 terrestrial carbon to mangrove sediments

The relative contribution of C_3 terrestrial plants to mangrove sediments is significantly different between eroding and expanding conditions in Vietnam (W = 442, p-value = 1.869e-05). Eroding sites showed a greater contribution than expanding sites. The relative contribution was not significantly different between eroding and expanding conditions in Florida (t(17) = 1.1539; p-value = 0.2645).

4.3.3 Sediment – atmosphere CO_2 emissions

CO_2 flux was not significantly different between eroding and expanding conditions for Vietnam (t = -2.135, p-value = 0.165) or Florida (t = 0.958, p-value = 0.406). Showing on average larger CO_2 emissions at eroding sites (Figure 4.5).

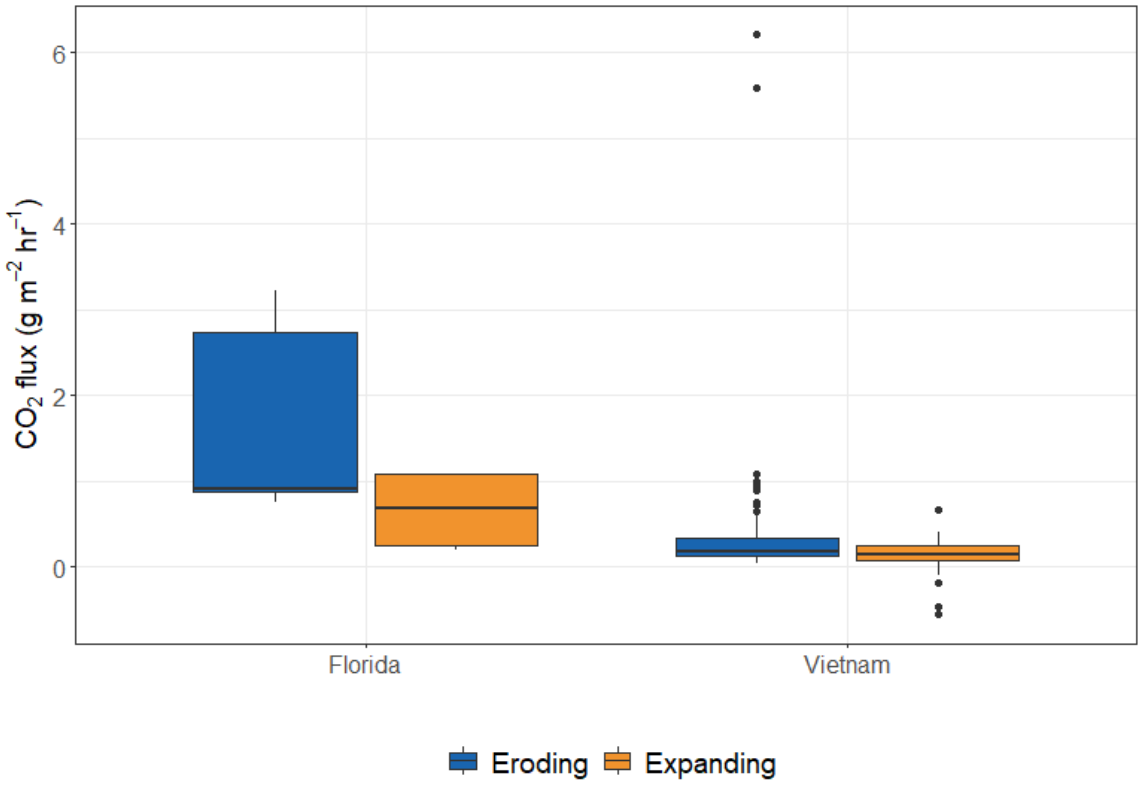

Figure 4.5 CO_2 flux (g m^{-2} hr^{-1}) between mangrove forests in Florida and Vietnam and between geomorphic conditions (blue = eroding; orange = expanding).

4.3.4 Correlations

There is a moderate correlation between the $\delta^{13}C$ signature and LRR (cor = 0.67, p-value <0.001) as well to carbon concentration (cor = -0.51, p-value < 0.001; Figure 4.6). Significant correlations also show among grain size percentages (clay, silt, sand) and among the different representations of carbon concentrations (carbon concentration, carbon percentage and LOI).

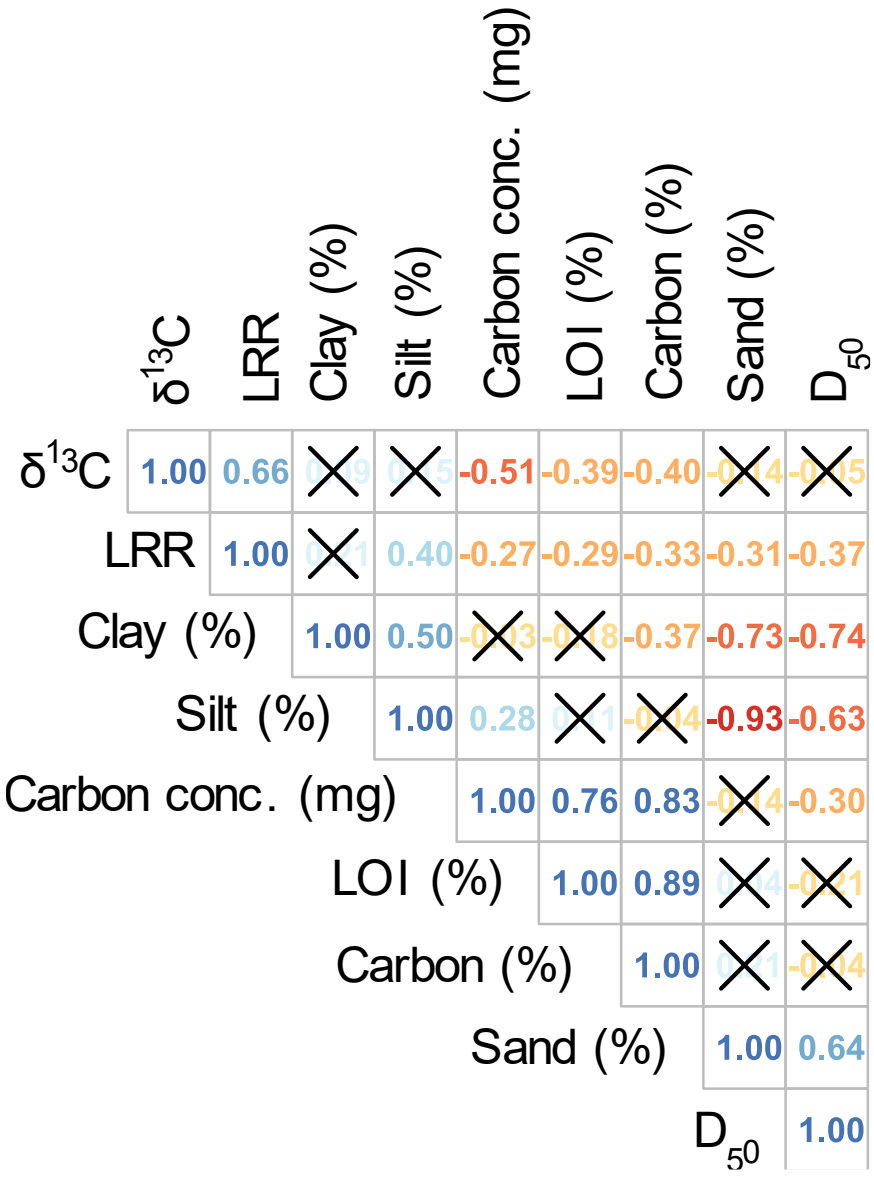

Figure 4.6 Correlation matrix for eroding and expanding sites including Florida and Vietnam sites. Numbers and colours represent correlation coefficient and crossed out circles are not significant correlations (p-value <0.05). $\delta^{13}C$ = carbon stable isotope signature; LRR = Linear Regression Rate (m yr^{-1}); Clay, silt, sand percentage; LOI (%) = Loss on ignition percentage; Carbon (%) = total carbon percentage; D_{50} = median grain size (µm).

4.3.5 PCA of sediment characteristics

PCA was performed on sediment and site characteristics from Florida and Vietnam to explore the differences between sites and locations (eroding vs expanding) and determine characterising variables. PCA performed on the combined data from Florida and Vietnam showed principal components 1 and 2 (PC1, PC2) that explained a total of 72.5% of the variation within the data (Figure 4.7). PC1 accounted for 39.02% of variation with clay percentage and LRR with negative loadings and sand percentage and carbon percentage with positive loadings. PC2 represented 33.49% of variation with negative loadings for carbon concentration and LOI, and positive loadings for median grain size (Figure 4.7). Soil samples from Florida were characterized by lower LRR, and lower clay and silt percentages, but higher carbon and sand percentages. Samples from Vietnam could be divided into separate groups. Samples from Soc Trang and Ca Mau being mostly separated along the PC1 axis. Samples taken from Kien Giang overlapped with both sites and could be characterized by lower PC2 loadings (lower LRR, $\delta^{13}C$, clay and silt percentages).

Principal component analysis performed separately on data from Vietnam showed that a total of 75.71% of the variation in the data was explained by PC1 and PC2 (Figure 4.8). Grouped together are the Carbon percentage representations, clay, and silt, as well as Sand and D_{50}.

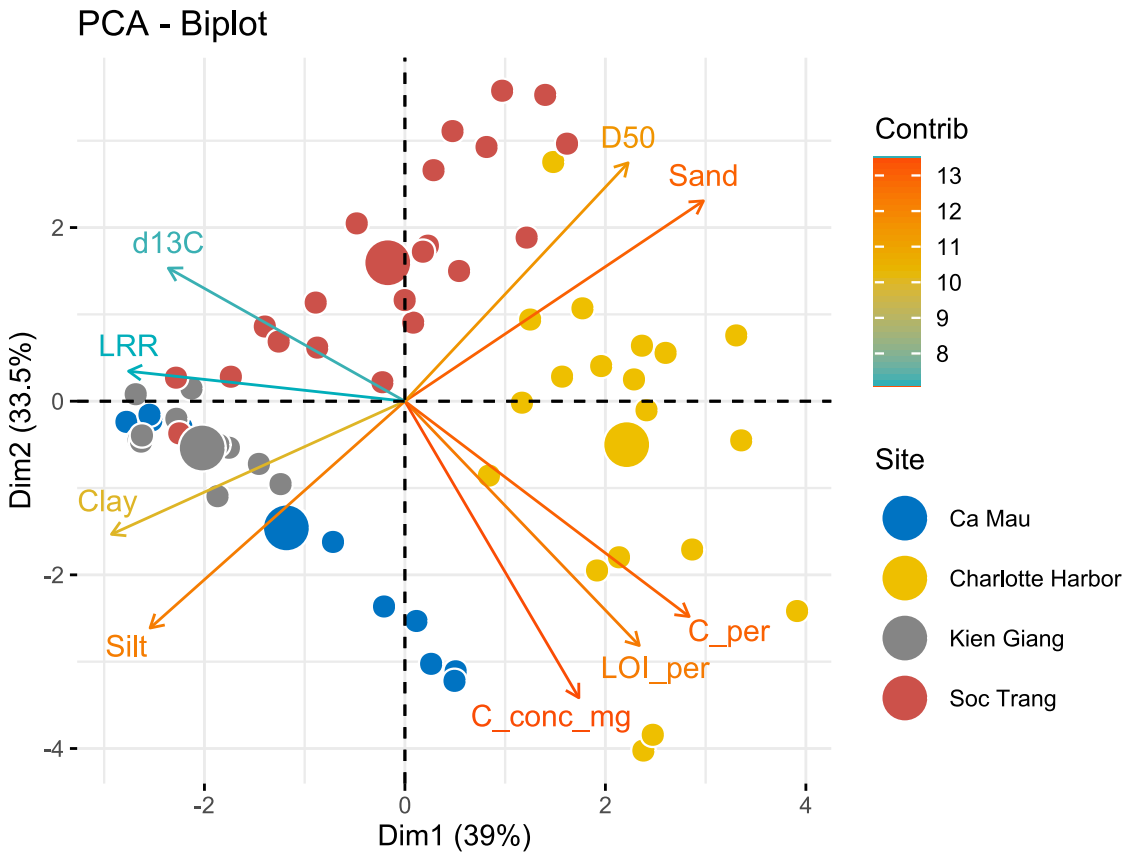

Figure 4.7 Principal component analysis (PCA) of sediment and site characteristics from sediment from Vietnam and Florida, eroding and prograding sites combined, blue circles = Ca Mau (Vietnam); yellow circle = Charlotte Harbor (Florida); grey circle = Kien Giang (Vietnam); red circle = Soc Trang (Vietnam). Contribution scale refers to Eigenvalues. Sediment characteristics are LOI = loss on ignition percentage; d13C = $\delta^{13}C$ (carbon stable isotope ratio); C_conc_mg = Carbon concentration (mg/mg); C_per = Carbon percentage; Clay = clay percentage, Silt = silt percentage; Sand = sand percentage, D50 = median grain size (d_{50}); LRR = linear regression rate (m yr-1). Point size represents Site mean.

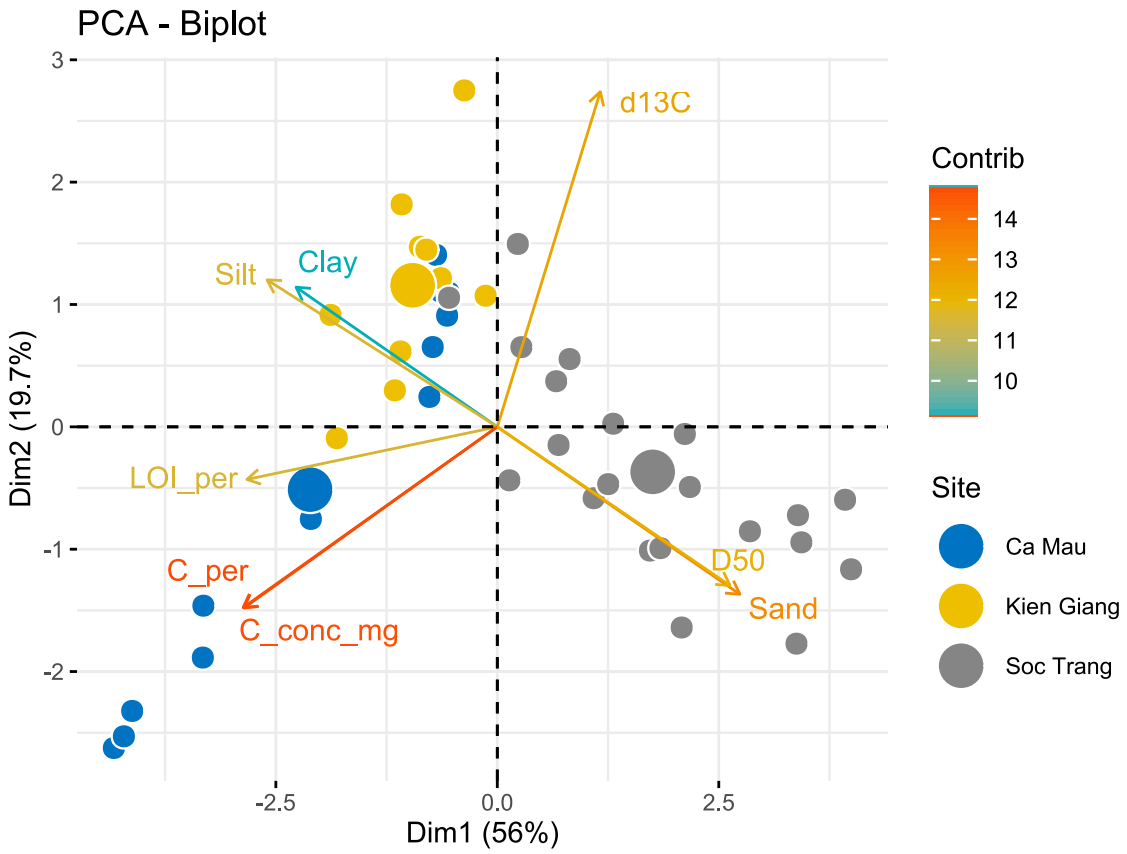

Figure 4.8 Principal component analysis (PCA) of sediment and site characteristics from sediment from Vietnam, combining eroding and prograding sites, blue circle = Ca Mau, yellow circle = Kien Giang; grey circle = Soc Trang. Contribution scale refers to Eigenvalues. Sediment characteristics are LOI = loss on ignition percentage; d13C = $\delta^{13}C$ (carbon stable isotope ratio); C_conc_mg = Carbon concentration (mg/mg); C_per = Carbon percentage; Clay = clay percentage, Silt = silt percentage; Sand = sand percentage, D50 = median grain size (d_{50}); LRR = linear regression rate (m yr^{-1}). Point size represents Site mean.

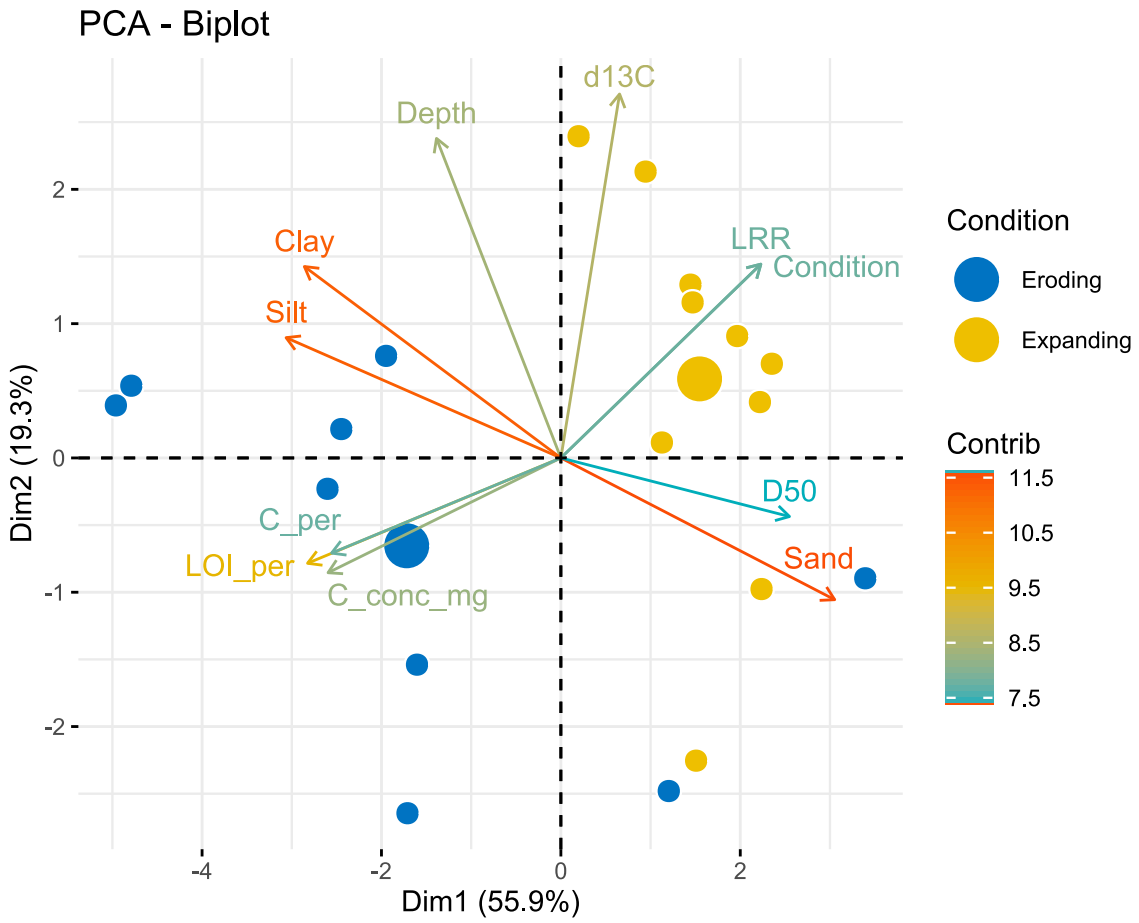

Figure 4.9 Principal component analysis (PCA) of sediment and site characteristics from sediment from Florida, blue circles = eroding site, yellow circles = expanding site. Contribution scale refers to Eigenvalues. Sediment characteristics are LOI = loss on ignition percentage; d13C = $\delta^{13}C$ (carbon stable isotope ratio); C_conc_mg = Carbon concentration (mg/mg); C_per = Carbon percentage; Clay = clay percentage, Silt = silt percentage; Sand = sand percentage, D50 = median grain size (d_{50}); LRR = linear regression rate (m yr-1). Point size represents Site mean.

4.4 Discussion

4.4.1 Stable isotope analysis

The objective of the study was to determine the difference between carbon sources contributing to soil carbon between differing geomorphic mangrove conditions. Further, possible differences in organic matter decomposition state downcore, as well as influencing soil conditions on soil to atmosphere CO_2 emissions were studied.

There was no significant difference in carbon sources to soil carbon between eroding and expanding mangrove forests at sites sampled in Vietnam or Florida, indicated by differing carbon stable isotope signatures ($\delta^{13}C$). These results are not in favour of our working hypothesis. Eroding sites were expected to have a lower $\delta^{13}C$ signature, indicating an autochthonous carbon source. The results do however show high site-specific variations, with Ca Mau showing a greater difference in $\delta^{13}C$ signatures between geomorphic conditions. The $\delta^{13}C$ values measured at eroding sites (-27.6 ± 2.3 ‰) are within reported $\delta^{13}C$ values for mangrove leaves (-29.4 ‰ to -27 ‰; (Arias-Ortiz et al., 2020; Bouillon et al., 2008). The increase in importance of organic matter derived from C_3 terrestrial plants at eroding sites with contributions at 100 % also suggests other organic matter sources than mangroves. Satellite and land use maps indicate rice farming, melaleuca forests as dominating land cover and land uses (Hauser et al., 2017; Son et al., 2015). Both, rice as well as melaleuca being C_3 plants, can contribute to the depletion of $\delta^{13}C$ signature and a relatively high C_3 plant contribution to sedimentary organic matter (Sun et al., 2021). With an LRR of -0.845 m yr^{-1}, current mangrove sites at Kien Giang were previously rice dominated, based on satellite image observations from 2012 (“Google Earth Pro,” 2024). Carbon could also have been transported from further inland onto the mangrove forests during the wet season through run-off (Call et al., 2019).

Expanding sites had higher $\delta^{13}C$ values (-25.76 ± 1.29 ‰ vs -28.62 ± 2.85 ‰) this suggests a change in importance from autochthonous to allochthonous carbon, imported into the system from the marine environment (Barber et al., 2017). The expanding sites at Ca Mau and Soc Trang show significantly lower contribution of C_3 terrestrial plant material and a greater contribution of marine phytoplankton, demonstrating the relative importance of marine sediments in mudflat sedimentation and thus the expansion and growth of mangrove ecosystems (Cinco-Castro et al., 2022). Further it strongly suggests lower elevation and higher inundation frequencies at expanding sites. The high expansion rate of 50.41 m yr^{-1} at the expanding site at Ca Mau (Hauser et al., 2017; Son et al., 2015), further shows the sediment influx and change from a mudflat to the expanding site, while relying on the

external organic matter supply. Furthermore, the higher carbon stable isotope values at the expanding site could indicate tidal flushing and export of mangrove organic matter before it could be incorporated into the soil (Marchand et al., 2003).

As well as indicating the source of organic matter, $\delta^{13}C$ can also provide insight into its decomposition stage (Adame and Fry, 2016). The $\delta^{13}C$ values decrease throughout the cores for sites in Vietnam. But only for the expanding sites these values are significantly different between the surface, i.e., depth of 0 cm, and at a depth of 50 cm (-26.0 ± 0.481 ‰ and -24.6 ± 0.806 ‰, respectively). With an enrichment of +1.4 ‰, this is indicating decomposition and oxic conditions (Adame and Fry, 2016). Eroding sites are also showing an enrichment of $\delta^{13}C$ throughout the core, but at the same time have a higher standard deviation associated with them. An increase in $\delta^{13}C$ values was also observed following the cutting of mangroves by Adame et al., (2018), attributed to decomposition of organic matter within the sediment. Comparing the $\delta^{13}C$ signature to the organic carbon percentage at eroding sites, could show if the signature is considered indicative of either the source of carbon or the decomposition of organic matter. The $\delta^{13}C$ signatures, however, only showed a slight negative correlation to carbon percentage at eroding sites (cor = -0.64) and no correlation for eroding and expanding sites combined. Thus, $\delta^{13}C$ signatures are therefore mainly denoting the source of organic matter within the system, rather than organic matter decomposition. Which also becomes apparent when looking at the anomaly of the $\delta^{13}C$ value of the surface sediment in Florida. The eroding site had a high $\delta^{13}C$ value, opposed to the expanding site. Here the high $\delta^{13}C$ value is most likely due to the influence of marine organic matter (Adame et al., 2018; Lovelock, 2008).

4.4.2 CO_2 flux - no geomorphic influence

The CO_2 flux from the mangrove sediment to the atmosphere is within the range of other studies performed within the Mekong Delta (Dušek et al., 2021; Vinh et al., 2019). With a CO_2 emission of 0.31 ± 0.74 g m^{-2} hr^{-1} our measurements are within the range previously reported for the wet season of 0.56 ± 0.28 g m^{-2} hr^{-1} (Vinh et al., 2019). There was however no geomorphic influence on soil – atmosphere CO_2 emissions, contrary to our hypothesis. The CO_2 emissions were expected to be greater at eroding sites than prograding sites, as mature landwards sites were shown to emit more CO_2 than seaward fringing sites, predominantly due to less tidal inundation and drier soils (Cameron et al., 2019; Chapter 2). The CO_2 flux between geomorphic conditions may show differences when repeated during the dry season. Differences in conditions between sites (i.e., hydroperiod, soil temperature)

driving CO_2 emissions could be more variable and pronounced between seasons (Cameron et al., 2019; Lovelock, 2008; Vinh et al., 2019). Indeed, lower CO_2 fluxes were measured during the mid wet season, due to increased photosynthetic rate and lower respiration (Vinh et al., 2019). Although also opposing trends were found. Where the higher rainfall during the end of the wet season let to increased GHG emissions (Cameron et al., 2021; Hien et al., 2018) mobilising organic-rich sediments and making those available for respiration (Spivak et al., 2019).

4.4.3 Geomorphic conditions and implications for blue carbon

Mangrove sites have been identified as important sites for carbon sequestration due to their organic-rich soils but low emissions of greenhouse gases due to anaerobic conditions (Kristensen et al., 2008). There is however a difference in the origin of soil carbon between geomorphic conditions, carrying implications for restoration projects. Mature mangrove ecosystems are a significant store of autochthonous carbon, owing to their higher productivity and greater above-ground biomass sequestering carbon through the fixation of CO_2 from the atmosphere (Breithaupt et al., 2012; Komada et al., 2022; Marchand, 2017). Expanding and younger mangrove sites on the other hand are a greater sink for allochthonous carbon, allowing them to accrete vertically (Yang et al., 2014). Edge-erosion of mature mangrove sites will need to be prevented, in order to preserve these habitats and guarantee continuous sequestration of "fast" carbon (Komada et al., 2022).

Adding to the CO_2 fluxes from mangrove forests is the emission of methane (CH_4), considered a more potent greenhouse gas than CO_2 (Rosentreter et al., 2018). Methane is produced under anaerobic conditions and high fluxes have been measured in water-saturated soils (Dušek et al., 2021). With an average CH_4 flux of 4,556.96 ± 1,102.06 µmol CH_4 m^{-2} day^{-1} ("Corrigendum," 2020) and an average global carbon burial of 31.1 ± 5.4 Tg C $year^{-1}$, mangroves are contributing to the global warming potential, releasing ~1 – 1.5 g of CO_2 equivalent of CH_4 for every gram of CO_2-eq C stored, making them net emitters of carbon ("Corrigendum," 2020). Methane emissions from mangroves are however highly variable, differing between systems and no clear environmental drivers have been identified (Al-Haj & Fulweiler, 2020). Potential methane emissions have however been shown to be lower from older mangrove forests (Comer-Warner et al., 2022). Strengthening the case for further studies including geomorphic conditions.

4.5 Conclusion

The present study determined the geomorphic impact of eroding and expanding conditions on soil properties and CO_2 emissions from mangrove habitat in the Mekong Delta in Vietnam and Charlotte Harbor National Park in Florida, US. The carbon stable isotope ratios showed no significant differences between geomorphic conditions but indicated site specific reliance on marine derived organic matter at expanding sites and terrestrial/mangrove organic matter at eroding sites (Marchand, 2017). Contrary to our hypothesis, the CO_2 emissions were not different between eroding and expanding conditions, which could be investigated in a follow-up study further including seasonal variation. This study demonstrated that mangrove rehabilitation projects can use carbon isotope ratios as a further assessment tool to determine rehabilitation sites, prioritising sites with higher carbon sequestration potential.

Acknowledgements

Florida research permit 06032224 from the Florida Department of Environmental Protection. Many thanks to the team of Charlotte Harbor Aquatic Preserves Team for fieldwork assistance and to Dr Chambers for planning and organization. We would also like to thank Nguyen Xuan Lan, Mr. Nguyen Trung Quoc, Mr. Cao Ngoc Trung, Mr. Hoang Van Giang, Mr. Nguyen Huu Phuc, Mr. To Thanh Huynh, Mr. Duong Trang Trong for fieldwork assistance in the Mekong Delta, Vietnam. The Living Deltas Hub is part of the UKRI GCRF Research HUB (Grant Reference NE/S008926/1).

References

Adame, M.F., Zakaria, R.M., Fry, B., Chong, V.C., Then, Y.H.A., Brown, C.J., Lee, S.Y., 2018. Loss and recovery of carbon and nitrogen after mangrove clearing. Ocean & Coastal Management 161, 117–126. https://doi.org/10.1016/j.ocecoaman.2018.04.019

Al-Haj, A.N., Fulweiler, R.W., 2020. A synthesis of methane emissions from shallow vegetated coastal ecosystems. Global Change Biology 26, 2988–3005. https://doi.org/10.1111/gcb.15046

Alongi, D.M., Sasekumar, A., Chong, V.C., Pfitzner, J., Trott, L.A., Tirendi, F., Dixon, P., Brunskill, G.J., 2004. Sediment accumulation and organic material flux in a managed mangrove ecosystem: estimates of land–ocean–atmosphere exchange in peninsular Malaysia. Marine Geology, Material Exchange Between the Upper Continental Shelf and Mangrove Fringed Coasts with Special Reference to the N. Amazon-Guianas Coast 208, 383–402. https://doi.org/10.1016/j.margeo.2004.04.016

Arias-Ortiz, A., Masqué, P., Glass, L., Benson, L., Kennedy, H., Duarte, C.M., Garcia-Orellana, J., Benitez-Nelson, C.R., Humphries, M.S., Ratefinjanahary, I., Ravelonjatovo, J., Lovelock, C.E., 2020. Losses of Soil Organic Carbon with Deforestation in Mangroves of Madagascar. Ecosystems. https://doi.org/10.1007/s10021-020-00500-z

Barber, A., Sirois, M., Chaillou, G., Gélinas, Y., 2017. Stable isotope analysis of dissolved organic carbon in Canada's eastern coastal waters. Limnology and Oceanography 62, S71–S84. https://doi.org/10.1002/lno.10666

Barbier, E.B., Hacker, S.D., Kennedy, C., Koch, E.W., Stier, A.C., Silliman, B.R., 2011. The value of estuarine and coastal ecosystem services. Ecological Monographs 81, 169–193. https://doi.org/10.1890/10-1510.1

Bouillon, S., Connolly, R.M., Lee, S.Y., 2008. Organic matter exchange and cycling in mangrove ecosystems: Recent insights from stable isotope studies. Journal of Sea Research, Mangrove Macrobenthos Special Issue 59, 44–58. https://doi.org/10.1016/j.seares.2007.05.001

Breithaupt, J.L., Smoak, J.M., Smith, T.J., Sanders, C.J., Hoare, A., 2012. Organic carbon burial rates in mangrove sediments: Strengthening the global budget. Global Biogeochemical Cycles 26. https://doi.org/10.1029/2012GB004375

Call, M., Sanders, C.J., Macklin, P.A., Santos, I.R., Maher, D.T., 2019. Carbon outwelling and emissions from two contrasting mangrove creeks during the monsoon storm season in Palau, Micronesia. Estuarine, Coastal and Shelf Science 218, 340–348. https://doi.org/10.1016/j.ecss.2019.01.002

Cameron, C., Hutley, L.B., Friess, D.A., Munksgaard, N.C., 2019. Hydroperiod, soil moisture and bioturbation are critical drivers of greenhouse gas fluxes and vary as a function of landuse change in mangroves of Sulawesi, Indonesia. Science of The Total Environment 654, 365–377. https://doi.org/10.1016/j.scitotenv.2018.11.092

Cameron, C., Hutley, L.B., Munksgaard, N.C., Phan, S., Aung, T., Thinn, T., Aye, W.M., Lovelock, C.E., 2021. Impact of an extreme monsoon on CO2 and CH4 fluxes from mangrove soils of the Ayeyarwady Delta, Myanmar. Science of The Total Environment 760, 143422. https://doi.org/10.1016/j.scitotenv.2020.143422

Chen, G., Gao, M., Pang, B., Chen, S., Ye, Y., 2018. Top-meter soil organic carbon stocks and sources in restored mangrove forests of different ages. Forest Ecology and Management 422, 87–94. https://doi.org/10.1016/j.foreco.2018.03.044

Chen, S., Chen, B., Chen, Guangcheng, Ji, J., Yu, W., Liao, J., Chen, Ganlin, 2021. Higher soil organic carbon sequestration potential at a rehabilitated mangrove comprised of Aegiceras corniculatum compared to Kandelia obovata. Science of The Total Environment 752, 142279. https://doi.org/10.1016/j.scitotenv.2020.142279

Cinco-Castro, S., Herrera-Silveira, J., Comín, F., 2022. Sedimentation as a Support Ecosystem Service in Different Ecological Types of Mangroves. Frontiers in Forests and Global Change 5.

Comer-Warner, S.A., Nguyen, A.T.Q., Nguyen, M.N., Wang, M., Turner, A., Le, H., Sgouridis, F., Krause, S., Kettridge, N., Nguyen, N., Hamilton, R.L., Ullah, S., 2022. Restoration impacts on rates of denitrification and greenhouse gas fluxes from tropical coastal wetlands. Science of The Total Environment 803, 149577. https://doi.org/10.1016/j.scitotenv.2021.149577

Corrigendum, 2020. . Global Change Biology 26, 5342–5342. https://doi.org/10.1111/gcb.15192

Dušek, J., Nguyen, V.X., Le, T.X., Pavelka, M., 2021. Methane and carbon dioxide emissions from different ecosystems at the end of dry period in South Vietnam. Trop Ecol 62, 1–16. https://doi.org/10.1007/s42965-020-00118-1

Google Earth Pro, 2024.

Hauser, L.T., Nguyen Vu, G., Nguyen, B.A., Dade, E., Nguyen, H.M., Nguyen, T.T.Q., Le, T.Q., Vu, L.H., Tong, A.T.H., Pham, H.V., 2017. Uncovering the spatio-temporal dynamics of land cover change and fragmentation of mangroves in the Ca Mau peninsula, Vietnam using multi-temporal SPOT satellite imagery (2004–2013). Applied Geography 86, 197–207. https://doi.org/10.1016/j.apgeog.2017.06.019

He, Z., Peng, Y., Guan, D., Hu, Z., Chen, Y., Lee, S.Y., 2018. Appearance can be deceptive: shrubby native mangrove species contributes more to soil carbon sequestration than fast-growing exotic species. Plant Soil 432, 425–436. https://doi.org/10.1007/s11104-018-3821-4

Hien, H.T., Marchand, C., Aimé, J., Cuc, N.T.K., 2018. Seasonal variability of CO2 emissions from sediments in planted mangroves (Northern Viet Nam). Estuarine, Coastal and Shelf Science 213, 28–39. https://doi.org/10.1016/j.ecss.2018.08.006

Himmelstoss, E.A., Henderson, R.E., Kratzmann, M.G., Farris, A.S., 2021. Digital Shoreline Analysis System (DSAS) Version 5.1 User Guide: U.S. Geological Survey Open-File Report 2021-1091 (User Guide). U.S. Geological Survey.

Hong, H.T.C., Avtar, R., Fujii, M., 2019. Monitoring changes in land use and distribution of mangroves in the southeastern part of the Mekong River Delta, Vietnam. Trop Ecol 60, 552–565. https://doi.org/10.1007/s42965-020-00053-1

Komada, T., Bravo, A., Brinkmann, M., Lu, K., Wong, L., Shields, G., 2022. "Slow" and "fast" in blue carbon: Differential turnover of allochthonous and autochthonous organic matter in minerogenic salt marsh sediments. Limnology & Oceanography 67. https://doi.org/10.1002/lno.12090

Kristensen, E., Bouillon, S., Dittmar, T., Marchand, C., 2008. Organic carbon dynamics in mangrove ecosystems: A review. Aquatic Botany 89, 201–219. https://doi.org/10.1016/j.aquabot.2007.12.005

Liu, K.-K., Kao, S.-J., Hu, H.-C., Chou, W.-C., Hung, G.-W., Tseng, C.-M., 2007. Carbon isotopic composition of suspended and sinking particulate organic matter in the northern South China Sea—From production to deposition. Deep Sea Research Part II: Topical Studies in Oceanography 54, 1504–1527. https://doi.org/10.1016/j.dsr2.2007.05.010

Lovelock, C.E., 2008. Soil Respiration and Belowground Carbon Allocation in Mangrove Forests. Ecosystems 11, 342–354. https://doi.org/10.1007/s10021-008-9125-4

Marchand, C., 2017. Soil carbon stocks and burial rates along a mangrove forest chronosequence. Forest ecology and management 384, 92. https://doi.org/10.1016/j.foreco.2016.10.030

Marchand, C., Lallier-Vergès, E., Baltzer, F., 2003. The composition of sedimentary organic matter in relation to the dynamic features of a mangrove-fringed coast in French Guiana. Estuarine, Coastal and Shelf Science 56, 119–130. https://doi.org/10.1016/S0272-7714(02)00134-8

Mcleod, E., Chmura, G.L., Bouillon, S., Salm, R., Björk, M., Duarte, C.M., Lovelock, C.E., Schlesinger, W.H., Silliman, B.R., 2011. A blueprint for blue carbon: toward an improved understanding of the role of vegetated coastal habitats in sequestering CO2. Frontiers in Ecology and the Environment 9, 552–560. https://doi.org/10.1890/110004

Natural Earth Data [WWW Document], 2009. . Natural Earth Data. URL naturalearthdata.com

Osland, M.J., Feher, L.C., Spivak, A.C., Nestlerode, J.A., Almario, A.E., Cormier, N., From, A.S., Krauss, K.W., Russell, M.J., Alvarez, F., Dantin, D.D., Harvey, J.E., Stagg, C.L., 2020. Rapid peat development beneath created, maturing mangrove forests: ecosystem changes across a 25-yr chronosequence. Ecol Appl 30. https://doi.org/10.1002/eap.2085

Osland, M.J., Spivak, A.C., Nestlerode, J.A., Lessmann, J.M., Almario, A.E., Heitmuller, P.T., Russell, M.J., Krauss, K.W., Alvarez, F., Dantin, D.D., Harvey, J.E., From, A.S., Cormier, N., Stagg, C.L., 2012. Ecosystem Development After Mangrove Wetland Creation: Plant–Soil Change Across a 20-Year Chronosequence. Ecosystems 15, 848–866. https://doi.org/10.1007/s10021-012-9551-1

Ouyang, X., Lee, S.Y., 2020. Improved estimates on global carbon stock and carbon pools in tidal wetlands. Nat Commun 11, 317. https://doi.org/10.1038/s41467-019-14120-2

Picarro, 2019. δ13C for Carbon Dioxide (CO2) CM-CRDS System.

Pribyl, D.W., 2010. A critical review of the conventional SOC to SOM conversion factor. Geoderma 156, 75–83. https://doi.org/10.1016/j.geoderma.2010.02.003

R Core Team, 2017. R: A language and environment for statistical computing.

Richards, D.R., Friess, D.A., 2016. Rates and drivers of mangrove deforestation in Southeast Asia, 2000–2012. Proc Natl Acad Sci USA 113, 344–349. https://doi.org/10.1073/pnas.1510272113

Rosentreter, J.A., Maher, D.T., Erler, D.V., Murray, R.H., Eyre, B.D., 2018. Methane emissions partially offset “blue carbon” burial in mangroves. Sci. Adv. 4, eaao4985. https://doi.org/10.1126/sciadv.aao4985

Son, N.-T., Chen, C.-F., Chang, N.-B., Chen, C.-R., Chang, L.-Y., Thanh, B.-X., 2015. Mangrove Mapping and Change Detection in Ca Mau Peninsula, Vietnam, Using Landsat Data and Object-Based Image Analysis. IEEE Journal of Selected Topics in Applied Earth Observations and Remote Sensing 8, 503–510. https://doi.org/10.1109/JSTARS.2014.2360691

Spivak, A.C., Sanderman, J., Bowen, J.L., Canuel, E.A., Hopkinson, C.S., 2019. Global-change controls on soil-carbon accumulation and loss in coastal vegetated ecosystems. Nat. Geosci. 12, 685–692. https://doi.org/10.1038/s41561-019-0435-2

Sun, Y., Xiong, H., Lee, M.-T., Brodie, C., Zong, Y., 2021. Geochemical dynamics and depositional history from mangrove sediments within the Pearl River estuary. Palaeogeography, Palaeoclimatology, Palaeoecology 584, 110701. https://doi.org/10.1016/j.palaeo.2021.110701

Tue, N.T., Hamaoka, H., Sogabe, A., Quy, T.D., Nhuan, M.T., Omori, K., 2011. The application of δ13C and C/N ratios as indicators of organic carbon sources and paleoenvironmental change of the mangrove ecosystem from Ba Lat Estuary, Red River, Vietnam. Environ Earth Sci 64, 1475–1486. https://doi.org/10.1007/s12665-011-0970-7

5 Carbon flux from geomorphically contrasting salt marsh sites

Abstract

Salt marshes are important carbon stores, increasing anthropogenic stressors on coastal ecosystems are however threatening salt marsh survival in a period of accelerated sea level rise. Sufficient sediment supply is needed to maintain salt marsh elevation within the tidal frame and prevent erosion of sequestered soil carbon. This study investigates the differences in carbon fluxes of a macro-tidal salt marsh with differing geomorphic conditions (i.e., eroding and prograding) in the Solway Firth, Scotland, UK. Carbon fluxes of in- vs. outflowing tidal waters during winter (January/February) and summer (June/July) and differential sedimentation on the marsh platform during winter were measured. This study showed that the eroding salt marsh site had sediment deposited of significantly coarser grain size (65.07 ± 10.1 µm vs 64.36 ± 3.9 µm) and lower inorganic carbon percentage (0.77 ± 0.32 % vs 1.01 ± 0.42 %) than the prograding salt marsh site. Though the sediment suspended within the tidal creeks (averaged over in – and outflowing tides) showed no significant difference between geomorphic conditions. This suggests that the site characteristics are potentially significant influencers on sedimentation and thus the resilience of the marsh environment. Furthermore, these results highlight the differential inorganic carbon sequestration potential between geographically different marshes, adding to the growing number of studies advocating for this property's inclusion in carbon sequestration budgets.

5.1 Introduction

Salt marshes are important coastal ecosystems. Besides the other ecosystem services they provide (coastal flood protection and biodiverse habitat), their ability to sequester carbon is increasingly recognised and valued (Macreadie et al., 2019; Mcleod et al., 2011). Alongside being naturally prone to disturbances due to their situation between the coastal and terrestrial environment, coastal ecosystems receive multiple stressors, direct anthropogenic stresses, or related to climate change. Critically, threats related to sea level rise (SLR) need to be robustly constrained, as marshes are at the interface between coastal and terrestrial systems. Salt marshes are dynamic, cyclical systems and their continued existence is dependent on vertical accretion (Reed et al., 1999). Only with sufficient sediment deposition will salt marshes be able to keep up with SLR (Ladd et al., 2019). Indeed a global review of salt marsh accretion rates found that 60% of marshes will not be able to accrete enough sediment to keep up with SLR by 2100 (Crosby et al., 2016).

Marsh vulnerability to degradation, inability to accrete enough sediment, has conventionally been measured with suspended sediment concentration (Fagherazzi et al., 2012). However, suspended sediment concentration (SSC) alone has been shown not to be a reliable predictor, as high SSC can also stem from an eroding marsh condition (Ganju et al., 2015). Leading to the proposition that instead, the differential between flood and ebb SSC should be calculated, quantifying the import and export of sediment (Ganju et al., 2015).

Sediment deposition and suspended sediment characteristics are also vital in understanding the carbon flux in and out of the system and thus its carbon sequestration potential (Mudd et al., 2009; Theuerkauf et al., 2015). Through the process of erosion, organic rich sediment is lost from the salt marsh and may be a net source of carbon to the coastal environment (Theuerkauf et al., 2015).

Using a bi-directional sediment sampler described by Elliott et al., (2017) is an inexpensive way of measuring the SSC and characteristics of the flood and ebb tides separately. It further provides the opportunity to sample locations, which are not easily accessible at high tide.

This study's objective was to connect suspended sediment composition and sediment deposition on the marsh platform with the erosional/accretional state of the salt marsh. The specific aims of the study were to 1) determine sediment deposition at two tidal creek catchments (eroding and prograding); 2) determine physical & chemical characteristics of flood and ebb tide suspended sediment concentration (carbon content, carbon stable isotope ratio and grain size) within two tidal creek catchments (eroding and prograding); 3) determine the relationship between tidal levels at the salt marsh edge and sediment deposition/suspended sediment concentration.

It was hypothesised that eroding sites will have a greater percent of sediment originating from the salt marsh deposited as well as suspended within the tidal waters. Prograding sites will potentially show a greater percentage of sediment originating from the mud flat deposited on the marsh as well as suspended within the tidal creeks.

5.2 Materials & Methods

5.2.1 Field study site

The study was conducted at the Caerlaverock salt marsh, Solway Firth, UK (Figure 5.1). The salt marsh is 8 km in length (Clyne et al., 2007) and has geomorphic different conditions, i.e., cliffed-eroding towards the west and sloping-prograding towards the east (Hansom, 2003). The marsh is characterised as meso-tidal and inundated diurnally during spring tides (Cutts and Hemingway, 1996; Chapter 2). The Solway Firth salt marsh is predominately comprised of C_3 plants, resulting in a $\delta^{13}C$ carbon stable isotope ratios of -20 ‰ to -26 ‰, such as *Puccinellia maritima*, however also *Spartina anglica*, as a plant with the C_4 photosynthetic pathway has been introduced to the UK, which results in a carbon stable isotope ratio of -12.4 ‰ to -14 ‰ (MacKenzie et al., 2004). A vegetation survey conducted during the June deployment within 1m radius of the sediment deposition cups showed no plant species utilising the C_4 photosynthetic pathway (i.e., *Spartina spp*.).

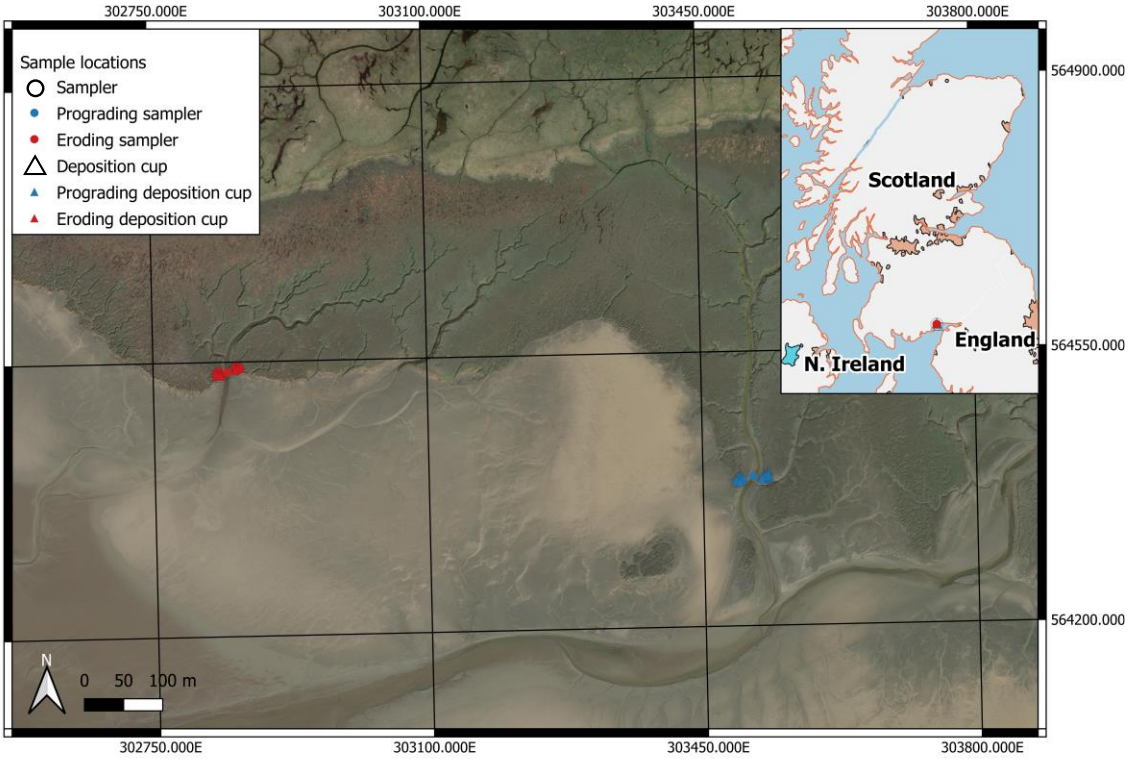

Figure 5.1 Map of study location at Caerlaverock salt marsh in Scotland, Solway Firth, UK. Circle = suspended sediment sampler; triangle = sediment deposition cup; blue = prograding site; red = eroding site. Inset map showing study location within Scotland.

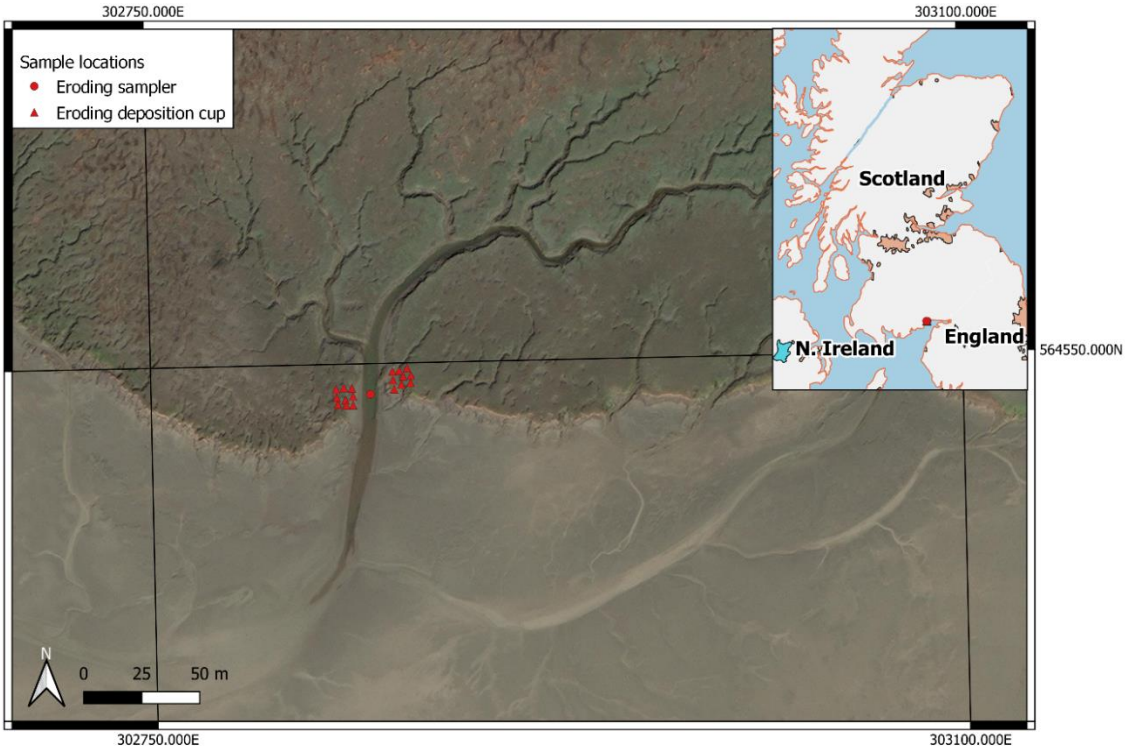

Figure 5.2 Map of eroding salt marsh study location at Caerlaverock salt marsh in Scotland, Solway Firth, UK. Circle = suspended sediment sampler; triangle = sediment deposition cup; red = eroding site. Inset map showing study location within Scotland.

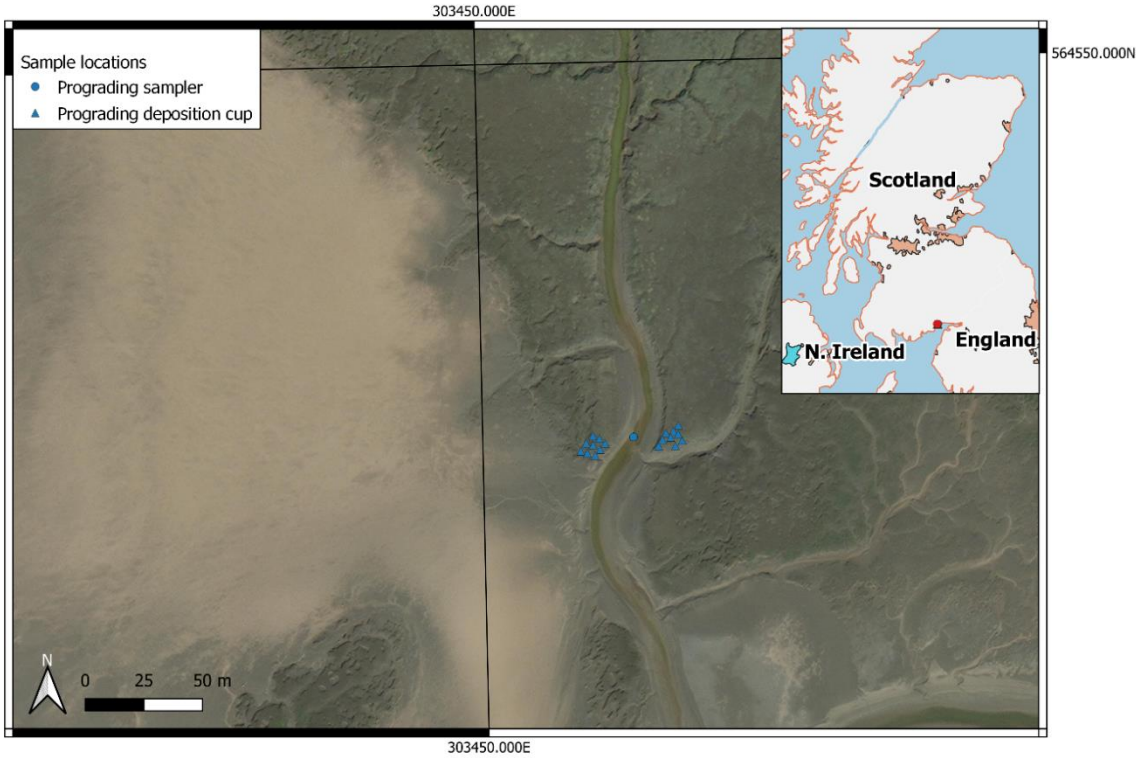

Figure 5.3 Map of prograding salt marsh study location at Caerlaverock salt marsh in Scotland, Solway Firth, UK. Circle = suspended sediment sampler; triangle = sediment deposition cup; blue = prograding site. Inset map showing study location within Scotland.

5.2.2 Sample collection

Two tidal creeks within the Caerlaverock salt marsh were selected, one creek draining an eroding stretch of marsh and one creek draining a prograding marsh (Figure 5.2, Figure 5.3). Sampling was conducted during 2 spring tidal cycles in winter 2023 and summer 2023 (Table 5.1).

Sediment deposition cups were deployed adjacent to the tidal creeks on the salt marsh flats in a 3x3 grid on both sites with a distance of 3m between cups. The sampling design encompassed: two eroding conditions, 18 sediment deposition cups per condition (locations), with two sampling times per deposition cup (Table 5.3).

Suspended sediment samplers were built following the instructions by Elliott et al., (2017). The samplers were collecting water from the tidal creek. Suspended sediment from either the inflowing or outflowing tide was retained within the sampler, depending on the direction and shape of the inflow tube (Figure 5.4). One pair (inflowing and outflowing) was placed in the tidal creek leading to an eroding site and another in a tidal creek to a prograding salt marsh site (Table 5.2, Figure 5.5).

Non-vented pressure loggers (Rugged TROLL 100) were attached to the sediment samplers and took readings with a frequency of 10 minutes. Water level pressure readings were corrected for atmospheric pressure from local measurements.

Table 5.1 Measurement campaigns.

Dates	**Season**	**Sediment deposition cups**	**Suspended sediment samplers**
17.01. – 31.01.2023	Winter	Yes	Yes
31.01. – 17.02.2023	Winter	Yes	Yes
08.06. – 22.06.2023	Summer	Yes	Yes
22.06. – 13.07.2023	Summer	No	Yes

Table 5.2 Suspended sediment sampler location and elevation of water level logger.

Site	**Season**	**Easting**	**Northing**	**Elevation**
Eroding	Winter	302844.453	564536.819	3.248
Prograding	Winter	303514.216	564390.44	3.235
Eroding	Summer	302843.379	564534.879	3.158
Prograding	Summer	303509.11	564385.581	3.093

Table 5.3 Deposited sediment sample size per sampling campaign.

Site	Location	Sampling campaigns	Analysis	Number of samples
Eroding	18	17.01. – 31.01.2023	Carbon analysis	8
			Grain size	12
			Sediment weight	14
		31.01.2023 – 17.02.2023	Carbon analysis	10
			Grain size	12
			Sediment weight	15
Prograding	18	17.01. – 31.01.2023	Carbon analysis	18
			Grain size	18
			Sediment weight	18
		31.01.2023 – 17.02.2023	Carbon analysis	10
			Grain size	10
			Sediment weight	18

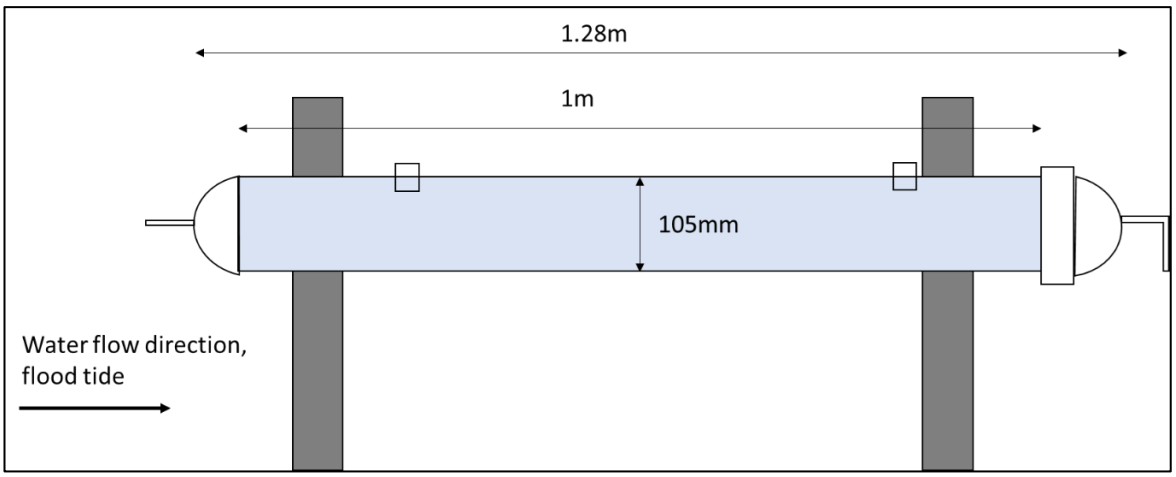

Figure 5.4 Schematic drawing of bi-directional suspended sediment sampler. Modified from Elliott et al., (2017).

Figure 5.5 Image of suspended sediment samplers within tidal creek.

5.2.3 Sample analysis

Sediment samples were freeze-dried for 48 hours following collection. Subsamples were taken to determine grain size, total carbon content, and total carbon stable isotope ratio ($\delta^{13}C$), as well as organic carbon content and organic carbon stable isotope ratio ($\delta^{13}C$). The grain size analysis could not be performed for some samples from the sediment deposition cups, as not enough material was available.

The grain size analysis was performed on an approx. 5 g subsample treated with hydrogen peroxide (100 volumes > 30%), which was left to react for two hours before more hydrogen peroxide was added and left overnight (Gray et al., 2010). Samples were consequently heated to 100 °C until the reaction ceased and a clear layer of supernatant formed. The samples were centrifuged at 2500 rpm after which they were dried at 90 °C for 24 hours. The grain size analysis was performed with Bettersize 2600 Particle Size analyser, for which 25 ml of water and 5 ml of Calgon were added to the dried sample and put into an ultrasonic bath for 3 minutes. The sample was then pipetted into the analyser.

Carbon stable isotope ratio ($\delta^{13}C$) and carbon content (mg/mg) were analysed from the freeze-dried subsamples using a Picarro Cavity Ring-down Spectrometer (G2201-*i*), which was coupled with a combustion module (A0201). Samples were weighed into tin capsules. The values of carbon stable isotope are presented in the standard delta notation (‰), which is relative to the Vienna Pee Dee Belemnite (VPDB) standard. The sample accuracy for $\delta^{13}C$ is between 0.2 to 0.3‰ (Picarro, 2019).

Organic carbon content and stable isotope signature ($\delta^{13}C_{org}$) was determined on a freeze-dried subsample. The sample was treated with HCl (3% vol) to remove inorganic carbon, until it ceased to effervesce, diluted to neutral pH, and dried before a known mass was placed in a tin capsule and analysed with the Picarro G2201-*i* coupled to a combustion module. The difference between total carbon content and organic carbon content was used to quantify inorganic carbon.

$$\boldsymbol{\delta X = 1000 * (\frac{R_{sample}}{R_{standard}} - 1)} \qquad \textbf{Equation 5.1}$$

Where X = $\delta^{13}C$ and R is ratio of heavy and light isotopes (^{13}C:^{12}C). $\delta^{13}C$ expressed as parts per mil (‰) differences relative to the Pee Dee belemnite international standard.

5.2.4 Statistical analysis

All statistical analyses were performed using R-Studio (2022.12.0). Inorganic carbon percentage below 0% was regarded as 0% percentage, further any samples with $\delta^{13}C_{org}$ signature below $\delta^{13}C_{TC}$ were regarded as having 0% inorganic carbon (Mueller et al., 2023). Statistical analyses on deposited sediment characteristics between geomorphic conditions were performed using Linear Mixed Effects Models (sampling date nested within erosion condition) with the lmer function of the *lme4* package (Bates et al., 2015). Data was transformed to meet normality assumptions (Table 5.4). Suspended sediment characteristics were analysed using two-way ANOVAs with an interaction between geomorphic condition and season. Log transformation and arcsine transformation were applied to data which did not meet the assumption of normal distribution of residuals. Statistical difference between total carbon and organic carbon stable isotope signatures of deposited, suspended and reference soil samples was calculated using paired t-tests, if differences between pairs were not normally distributed, the paired samples Wilcoxon rank test was used.

Sediment weight differences for eroding and prograding site was calculated by subtracting the weight of outflowing sediment from the inflowing sediment (Difference = Inflowing – Outflowing).

Sediment particle size distribution was determined using the Kolmogorov-Smirnov two-sample statistical test, following Phillips et al., (2000). The distribution of reference material taken from the mudflat and salt marsh at both eroding and prograding site was compared to i) deposited sediment at each geomorphic site; ii) retained suspended sediment during winter and summer sampling campaigns; iii) retained suspended sediment for in- and outflowing samplers.

Tidal inundations of sediment deposition cups were calculated for the entire winter deployment and differences between geomorphic condition was statistically tested using the Wilcoxon sign rank test. An exponential regression model was fitted to the relationship between deposited sediment weight and inundation time. Correlations between organic carbon percentage and the elevation of deposition cups and the distance to the tidal channel were calculated using the Spearman's rank correlation test, as the assumption of normal distribution was not met.

Difference in inundation duration of the suspended sediment samplers was tested using the unpaired two-sample t-test between seasons for grouped geomorphic conditions (eroding and prograding together).

5.3 Results

5.3.1 Sediment deposition

Sediment deposited on the salt marsh flat at eroding and prograding sites during the winter differed significantly in their sediment weight as well as in their clay and silt percentage (Table 5.4). Silt percentage was significantly greater at prograding sites, whereas clay percentage and sediment weight were significantly lower at prograding sites (Figure 5.6). The difference between total and organic carbon stable isotope ratios ($\delta^{13}C_{TC}$, $\delta^{13}C_{org}$) of deposited sediment during winter was significant (t=16.784; df = 45; p-value < 0.001).

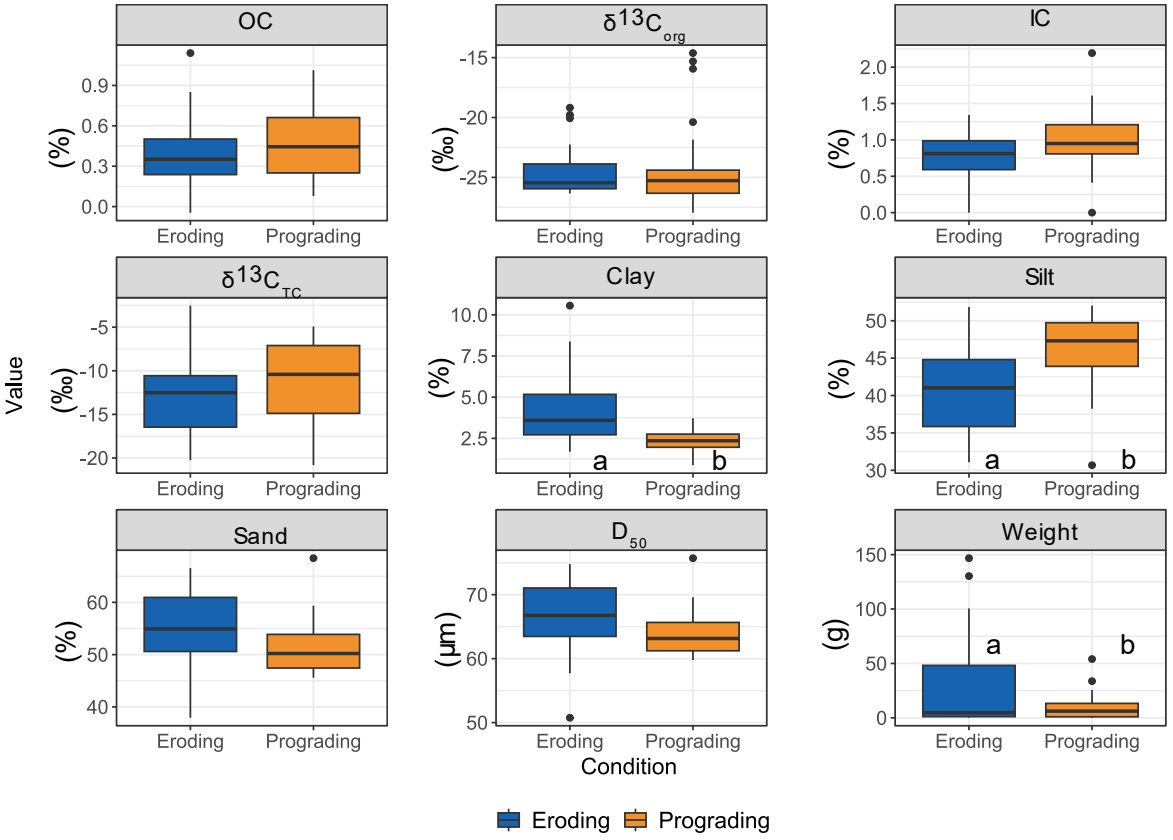

Figure 5.6 Boxplots of deposited sediment on salt marsh during winter (January and February 2023) between eroding (n=44) and prograding (n=54) marsh. OC = organic carbon percentage; $\delta^{13}C_{org}$ = organic carbon stable isotope ratio; IC = inorganic carbon percentage; $\delta^{13}C_{TC}$ = total carbon stable isotope ratio; Clay = clay percentage; Silt = silt percentage; Sand = sand percentage; D_{50} = Median grain size (µm); Weight = Deposited sediment weight (g).

Table 5.4 Statistical summary of predictor variables from the Linear Mixed Effects Model (LMM) of deposited sediment characteristics with "Sampling Date" as random intercept, i.e., nested within condition (Variable ~ Condition + (1 | Cup)).

Variable ~ Condition [prograding]	**Transformation**	**Estimate**	**SE**	**t-value**	**P-value**
Organic carbon percentage	log	0.05	0.056	0.898	0.374
$\delta^{13}C_{org}$	reciprocal	0.046	0.055	0.835	0.408
Inorganic carbon percentage	NA	0.246	0.125	1.964	0.062
$\delta^{13}C_{TC}$	square	-41.69	27.31	-1.526	0.136
Clay percentage	**log**	**-0.531**	**0.115**	**-4.6**	**<0.001**
Silt percentage	**NA**	**5.435**	**1.753**	**3.10**	**0.004**
Sand percentage	NA	-3.71	2.014	-1.842	0.075
Median grain size	NA	-2.573	1.528	-1.683	0.102
Sediment weight (g)	**NA**	**-21.738**	**10.287**	**-2.113**	**0.043**

5.3.2 Suspended sediment

The suspended sediment characteristics differed significantly between seasons for organic and inorganic carbon percentage, and $\delta^{13}C_{TC}$ signature. With higher values during winter for IC and $\delta^{13}C_{TC}$. Clay, silt, and sand percentages of the suspended sediment samples showed a significantly different interaction of geomorphic condition and season (Table 5.5). However, not between sites during the same season (Table 5.5). Clay and silt percentages were significantly greater during summer at both the eroding and prograding site than during the winter, whereas the sand percentage was significantly higher during winter than summer (Figure 5.7).

The difference between $\delta^{13}C_{TC}$ and $\delta^{13}C_{org}$ was significant ($t=16.483$; $df = 14$; p-value < 0.001). $\delta^{13}C_{org}$ was significantly lower than $\delta^{13}C_{TC}$.

Given the small sample size per inflowing and outflowing sampling during each season, the differences in sediment characteristics could not be statistically tested, though initial data suggests some potential variability (Figure 5.8, Figure 5.9). Organic carbon percentage was higher at the inflowing eroding site during winter than prograding or outflowing samples. During the summer deployment, the prograding site had the highest percentage of organic carbon compared to the eroding site for both inflowing and outflowing sampling. A clear difference could also be seen regarding the $\delta^{13}C_{org}$, being highest at the eroding inflowing site during winter. During summer, the highest signature was measured at the prograding outflowing site. During winter, the inorganic carbon percentage was higher for the eroding site from the outflowing than the inflowing tide. $\delta^{13}C_{TC}$ was during both seasons higher for

the inflowing tide. The percentage of clay was greater in the outflowing tide than inflowing tide for the winter sampling campaign for the prograding site (Figure 5.9). The eroding site had a greater silt percentage during winter in the sediment from the outflowing tide than the inflowing tide. The sand percentage at the eroding site showed that during winter more sand was transported in than out.

The sediment weight difference between inflowing and outflowing tides showed that more sediment is being transported into the salt marsh during inflowing tides at the eroding site (Figure 5.10). At the prograding site, more sediment is however transported out of the salt marsh than into the system.

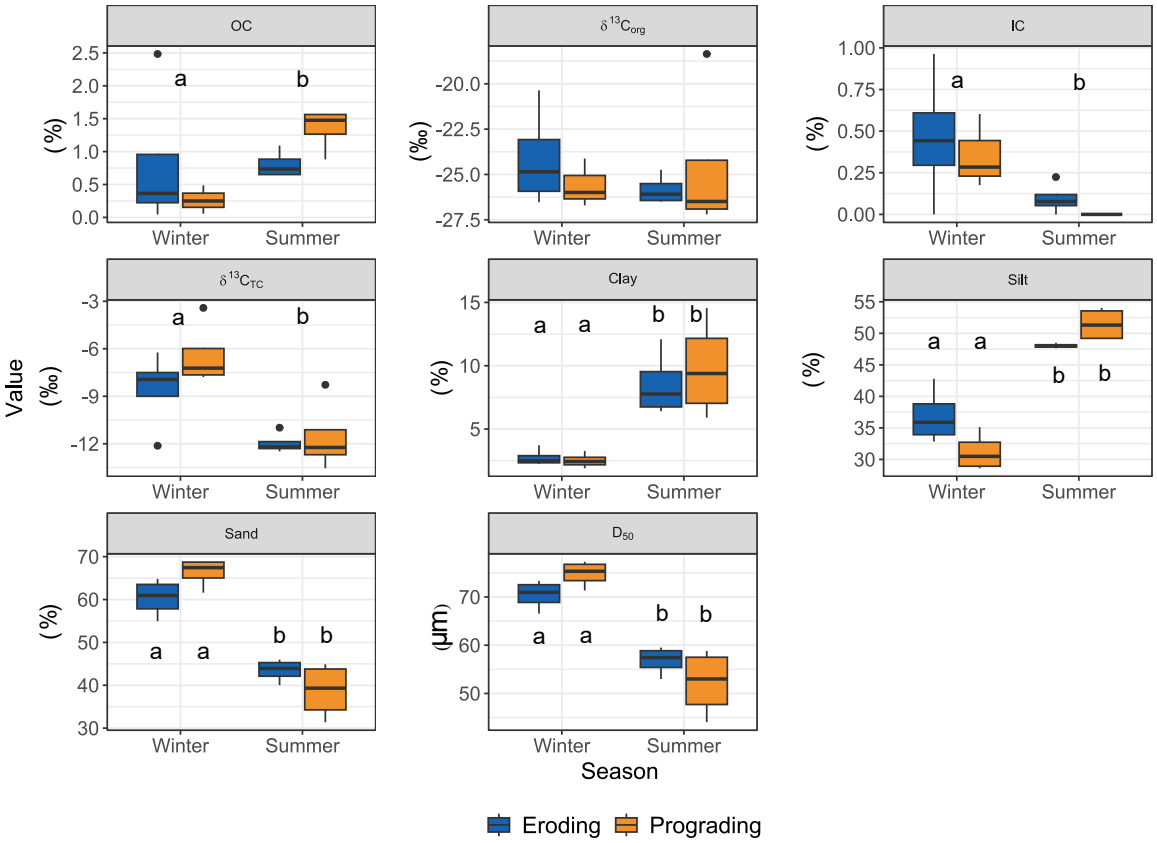

Figure 5.7 Suspended sediment characteristics between eroding and prograding sites between winter and summer. OC = organic carbon percentage; $\delta^{13}C_{org}$ = organic carbon stable isotope ratio; IC = inorganic carbon percentage; $\delta^{13}C_{TC}$ = total carbon stable isotope ratio; Clay = clay percentage; Silt = silt percentage; Sand = sand percentage; D_{50} = Median grain size (µm). Post-hoc analyses: two letter = Season factor difference; four letters = Condition:Season interaction difference.

Table 5.5 Two-way ANOVA results of sediment characteristics of suspended sediment sampled during winter (January, February) and summer (June, July) deployment.

Response	Factor	Df	Sum Sq	Mean Sq	F value	PR(>F)
$\delta^{13}C_{TC}$	Condition	1	6.46	6.46	1.602	0.2297
	Season	**1**	**73.37**	**73.37**	**18.189**	**0.0011**
	Condition:Season	1	3.08	3.08	0.763	0.3995
	Residuals	12	48.41	4.03		
Clay percentage (log transformed)	Condition	1	0.001	0.001	0.007	0.934
	Season	**1**	**5.967**	**5.967**	**67.751**	**2.81e-06**
	Condition:Season	1	0.040	0.040	0.453	0.514
	Residuals	12	1.057	0.088		
Sand percentage	Condition	1	1.4	1.4	0.069	0.7977
	Season	**1**	**1983.6**	**1983.6**	**99.115**	**3.76e-07**
	Condition:Season	**1**	**113.3**	**113.3**	**5.659**	**0.0348**
	Residuals	12	240.2	20.0		
Silt percentage	Condition	1	5.1	5.1	0.567	0.466
	Season	**1**	**990.2**	**990.2**	**111.120**	**2.02e-07**
	Condition:Season	**1**	**83.0**	**83.0**	**9.318**	**0.010**
	Residuals	12	106.9	8.9		
Organic carbon percentage (log transformed)	Condition	1	0.038	0.038	0.038	0.8495
	Season	**1**	**6.600**	**6.600**	**6.635**	**0.0258**
	Condition:Season	1	1.154	1.154	1.160	0.3045
	Residuals	11	10.942	0.995		
Inorganic carbon percentage (Arcsine transformed)	Condition	1	0.001086	0.001086	1.714	0.21716
	Season	**1**	**0.007156**	**0.007156**	**11.294**	**0.00636**
	Condition:Season	1	0.000603	0.000603	0.952	0.35011
	Residuals	11	0.006970	0.000634		
$\delta^{13}C_{org}$ (Arcsine transformed)	Condition	1	0.153	0.1533	0.276	0.610
	Season	1	0.269	0.2689	0.484	0.501
	Condition:Season	1	0.132	0.1316	0.237	0.636
	Residuals	11	6.116	0.5560		
Median grain size (square transformed)	Condition	1	25749	25749	0.107	0.7492
	Season	**1**	**20945891**	**20945891**	**87.072**	**7.53e-07**
	Condition:Season	**1**	**1227555**	**1227555**	**5.103**	**0.0433**
	Residuals	12	2886698	240558		

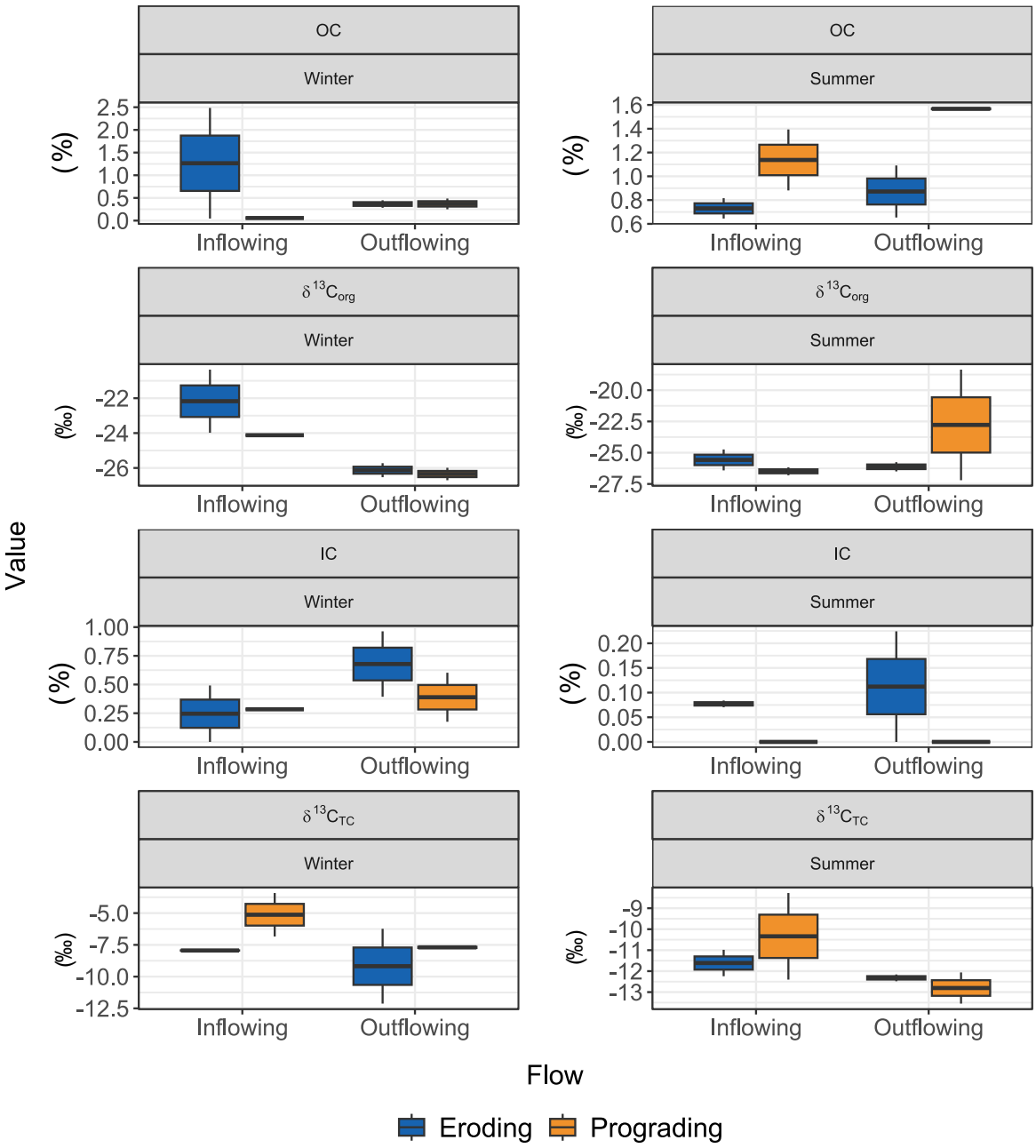

Figure 5.8 Suspended sediment characteristics between eroding and prograding site for summer and winter and in- and outflowing tide. OC = organic carbon percentage; $\delta^{13}C_{org}$ = organic carbon stable isotope ratio; IC = inorganic carbon percentage; $\delta^{13}C_{TC}$ = total carbon stable isotope ratio.

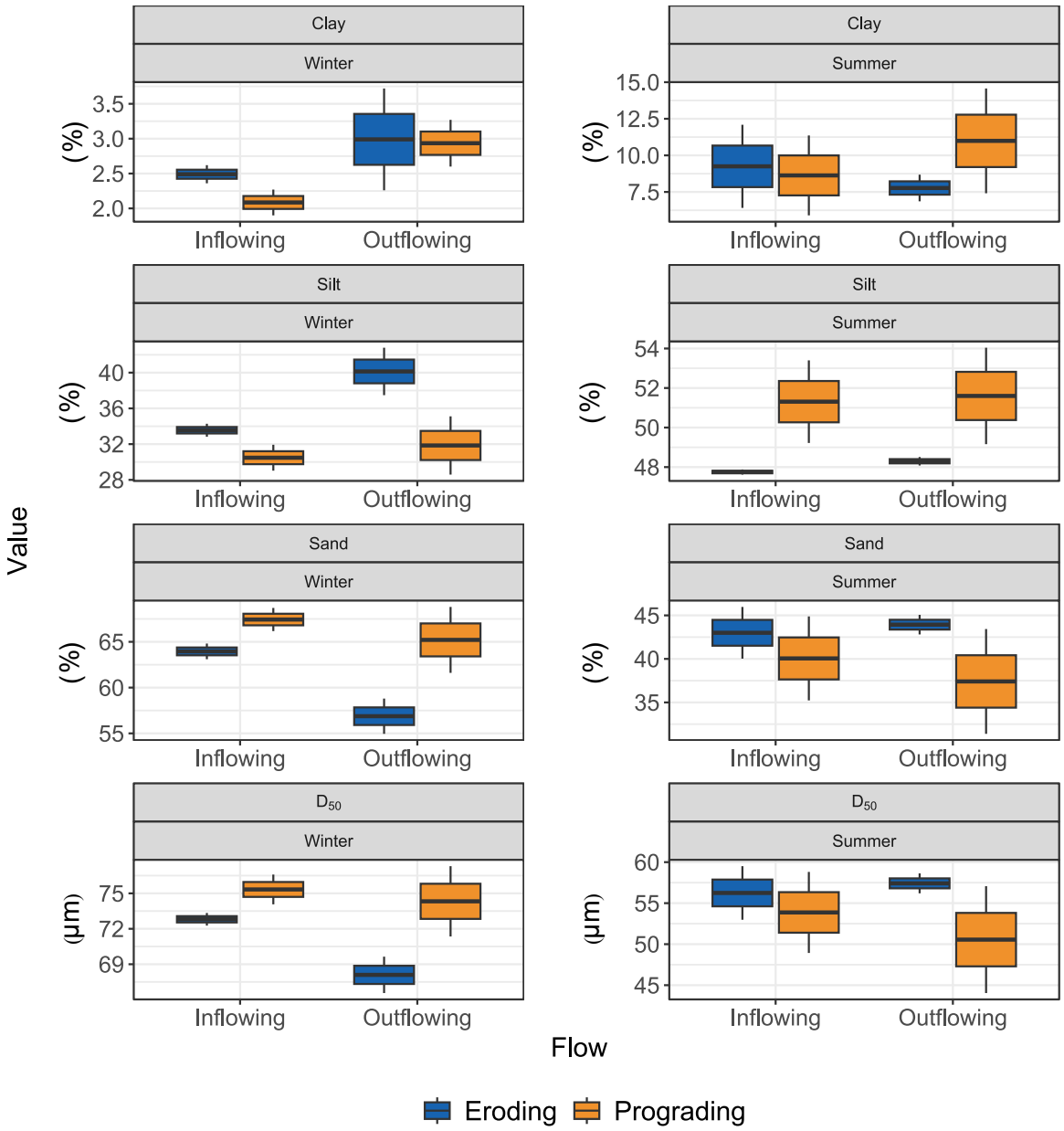

Figure 5.9 Suspended sediment characteristics between eroding and prograding site for summer and winter and in- and outflowing tide. Clay = clay percentage; Silt = silt percentage; Sand = sand percentage; D50 = Median grain size (µm).

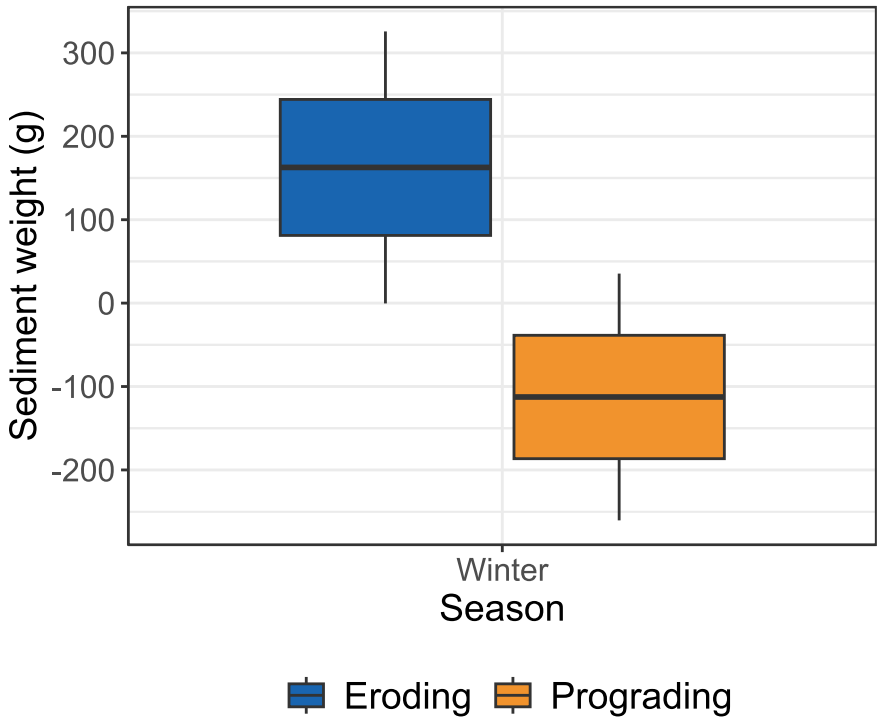

Figure 5.10 Suspended sediment weight difference (g) between inflowing and outflowing sampler (Difference = Inflowing - outflowing) for eroding and prograding site during the winter sampling campaign. Higher sediment weight = more sediment inflowing than outflowing.

5.3.3 Mudflat and Salt marsh sediment

Mud flat surface soil samples had a greater organic carbon concentration, organic carbon stable isotope ratio, clay percentage, and sand percentage at the prograding site than the eroding site (Figure 5.11). The mud flat inorganic carbon percentage, total carbon stable isotope ratio and silt percentage were greater at the eroding than prograding site. Soil surface samples from the salt marsh were higher at prograding sites for inorganic carbon percentage as well as the silt percentage (Figure 5.11). Only the sand percentage at the eroding site was greater value than the prograding site. The clay percentage, $\delta^{13}C_{org}$, and $\delta^{13}C_{TC}$ the signatures were similar for salt marsh surface soil samples. There was a significant difference between the isotopic signatures of total carbon and organic carbon (V=36; p-value < 0.01).

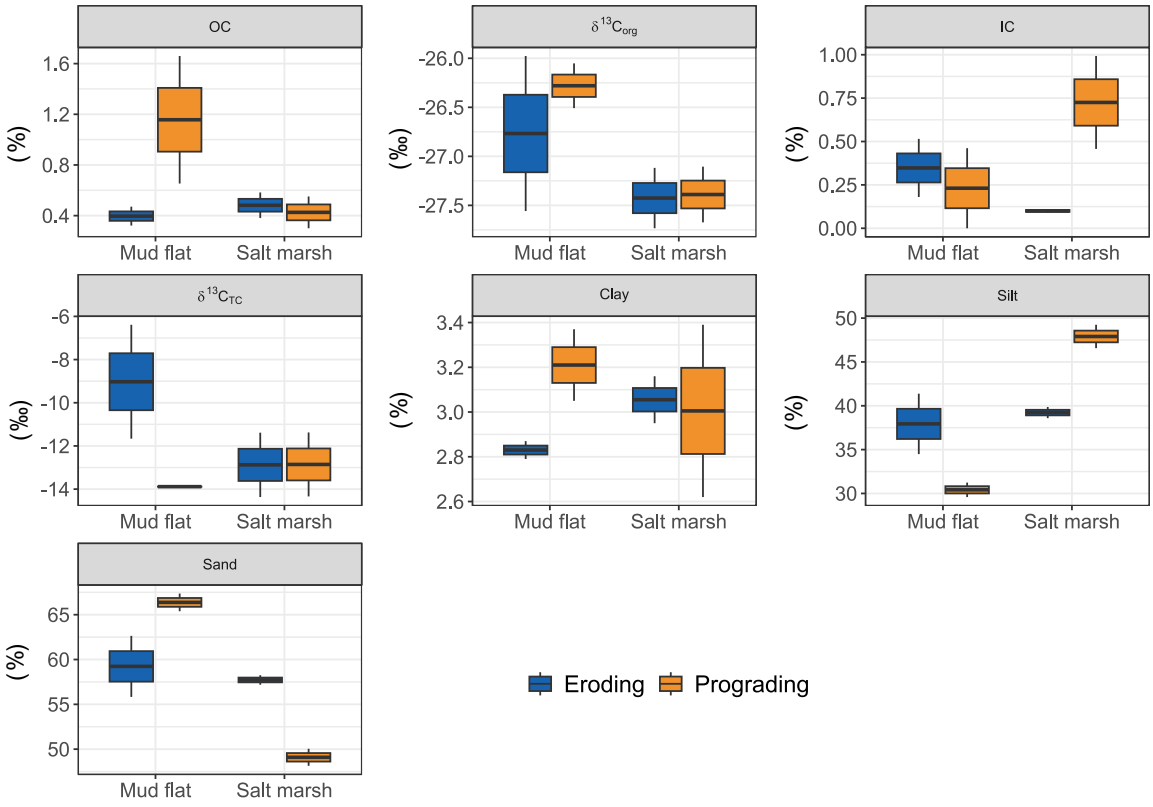

Figure 5.11 Sediment characteristics of mud flat and salt marsh surface soil samples at eroding and prograding sites. OC = organic carbon percentage; $\delta^{13}C_{org}$ = organic carbon stable isotope ratio; IC = inorganic carbon percentage; $\delta^{13}C_{TC}$ = total carbon stable isotope ratio; Clay = clay percentage; Silt = silt percentage; Sand = sand percentage.

5.3.4 Particle size distribution

The average particle size distribution of the deposited sediment at the eroding site was significantly different to the reference distribution of both the salt marsh and mudflat sample, D = 0.28, p-value < 0.001 and D = 0.28, p-value < 0.001, respectively. At the prograding site, the distribution of the deposited sediment was not significantly different to the reference distribution (Figure 5.12). The deposited sediment particle size distributions were significantly different between the eroding and prograding site (D = 0.28, p-value < 0.0007873).

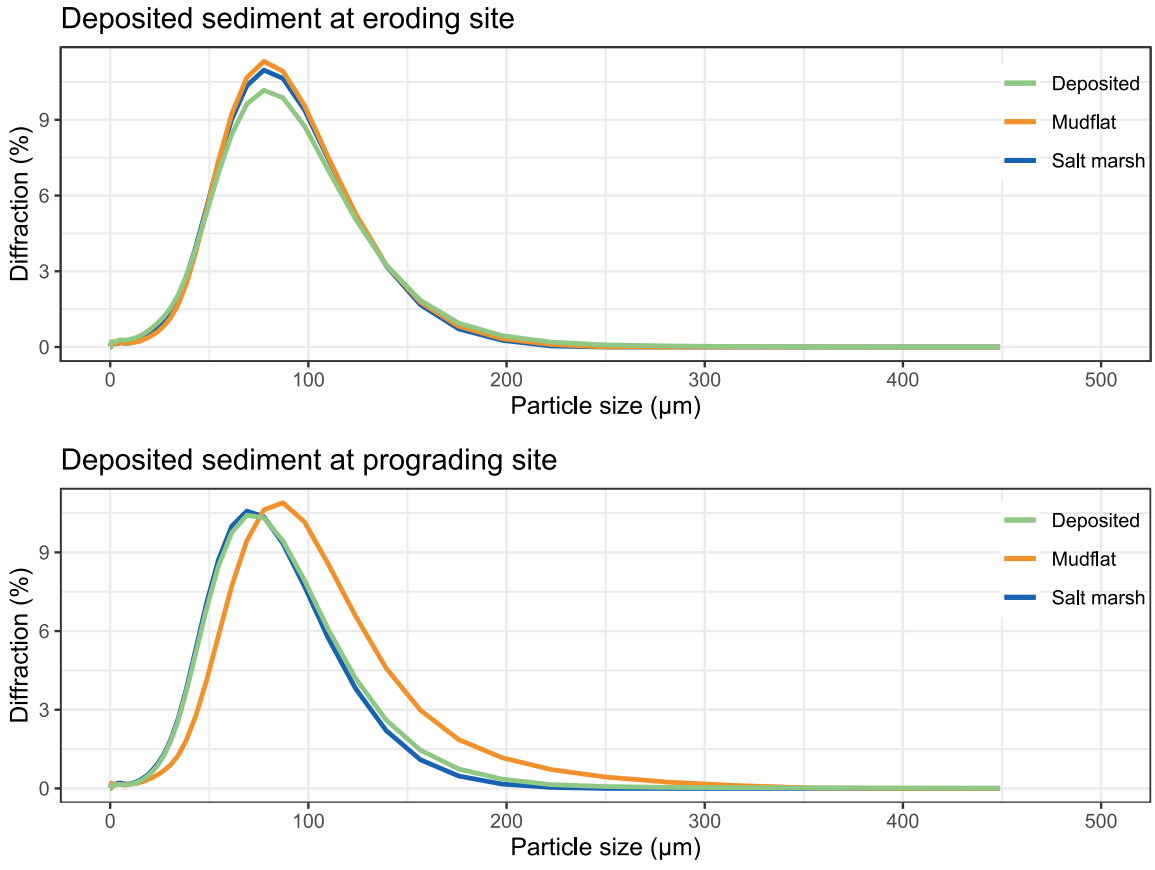

Condition	Sample ID	Sediment d_{50} (µm)
Eroding	Salt marsh	68.69
	Mudflat	69.555
	Deposited sediment - winter	65.068
Prograding	Salt marsh	62.37
	Mudflat	76.095
	Deposited sediment - winter	64.357

Figure 5.12 Top: Particle size distribution of deposited sediment during winter sampling campaign at eroding and prograding site; Bottom: Median grain size (d_{50}) of reference and deposited sediment.

The particle size distribution of suspended sediment retained within the sampler during summer was significantly different from the salt marsh ($D = 0.31$, p-value < 0.001) as well as the mudflat ($D = 0.32$, p-value < 0.0001). There was no significant difference during winter at the eroding site (Figure 5.13). Comparing the particle size distribution of suspended sediment, there is also a significant difference between the distribution during winter and summer ($D = 0.31$, p-value < 0.001). The distribution of retained suspended sediment at the prograding site was significantly different during summer from both the salt marsh and the mudflat, $D = 0.31$, p-value < 0.001 and $D = 0.3$, p-value < 0.001, respectively (Figure 5.13). During winter the sediment was further significantly different from the mudflat ($D = 0.21$, p-value 0.024), however not from the salt marsh. The retained suspended sediment at the prograding site was also significantly different between seasons ($D = 0.33$, p-value < 0.0001).

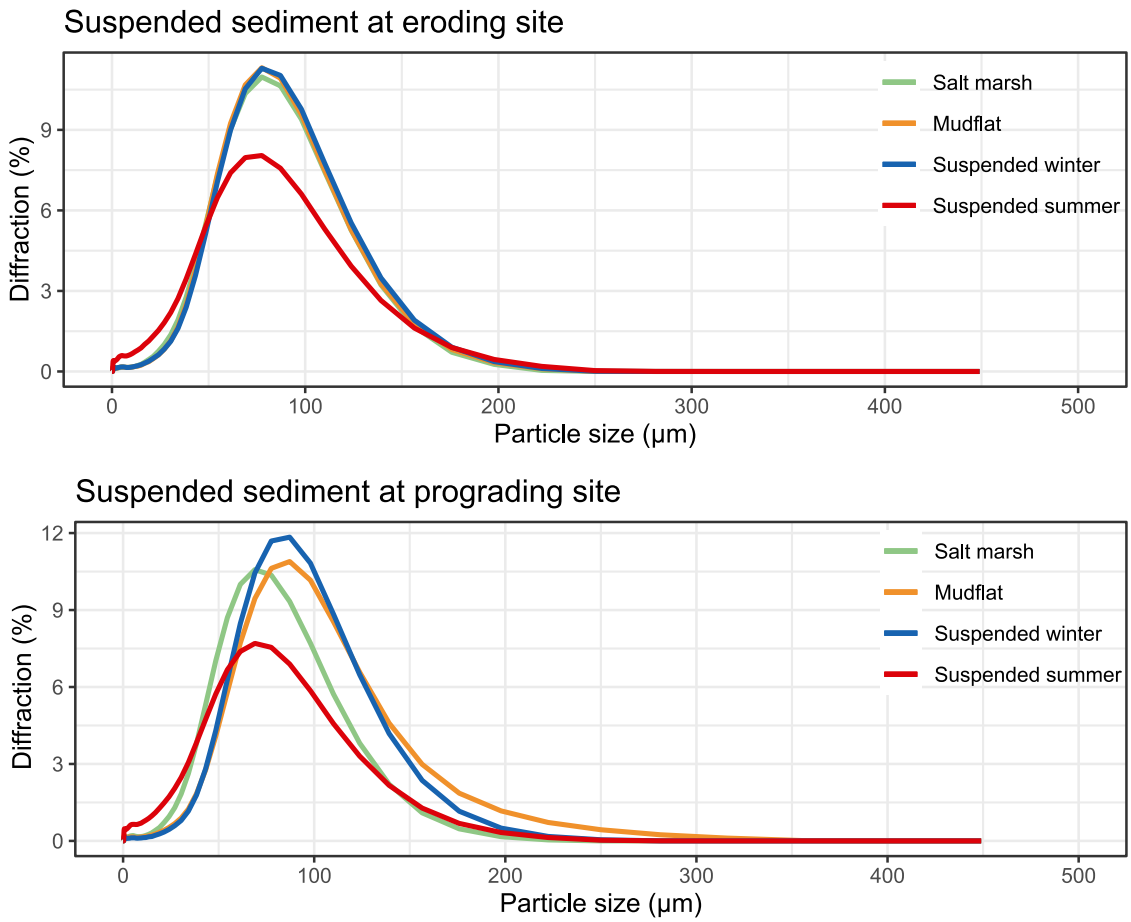

Condition	Sample ID	Sediment d_{50} (µm)
Eroding	Salt marsh	68.69
	Mudflat	69.555
	Suspended sediment - winter	70.4525
	Suspended sediment - summer	56.83
Prograding	Salt marsh	62.37
	Mudflat	76.095
	Suspended sediment - winter	74.8275
	Suspended sediment - summer	52.2125

Figure 5.13 Top: Sediment particle size distribution of retained suspended sediment within sediment sampler during winter (blue) and summer (red) sampling campaigns at eroding and prograding site; Bottom: Median grain size (d_{50}) of reference and retained suspended sediment.

The particle size distribution between the reference salt marsh at the eroding site was significantly different to the inflowing and outflowing retained suspended sediment samples (D = 0.3, p-value < 0.001 and D = 0.28, p-value < 0.001, respectively), same for the mudflat reference sample (Figure 5.14). The particle size distribution for the prograding site was significantly different for all reference samples to in- and outflowing retained sediments. The distribution was not significantly different between in-and outflowing samples.

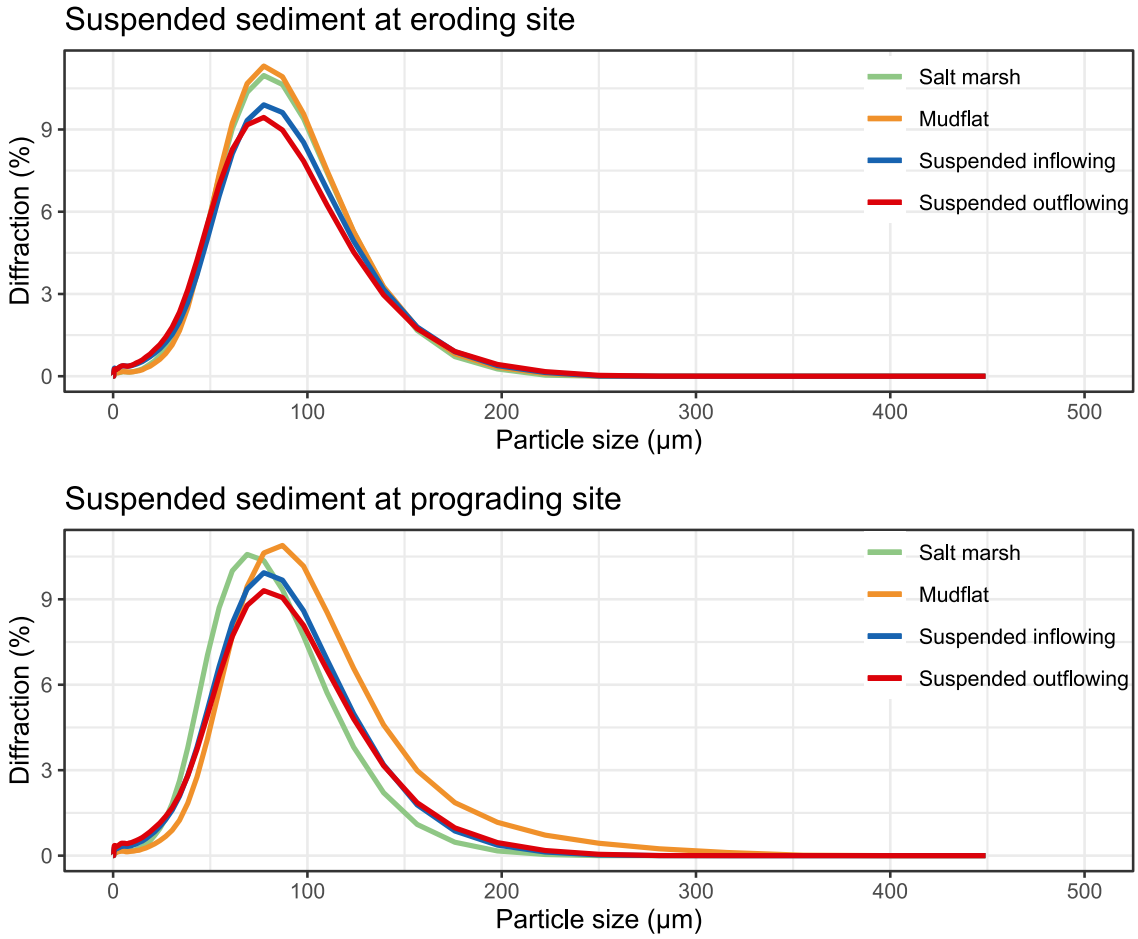

Condition	Sample ID	Sediment d_{50} (µm)
Eroding	Salt marsh	68.69
	Mudflat	69.555
	Suspended sediment – inflowing	64.525
	Suspended sediment – outflowing	62.7575
Prograding	Salt marsh	62.37
	Mudflat	76.095
	Suspended sediment – inflowing	64.6
	Suspended sediment - outflowing	62.44

Figure 5.14 Top: Sediment particle distribution of retained suspended sediment within sampler for inflowing (blue) and outflowing (red) tides for eroding and prograding site combined for all seasons; Bottom: Median grain size (d_{50}) of reference and retained suspended sediment.

5.3.5 Tidal inundation

The tidal inundations of the sediment deposition cups during winter deployment (January and February 2023) were significantly greater at the eroding than the prograding salt marsh site (W = 748, p-value < 0.001; Figure 5.15). Sediment weight deposited within the cups at both salt marsh sites is significantly exponentially related to the inundation time (F = 51.89; p-value < 0.0001; Figure 5.15). The organic carbon percentage is not significantly correlated with the elevation of the deposition cups (r = 0.26; p-value = 0.08), nor with the distance to the channel (r = -0.07; p-value = 0.597).

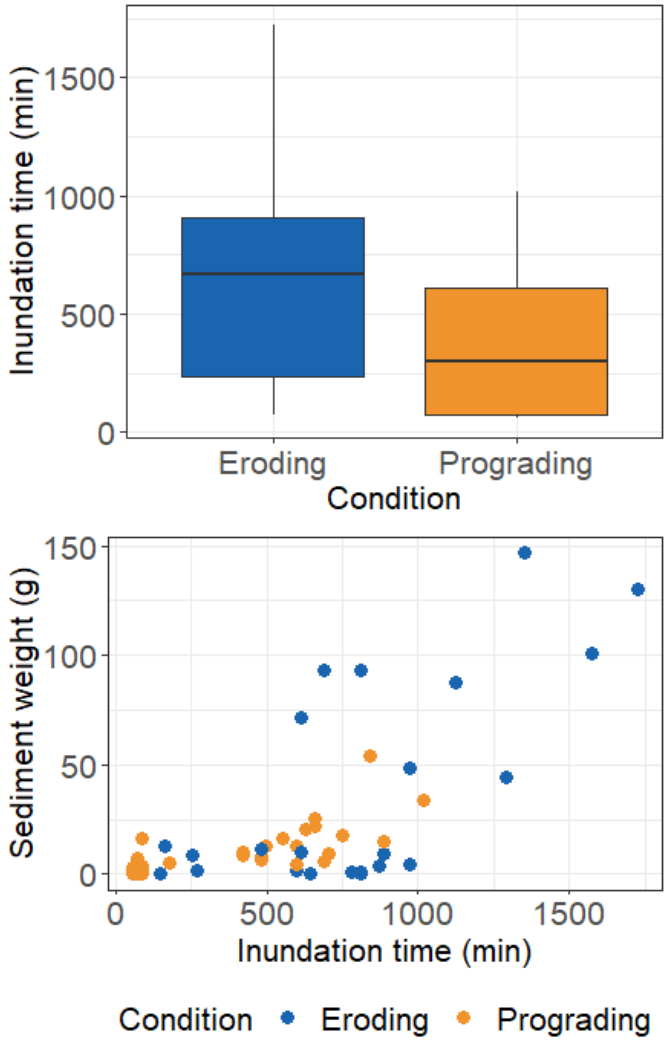

Figure 5.15 Top: Average inundation time (min) for sediment cups between eroding and prograding site for winter (January, February) deployment; Bottom: Sediment weight vs inundation time (min) between eroding and prograding sites.

The average inundation time of the sediment samplers was not significantly different between seasons (t= -1.3272, df = 6; p-value = 0.233; Figure 5.16).

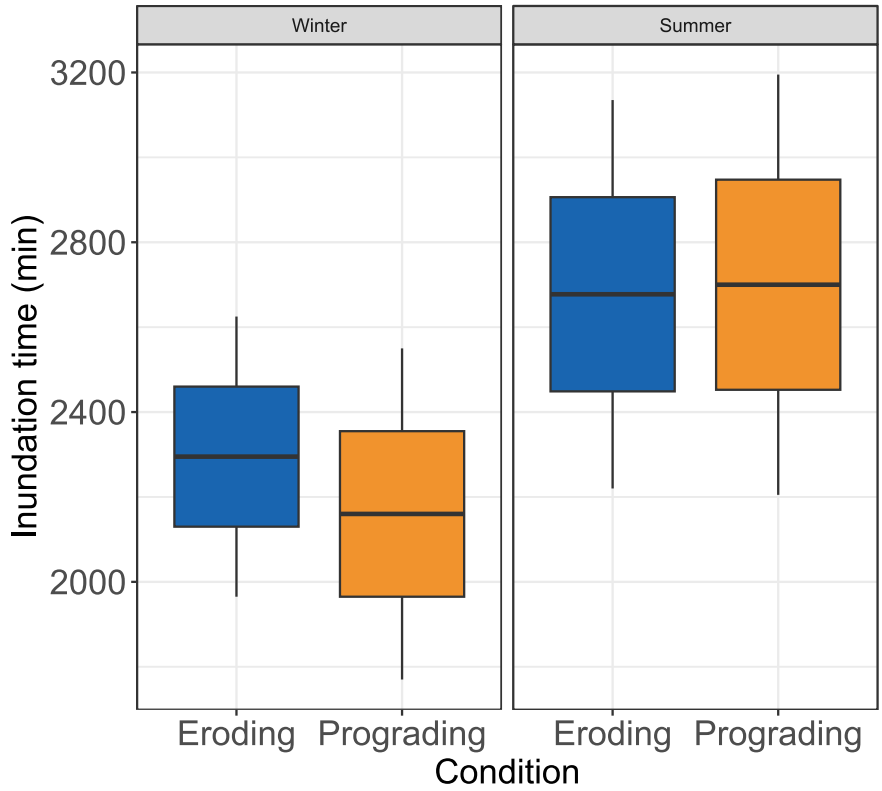

Figure 5.16 Average inundation time (min) for suspended sediment samplers at eroding and prograding sites between seasons (Winter, Summer).

5.4 Discussion

This study aimed to determine the carbon fluxes of different salt marsh sites with different geomorphic properties. To this end the suspended sediment associated with flood and ebb tides in two tidal creeks were characterised as well as the deposited sediment between the eroding and prograding salt marsh sites. Comparing those to the reference samples collected from the mud flat and salt marsh at both geomorphic conditions the dynamics of saltmarsh carbon stocks were examined.

5.4.1 Suspended sediment

Suspended sediment was analysed between an eroding and a prograding site as well as between winter (January, February) and summer (June, July). Inorganic carbon percentage and $\delta^{13}C_{TC}$ were significantly greater during winter than summer, the organic carbon percentage showed the opposite trend. The high $\delta^{13}C_{TC}$ indicates greater amounts of carbonate within the sediment, further apparent by the greater inorganic carbon percentage. The influence of carbonates to $\delta^{13}C_{TC}$ is high, evident through the significant change in isotope ratios upon removing of carbonates ($\delta^{13}C_{TC}$ vs $\delta^{13}C_{org}$). Supported by previous measurements of carbonate $\delta^{13}C$ ratios of 0.1 to 0.8 ‰ within surface sediments of the northeast Irish Sea (MacKenzie et al., 2004). Inorganic carbon percentages were higher during winter, driven by the outflowing sediment. This could also be due to reduced trapping of predominantly sedimentary material within less dense marsh vegetation during winter (Mueller et al., 2023).

The organic carbon percentage of the suspended sediment was significantly different between seasons, with higher percentages during summer. This trend was expected, as the productivity of the salt marsh increases during summer, therefore more salt marsh organic matter can be transported out of the system through the tidal creeks during tidal inundations (Smeaton et al., 2022).

Carbon percentages and carbon origins were assumed to be different between geomorphic conditions. However, no significant differences were observed. Greater $\delta^{13}C_{org}$ ratios were hypothesised for prograding than eroding sites, showing the reliance on marine organic matter at prograding sites, whereas the majority of organic matter at eroding sites was assumed to be autochthonous carbon (Chen et al., 2016).

The in- and outflowing tides showed a clearer difference between $\delta^{13}C_{org}$. The variation between the in- and outflowing suspended sediment could however not be attributed to the geomorphic condition.

Suspended sediment from eroding and prograding sites differed in their particle size distributions and grain size percentages as well as between seasons, though not between geomorphic conditions. A greater percentage of sand and a greater median grain size was measured during winter than summer. Which could however not be attributed to different inundation durations, as they were not significantly different between eroding and prograding samplers. An oversampling of coarser sediments, as observed by Elliott et al., (2017), was not noted during our study, as for example the suspended sediment retained during the summer sampling campaigns had a significantly smaller particle size distribution. Contrary to expectations, the particle size distribution of the inflowing and outflowing tide for both geomorphic conditions did not differ. It was expected that more fine-grained sediment got transported into the system, where it would be trapped by the vegetation (Mudd et al., 2010).

5.4.2 Sediment deposition

The study further aimed to determine the characteristics of sediment deposited on the salt marsh flat and if there are differences between sites with contrasting geomorphic conditions (i.e., eroding and prograding). The eroding salt marsh site was found to have more sediment deposited than the prograding site. The sediment was characterized by significantly lower silt percentage, but significantly greater clay percentage than at the prograding site.

The deposited sediment at the eroding site had less inorganic carbon percentage than the prograding site, but was however, higher than the inorganic carbon percentage of the eroding salt marsh reference samples. Indicating that inorganic material from outside the system is being deposited on the eroding salt marsh. The inorganic carbon percentage of the deposited sediment at the prograding site is within the range of the prograding salt marsh reference sample, indicating resuspension and further deposition of new material.

A clear indication of different organic matter origin of the deposited sediment between the geomorphic conditions could not be made. Neither the total nor the organic carbon stable isotope signatures were significantly different between geomorphic conditions. This could be due to the limited number of replicates. Differences were observed, although not statistically significant and repetition of the study over a longer time frame and other study locations would be beneficial. Differences in organic matter deposition between geomorphic varying salt marshes have previously been found (Chen et al., 2016). An old marsh had a greater contribution of marine source organic matter than the new marsh, where a higher autochthonous source was identified (Chen et al., 2016). They further found that the percentage of deposited organic matter varied with marsh elevation. And consequently,

attributed it to the inundation duration affecting the grain size of deposited sediment and their association with organic matter (Chen et al., 2016; Kelleway et al., 2016). At higher elevations, sediment with higher grain sizes was deposited, which is low in organic matter content (Chen et al., 2016). Such a significant change in organic matter driven by elevation was not measured in our study, probably given the relatively shorter distance covered by the transects. We however found that the deposited sediment weight within a spring tidal cycle showed an exponential relationship with inundation time, greater inundation time leading to more opportunities of sediment deposition (Oosterlee et al., 2018). In this regard, the marsh elevation, determining inundation time, had a strong influence over the weight of the deposited sediment, rather than the distance to the tidal channel (Chen et al., 2016).

Furthermore, the sediment deposited differed, although not statistically significant, between geomorphic conditions regarding its inorganic carbon percentage. The sloping-prograding site received sediment with higher inorganic carbon percentage than the eroding site. This pattern has been observed at sites contrasting in geomorphic settings (Mueller et al., 2023). Hydrodynamically exposed sites received a greater percentage of inorganic carbon than sheltered sites, attributed to the connectivity with the marine environment and marine carbonates.

The median grain size of sediment deposited onto the eroding marsh was significantly lower than the suspended sediment within the tidal creeks. The sediment grain size distribution of the deposited sediment on the prograding marsh does however not vary significantly from the suspended sediment. The differential pattern of sedimentation determined by geomorphic condition is due to elevation and topographic differences influencing tidal flooding (Temmerman et al., 2005). Lower and seaward sloping marshes predominantly flooded from the marsh edge, whereas old marsh with higher elevation flooded from the tidal creek (Temmerman et al., 2005). The elevation on the older marsh is thus determining sedimentation patterns, as sediment settles out progressively during its transportation via the tidal creeks.

5.4.3 Implications for salt marsh resilience

Sediment retention on salt marshes is crucial to support their vertical growth and to maintain their elevation within the tidal frame, particularly when considering sea level rise (Crosby et al., 2016; Reed et al., 1999). However, even without a rise in sea level, a salt marsh experiencing insufficient sediment supply can drown (Fagherazzi et al., 2013; Ladd et al., 2019). Lower sediment supply is further connected to eroding site conditions (Ladd et al., 2019). To differentiate between in-system resuspension and external sediment supply the

flood-ebb SSC differential has been proposed (Ganju et al., 2015). Applying it to our study, there was no significant difference, however a slight difference in flood-ebb SSC differential between geomorphic conditions during the winter sampling campaign. The eroding marsh received more sediment than was lost from the system, whereas the prograding site lost more sediments. The great deviation in sediment weight could be due to the different sampling technique used in comparison to Ganju et al., (2015), where the loss of sediment is possible and tidal water collection is not the main priority. Furthermore, the sampling duration employed in our study lasted over the entire spring tidal cycle. Rapid accretion of sediment does not necessarily imply a healthy system and can stem from resuspended eroded material (Ganju et al., 2013).

Instead of using the weight difference between flood-ebb SSC, using differences in sediment characteristics of the suspended sediment and deposited sediment, i.e., carbon stable isotope ratios, carbon percentages or grain size, can provide information on the resilience of the marsh. The sediment characteristics suspended within the tidal creeks did not differ significantly between the two geomorphic conditions sampled. Confirming that both sites received sediment from the same source. The sediment which eventually did get deposited on the salt marsh flat did however significantly differ between geomorphic conditions. The prograding site had a greater deposition of sediment with higher inorganic carbon percentage, which will not only have consequences for the vertical soil development (Allen, 2000), but also for the carbon storage ability of the marsh (Macreadie et al., 2017; Saderne et al., 2019). The deposition of mineral sediments is particularly important for marshes with low autochthonous carbon input to reach and maintain equilibrium in the tidal frame (Allen, 2000). This might have been the prevailing mechanism of marsh growth at the prograding site, whereas the eroding site is not receiving these mineral deposits and through the combined effect on has a lower elevation within the tidal frame. However, without sufficient external sediment supply, the eroding salt marsh site will not be able to accrete enough sediment to grow vertically and avoid loss of habitat through sea level rise.

Salt marshes are characterised as depositional environments for inorganic carbon, predominantly comprised of calcium carbonates, and as such could act as a sink for inorganic carbon (Macreadie et al., 2017; Mueller et al., 2023). The dissolution of calcium carbonate will be lowering the pCO_2, as calcium and hydrogen carbon ions are formed (Anderson, 2013; Macreadie et al., 2017). Our results are taking the findings from Mueller et al., (2023) further and incorporate the suspended sediment fluxes into and out of salt marshes with differing geomorphic conditions providing a more holistic understanding.

5.5 Conclusion

Our study found that even though the sediment suspended within the tidal creek was not significantly different between geomorphic conditions, the deposited sediment on the salt marsh platform was. Showing that the salt marsh sites with differing geomorphic conditions are receiving sediment with the same characteristics through tidal inundations from the tidal creek systems, differ though in the sediment deposition. The eroding salt marsh site showed a greater deposition of sediment than the prograding site, which further differed through the grain size. Concluding that salt marshes with differing geomorphic conditions are retaining sediment with varying characteristics, driven by the grain size of deposited sediment, associated with varying carbon percentages. Understanding these carbon fluxes is crucial regarding assessing blue carbon storage. Determining tipping points of salt marshes based on their carbon fluxes, i.e., import and export, might assist restoration efforts. Especially considering the loss of carbon from eroding marshes, as this could hinder their ability to sequester carbon in the long term.

References

Allen, J.R.L., 2000. Morphodynamics of Holocene salt marshes: a review sketch from the Atlantic and Southern North Sea coasts of Europe. Quat. Sci. Rev. 19, 1155–1231. https://doi.org/10.1016/S0277-3791(99)00034-7

Anderson, L.G., 2013. Carbonate Dissolution, in: Harff, J., Meschede, M., Petersen, S., Thiede, J. (Eds.), Encyclopedia of Marine Geosciences. Springer Netherlands, Dordrecht, pp. 1–4. https://doi.org/10.1007/978-94-007-6644-0_46-1

Bates, D., Mächler, M., Bolker, B., Walker, S., 2015. Fitting Linear Mixed-Effects Models Using lme4. Journal of Statistical Software 67, 1–48. https://doi.org/10.18637/jss.v067.i01

Chen, S., Torres, R., Goñi, M.A., 2016. The Role of Salt Marsh Structure in the Distribution of Surface Sedimentary Organic Matter. Estuaries Coasts 39, 108–122. https://doi.org/10.1007/s12237-015-9957-z

Clyne, F.J., Garrod, C.J., Tipple, J.R., Jeffs, T.M., 2007. Radiological Habits Survey: Dumfries and Galloway Coast (Environment Report No. Final report RL 08/11).

Crosby, S.C., Sax, D.F., Palmer, M.E., Booth, H.S., Deegan, L.A., Bertness, M.D., Leslie, H.M., 2016. Salt marsh persistence is threatened by predicted sea-level rise. Estuar. Coast. Shelf Sci. 181, 93–99. https://doi.org/10.1016/j.ecss.2016.08.018

Cutts, N., Hemingway, K., 1996. The Solway Firth - broad scale habitat mapping (Scottish Natural Heritage Research, Survey and Monitoring Report No. 46).

Elliott, E.A., Monbureau, E., Walters, G.W., Elliott, M.A., McKee, B.A., Rodriguez, A.B., 2017. A novel method for sampling the suspended sediment load in the tidal environment using bi-directional time-integrated mass-flux sediment (TIMS) samplers. Estuar. Coast. Shelf Sci. 199, 14–24. https://doi.org/10.1016/j.ecss.2017.08.029

Fagherazzi, S., Kirwan, M.L., Mudd, S.M., Guntenspergen, G.R., Temmerman, S., D'Alpaos, A., van de Koppel, J., Rybczyk, J.M., Reyes, E., Craft, C., Clough, J., 2012. Numerical models of salt marsh evolution: Ecological, geomorphic, and climatic factors. Rev. Geophys. 50. https://doi.org/10.1029/2011RG000359

Fagherazzi, S., Mariotti, G., Wiberg, P., McGlathery, K., 2013. Marsh Collapse Does Not Require Sea Level Rise. Oceanography 26, 70–77. https://doi.org/10.5670/oceanog.2013.47

Ganju, N.K., Kirwan, M.L., Dickhudt, P.J., Guntenspergen, G.R., Cahoon, D.R., Kroeger, K.D., 2015. Sediment transport-based metrics of wetland stability. Geophys. Res. Lett. 42, 7992–8000. https://doi.org/10.1002/2015GL065980

Ganju, N.K., Nidzieko, N.J., Kirwan, M.L., 2013. Inferring tidal wetland stability from channel sediment fluxes: Observations and a conceptual model. J. Geophys. Res. Earth Surf. 118, 2045–2058. https://doi.org/10.1002/jgrf.20143

Gray, A.B., Pasternack, G.B., Watson, E.B., 2010. Hydrogen peroxide treatment effects on the particle size distribution of alluvial and marsh sediments. The Holocene 20, 293–301. https://doi.org/10.1177/0959683609350390

Hansom, J.D., 2003. Solway Firth (North Shore), in: Coastal Geomorphology of Great Britain, Geological Conservation Review Series. Joint Nature Conservation Committee: Peterborough, pp. 541–548.

Kelleway, J.J., Saintilan, N., Macreadie, P.I., Ralph, P.J., 2016. Sedimentary Factors are Key Predictors of Carbon Storage in SE Australian Saltmarshes. Ecosystems 19, 865–880. https://doi.org/10.1007/s10021-016-9972-3

Ladd, C.J.T., Duggan-Edwards, M.F., Bouma, T.J., Pagès, J.F., Skov, M.W., 2019. Sediment Supply Explains Long-Term and Large-Scale Patterns in Salt Marsh Lateral Expansion and Erosion. Geophys. Res. Lett. 46, 11178–11187. https://doi.org/10.1029/2019GL083315

MacKenzie, A.B., Cook, G.T., Barth, J., Gulliver, P., McDonald, P., 2004. ^{14}C and δ^{13}C characteristics of organic matter and carbonate in saltmarsh sediments from south west Scotland. J Env. Monit 6, 441–447. https://doi.org/10.1039/B315766K

Macreadie, P.I., Anton, A., Raven, J.A., Beaumont, N., Connolly, R.M., Friess, D.A., Kelleway, J.J., Kennedy, H., Kuwae, T., Lavery, P.S., Lovelock, C.E., Smale, D.A., Apostolaki, E.T., Atwood, T.B., Baldock, J., Bianchi, T.S., Chmura, G.L., Eyre, B.D., Fourqurean, J.W., Hall-Spencer, J.M., Huxham, M., Hendriks, I.E., Krause-Jensen, D., Laffoley, D., Luisetti, T., Marbà, N., Masque, P., McGlathery, K.J., Megonigal, J.P., Murdiyarso, D., Russell, B.D., Santos, R., Serrano, O., Silliman, B.R., Watanabe, K., Duarte, C.M., 2019. The future of Blue Carbon science. Nat. Commun. 10, 3998. https://doi.org/10.1038/s41467-019-11693-w

Macreadie, P.I., Serrano, O., Maher, D.T., Duarte, C.M., Beardall, J., 2017. Addressing calcium carbonate cycling in blue carbon accounting. Limnol. Oceanogr. Lett. 2, 195–201. https://doi.org/10.1002/lol2.10052

Mcleod, E., Chmura, G.L., Bouillon, S., Salm, R., Björk, M., Duarte, C.M., Lovelock, C.E., Schlesinger, W.H., Silliman, B.R., 2011. A blueprint for blue carbon: toward an improved understanding of the role of vegetated coastal habitats in sequestering CO2. Front. Ecol. Environ. 9, 552–560. https://doi.org/10.1890/110004

Mudd, S.M., D'Alpaos, A., Morris, J.T., 2010. How does vegetation affect sedimentation on tidal marshes? Investigating particle capture and hydrodynamic controls on biologically mediated sedimentation. J. Geophys. Res. Earth Surf. 115. https://doi.org/10.1029/2009JF001566

Mudd, S.M., Howell, S.M., Morris, J.T., 2009. Impact of dynamic feedbacks between sedimentation, sea-level rise, and biomass production on near-surface marsh stratigraphy and carbon accumulation. Estuar. Coast. Shelf Sci. 82, 377–389. https://doi.org/10.1016/j.ecss.2009.01.028

Mueller, P., Kutzbach, L., Mozdzer, T.J., Jespersen, E., Barber, D.C., Eller, F., 2023. Minerogenic salt marshes can function as important inorganic carbon stores. Limnol. Oceanogr. 68, 942–952. https://doi.org/10.1002/lno.12322

Oosterlee, L., Cox, T.J.S., Vandenbruwaene, W., Maris, T., Temmerman, S., Meire, P., 2018. Tidal Marsh Restoration Design Affects Feedbacks Between Inundation and Elevation Change. Estuaries Coasts 41, 613–625. https://doi.org/10.1007/s12237-017-0314-2

Phillips, J.M., Russell, M.A., Walling, D.E., 2000. Time-integrated sampling of fluvial suspended sediment: a simple methodology for small catchments. Hydrol. Process. 14, 2589–2602. https://doi.org/10.1002/1099-1085(20001015)14:14<2589::AID-HYP94>3.0.CO;2-D

Picarro, 2019. δ13C for Carbon Dioxide (CO2) CM-CRDS System.

Reed, D.J., Spencer, T., Murray, A.L., French, J.R., Leonard, L., 1999. Marsh Surface Sediment Deposition and the Role of Tidal Creeks: Implications for Created and Managed Coastal Marshes. J. Coast. Conserv. 5, 81–90.

Saderne, V., Geraldi, N.R., Macreadie, P.I., Maher, D.T., Middelburg, J.J., Serrano, O., Almahasheer, H., Arias-Ortiz, A., Cusack, M., Eyre, B.D., Fourqurean, J.W., Kennedy, H., Krause-Jensen, D., Kuwae, T., Lavery, P.S., Lovelock, C.E., Marba, N., Masqué, P., Mateo, M.A., Mazarrasa, I., McGlathery, K.J., Oreska, M.P.J., Sanders, C.J., Santos, I.R., Smoak, J.M., Tanaya, T., Watanabe, K., Duarte, C.M., 2019. Role of carbonate burial in Blue Carbon budgets. Nat. Commun. 10, 1106. https://doi.org/10.1038/s41467-019-08842-6

Smeaton, C., Miller, L.C., Ladd, C.J.T., O'Dell, A., Austin, W.E.N., 2022. Bulk elemental and stable isotope composition of organic matter from terrestrial, intertidal, and marine environments, UK, 2016-2021. https://doi.org/10.5285/A445A7A8-528D-4E0B-9094-28CBCD449367

Temmerman, S., Bouma, T.J., Govers, G., Lauwaet, D., 2005. Flow paths of water and sediment in a tidal marsh: Relations with marsh developmental stage and tidal inundation height. Estuaries 28, 338–352. https://doi.org/10.1007/BF02693917

Theuerkauf, E.J., Stephens, J.D., Ridge, J.T., Fodrie, F.J., Rodriguez, A.B., 2015. Carbon export from fringing saltmarsh shoreline erosion overwhelms carbon storage across a critical width threshold. Estuar. Coast. Shelf Sci. 164, 367–378. https://doi.org/10.1016/j.ecss.2015.08.001

6 Discussion

6.1 Summary

Vegetated coastal ecosystems are important for providing coastal protection, flooding control, and as part of the main aspect of this thesis their ability to store carbon. These systems, salt marshes and mangroves alike, are dynamic and grow at the interface between the coastal and the terrestrial environment. As such they are under multiple anthropogenic pressures. Increasing sea level and changes to the amount of sediment delivered are impacting not only the shape and form of these ecosystems but are also reinforcing the physical processes driving the development of landforms and vegetation (i.e., biogeomorphology; Xin et al., 2022).

Within the scope of this thesis, the influence of geomorphic conditions on the fluxes of carbon from salt marsh and mangrove systems was examined and a series of interacting drivers elucidated.

6.2 Hydrodynamic and soil influence on carbon respiration – Chapter 2 & 3

The emission of carbon dioxide from salt marshes and mangroves have been extensively studied (Alongi, 2020; Bouillon et al., 2008), investigating the impacts of a changing climate, including changes in sea level, changing soil temperature, and tidal inundation regimes (Abdul-Aziz et al., 2018; Kirwan et al., 2014). Increased temperature has for example been linked to greater primary production and an increase in carbon sequestration (Wang et al., 2021). This initial benefit could be offset by the increased emission of CO_2 due to the greater microbial activity and respiration during organic matter decay (Abdul-Aziz et al., 2018).

The geomorphic condition, as well as the maturity of marshes has been shown to influence the soil carbon stock (Kelleway et al., 2016; Sousa et al., 2010). In addition to the soil carbon stock, the emission of CO_2 also varies between geomorphic conditions, resulting in greater emissions of CO_2 from eroding sites (*Chapter 2*). Combining the dynamic and often cyclical environment of salt marshes, the main drivers influencing the soil to atmosphere CO_2 flux seem to be tidal cycles, distance to the vegetation edge, groundwater levels, and soil temperatures (*Chapter 2*). An approximate calculation shows that with an average carbon stock of 279.2 ± 6.53 Mg C ha^{-1} (Chapter 2), and a flux of 97.24 ± 67.45 Mg C ha^{-1} yr^{-1}, eroding salt marshes are losing between 10.42 % to 60.4% carbon each year. At the

prograding sites, the soil carbon stock is 186.73 ± 5.05 Mg C ha^{-1} and loses through CO_2 emissions are 77.09 ± 64.82 Mg C ha^{-1} yr^{-1} (*Chapter 2*), leading to a total loss between 6.4 % to 78.1% carbon per year. These calculations are taking into account the carbon loss measured at the seaward fringe of eroding and prograding salt marsh sites are further not considering the carbon additions throughout the same time frame. The remineralisation of carbon and consequent emission as CO_2 leads to a greater percentage loss of organic carbon at prograding sites relative to the total soil carbon stock. To be able to offset the loss of carbon through remineralisation, enough carbon needs to be sequestered through primary production, and/or deposited from allochthonous sediment supply (*Chapter 5*). The calculations of CO_2 emissions from the system assumes that sediment is not actively eroding, adding to the loss of sequestered carbon. Given the large uncertainty, and variables CO_2 emissions are dependent on, more research is needed to lower the uncertainty in emission calculations.

The results make a strong case for the inclusion of geomorphic condition during the calculation of salt marsh carbon budgets or during the selection of sites for restoration. This is in support of the prosed management planning guidelines by Burden et al., (2019). Differentiated calculations will possibly influence site selection for restoration as well as the time frame for carbon offsetting schemes. Sites for restoration and conservation could be selected based on their initial high carbon stock (i.e., mature marshes). The prioritisation of carbon storage in salt marsh management could thus further entail the focus on erosion control, to avoid the loss of carbon through CO_2 emissions and the loss through the active erosion of sediment.

Although prograding sites are potentially losing a higher percentage of initial carbon stock through CO_2 emissions, they have been shown to have a rapid initial accumulation of carbon (Burden et al., 2019). However, these marshes only reach a stable carbon stock as mature marshes after approximately 100 years (Burden et al., 2019). Thus, the time frame and carbon storage benefits might, counter-intuitively, be greater at salt marshes which are experiencing erosion, than at marshes that have recently been restored. Erosion control, i.e., sufficient sediment supply (Ladd et al., 2019), could thus not only maintain high carbon stocks, it could also preserve ecosystem functions of existing marshes and prevent an accreting marsh transitioning into an eroding one by aiding in marsh platform growth and securing the salt marsh against relative sea-level rise.

Chapter 3 highlighted the impact of tidal inundations on groundwater level and the combined effect with current velocity on soil temperature. As soil temperature is a primary controlling

factor of CO_2 emissions to the atmosphere, the tidal connection and groundwater level are key drivers and should thus be included in restoration planning. Restored marshes are typically characterized by reduced groundwater dynamics where groundwater fluctuates within a newly deposited soil layer on top of compacted soil (Van Putte et al., 2020). Increasing groundwater dynamics and aeration depth will enhance drainage from the salt marsh and create an environment more resembling a natural marsh aiding in the establishment of a more diverse plant community (Brooks et al., 2015). An adverse effect following the reintroduction of tidal inundation and higher groundwater dynamics on the carbon storage in restored salt marshes is expected through higher CO_2 emission as oxic soil environments are created (Xiao et al., 2021). However, balancing this loss of carbon is the increased carbon accumulation by new marsh vegetation (Burden et al., 2019).

The effect reduced groundwater level dynamics has on soil temperature is speculative. We observed different influences of high groundwater levels on soil temperature, dependent on current velocity. Further modified by seasonal cooling of warming. At restored salt marsh sites, we expect that higher groundwater levels with a higher current velocity will lead to on average lower soil temperatures (*Chapter 3*). However, the comparison between restored and natural marshes regarding soil temperature interaction with groundwater level and current velocity should be considered as a further future work avenue.

Additional carbon emissions from the coastal wetlands in the form of CH_4, might also be affected by restoration methods. Methane, as it is produced under anaerobic conditions might initially decrease through the restoration measures when tidal inundations are re-introduced and care taken to implement groundwater dynamics (Derby et al., 2022). Lower groundwater levels and shallow rooting depth of vegetation will potentially increase the soil oxygen content and suppresses CH_4 production (Derby et al., 2022).

6.3 Organic matter origin and geomorphic conditions – Chapter 2, 4, 5

The carbon sequestration potential of mangroves and salt marshes alike, is driven by the delivery of organic matter to the ecosystem and its primary production (Alongi, 2020). The reliance on external sediment and organic matter supply is greater within minerogenic ecosystems, or marshes not yet able to independently produce enough organic matter and accrete enough sediment to maintain their elevation in relation to the tidal frame (Nolte et al., 2013).

At our salt marsh study site, a minerogenic marsh in the UK (Nolte et al., 2013), the main delivery of sediment input is external from tidal inundations. The eroding sites had a lower supply of sediment than prograding marsh sites (Ladd et al., 2019), thus the source of organic matter delivered to geomorphic different coastal ecosystems was also expected to be different. Organic matter origin was delineated between terrestrial and marine derived sources, using the carbon stable isotope ratio of $\delta^{13}C$ (Bouillon et al., 2011; Kelleway et al., 2016). A short-term deposition study within a salt marsh could not show that the deposited organic matter at sites of different geomorphic conditions is from different origins (*Chapter 5*). Sites of different geomorphic conditions are however showing a difference in carbon stable isotope ratio averaged for a depth of 1 m (*Chapter 2*). Such a difference in isotope ratio could, instead of organic matter origin, denote the lability of carbon and thus its decomposition stage. An increase of 1-3‰ $\delta^{13}C$ has been attributed to the decomposition of carbon, with the more labile carbon, ^{13}C, being decomposed first (Adame and Fry, 2016). The carbon stable isotope ratio was however significantly different between mangrove sites of different geomorphic conditions and the carbon was interpreted to be of differing organic matter sources (*Chapter 4*). Eroding mangrove sites had a lower ratio, i.e., proportionally higher terrestrial organic matter source than prograding sites (*Chapter 4*).
The delivery of sediments to the coast and differences between geomorphic conditions has previously been found to be a determinant of the erosional status of salt marsh coasts (Ladd et al., 2019). Although the total weight of deposited sediment was greater at the eroding site, the results point towards the resuspension and deposition of salt marsh derived sediment (*Chapter 5*). The total suspended sediment weight of in- vs. outflowing tides differed between geomorphic conditions, however not statistically. When repeating this study, temporal and spatial variation should be included, i.e., measuring over shorter tidal cycles and including different salt marsh sites.

What the results from *Chapter 4* and *Chapter 5* do however highlight and reinforce, are the role of tidal inundation and vegetation on the delivery of sediments to coastal systems as well as their retention (Temmerman et al., 2005; Stijn Temmerman et al., 2012). Leading to varying developments of the vegetation. The sites did differ in the grain size distribution of the sediment deposited, deemed to be driven by elevation and thus inundation related factors, such as inundation duration and tidal current velocity (Kelleway et al., 2016). Further work could possibly delineate the relationship between sediment grain size, sediment carbon concentration and current/wave energy received by coasts (Kelleway et al., 2016). But also

the water level and wave energy received and connected to the export of carbon to the coastal environments (Braun and Theuerkauf, 2021).

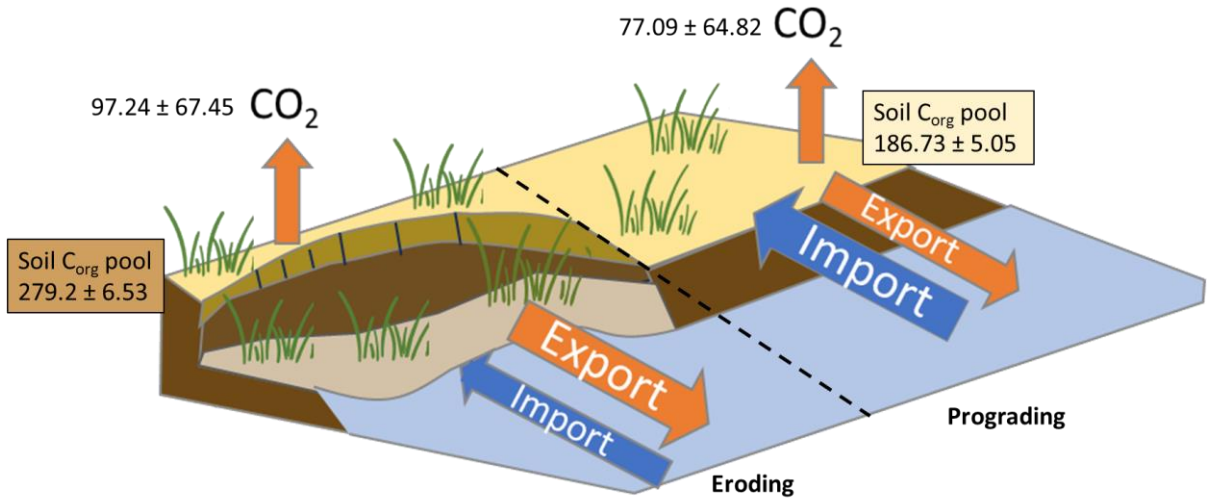

Figure 6.1 Schematic of findings from Chapter 2, 5. Soil C_{org} pool (Mg C ha^{-1}) and soil to atmosphere CO_2 flux (Mg C ha^{-1} yr^{-1}) from sites of different geomorphic condition (left: eroding; right: prograding). Mean ± Standard deviation.

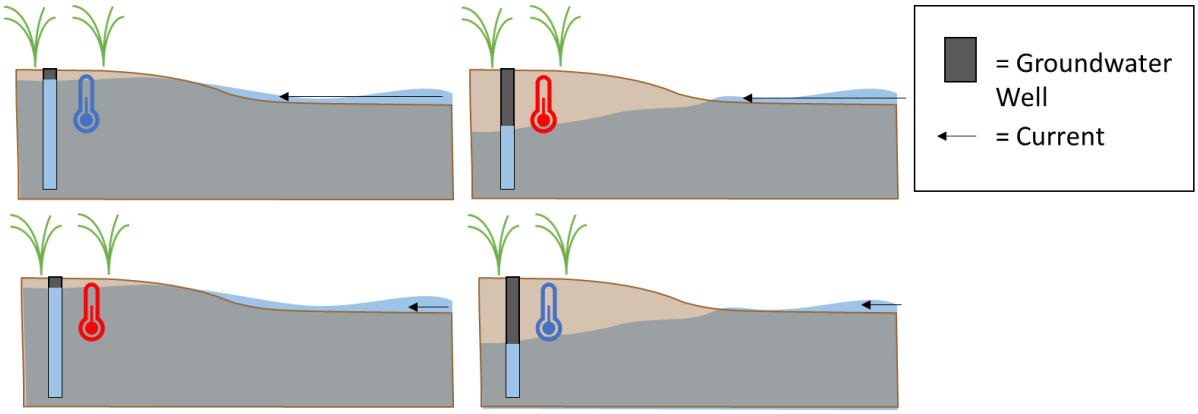

Figure 6.2 Schematic of finding from Chapter 3. Groundwater level and current velocity influence on salt marsh soil temperature. With greater currents (longer arrow; top), the soil temperature cools with higher groundwater level and warms with lower groundwater level, lower currents (shorter arrow; bottom) resulting in the opposite effect.

6.4 Future work

Future work, building on the results of this thesis could include the development of a greenhouse gas flux model. The model could calculate the loss of carbon from the soil to the atmosphere based on geomorphic condition and other influencing environmental factors. As described in *Chapter 2* and *Chapter 3* influencing factors to be included are tidal cycle, groundwater level, soil temperature, distance to vegetation edge and current velocity. Their combination could provide an estimate of soil to atmosphere CO_2 emission at cliffed-eroding and sloping-prograding salt marsh sites. The model would further benefit from including carbon lability measurements and their influence on CO_2 emissions, depending on the distance to the cliff as well as the cliff height. This would be an extension to the model produced by Lovelock et al., (2017), calculating the likelihood of CO_2 emissions based on the exposure of material to oxic environments. It could also link groundwater level dynamics, restored tidal channels to greenhouse gas fluxes (Van Putte et al., 2020; *Chapter 2, 3*). The model could help in the planning process of restoration projects to delineate between possible restoration sites and level of restoration and inform carbon ratings and be a decision-making tool in offsetting carbon emissions.

Additional research could further include measurements of methane (CH_4) fluxes. The emissions of methane from coastal ecosystems has received increased attention but the variability of fluxes is high and only a limited number of studies have been performed (Rosentreter et al., 2021). Methane is produced under anaerobic conditions, salt marshes with reduced groundwater dynamics might be low in CO_2 emissions, however, might have a considerable emission of CH_4.

Various other carbon fluxes potentially linked to geomorphic different salt marsh coasts could further be investigated. For example, fluxes associated with groundwater exchange, i.e., dissolved organic and inorganic carbon (DOC, DIC). Fluxes of DOC and DIC to the coastal ocean have previously been found to exceed the burial of carbon (Correa et al., 2022). As groundwater discharge is related to the tidal amplitude (Wilson et al., 2015), the varying groundwater levels between geomorphic conditions (*Chapter 2*) and influences of current velocity (*Chapter 3*) could lead to differential fluxes of DOC and DIC between eroding and prograding sites.

Even though no significant difference in CO_2 emission was measured from mangroves of geomorphic varying conditions (*Chapter 4*), further measurements including temporal variations should be conducted. The rainfall and conditions during the wet season could have

reduced any potential differences in emissions between sites and should be repeated during the dry season.

6.5 Conclusion

This thesis investigated the impact of geomorphic conditions on carbon fluxes at coastal wetland sites. The relationships with and impact of environmental factors on CO_2 emissions was identified as well as the carbon flux through tidal transport of sediments. Geomorphic condition influenced CO_2 emissions at salt marsh sites, through interacting effects of tidal cycle, groundwater level and soil temperature. Mangroves didn't show differential CO_2 emissions. However, like salt marsh sites, they showed a clear distinction between sediment organic carbon origins. My results show that salt marsh sites and mangrove forests are heavily reliant on external carbon supply, especially true during their initial growth phase before they can produce enough organic matter to accrete sediment vertically. As the ecosystems mature, the dominant carbon source within the soil shifts to autochthonous carbon. Providing an argument for the inclusion of carbon isotope signature in the analysis of tipping points and delineate between potential restoration sites.

Characterising carbon fluxes between salt marsh sites of different geomorphic conditions showed further differences in the deposition of sediment through tidal inundations. At eroding sites deposited sediment showed a greater median grain size and lower inorganic carbon concentration. No such difference in sediment characteristics was identified from suspended sediment between sites of different geomorphic conditions. Highlighting that sites of different geomorphic conditions are receiving sediments with similar characteristics but are retaining sediments with distinctly separate characteristics.

The retention of different sediments and the sedimentary make-up of sites with differing geomorphic condition further has significant effects on carbon emissions. Groundwater retention/drainage is affected, thus impacting the soil temperature and CO_2 emissions. Leading to greater CO_2 emissions at eroding sites in addition to soil carbon loss through erosion processes.

The connection between hydrological factors on the soil pore space has been further investigated. Revealing an overlooked link between tidal factors and soil temperature, having a direct effect on soil processes, i.e., carbon respiration. Emphasising that salt marshes are not uniform habitats and carbon budget calculations need to be adjusted to account for differential CO_2 emissions.

The inclusion of salt marsh restoration within the UK carbon market has been analysed within a feasibility study (Burden et al., 2023). The feasibility study is deducting allochthonous carbon from the accumulated carbon following restoration. However, in line with the results of this thesis, deducting allochthonous carbon from the carbon income of restoration sites, would decrease the viability of the restoration. Coastal blue carbon ecosystems store however the carbon and prevent its remineralisation and return to the atmosphere.

References

Abdul-Aziz, O.I., Ishtiaq, K.S., Tang, J., Moseman-Valtierra, S., Kroeger, K.D., Gonneea, M.E., Mora, J., Morkeski, K., 2018. Environmental Controls, Emergent Scaling, and Predictions of Greenhouse Gas (GHG) Fluxes in Coastal Salt Marshes. Journal of Geophysical Research: Biogeosciences 123, 2234–2256. https://doi.org/10.1029/2018JG004556

Adame, M.F., Fry, B., 2016. Source and stability of soil carbon in mangrove and freshwater wetlands of the Mexican Pacific coast. Wetlands Ecol Manage 24, 129–137. https://doi.org/10.1007/s11273-015-9475-6

Alongi, D.M., 2020. Carbon Balance in Salt Marsh and Mangrove Ecosystems: A Global Synthesis. J. Mar. Sci. Eng. 8, 767. https://doi.org/10.3390/jmse8100767

Bouillon, S., Borges, A.V., Castañeda-Moya, E., Diele, K., Dittmar, T., Duke, N.C., Kristensen, E., Lee, S.Y., Marchand, C., Middelburg, J.J., Rivera-Monroy, V.H., Smith, T.J., Twilley, R.R., 2008. Mangrove production and carbon sinks: A revision of global budget estimates. Global Biogeochem. Cycles 22. https://doi.org/10.1029/2007GB003052

Bouillon, S., Connolly, R.M., Gillikin, D.P., 2011. Use of Stable Isotopes to Understand Food Webs and Ecosystem Functioning in Estuaries, in: Treatise on Estuarine and Coastal Science. Elsevier, pp. 143–173. https://doi.org/10.1016/B978-0-12-374711-2.00711-7

Braun, K.N., Theuerkauf, E.J., 2021. The role of short-term and long-term water level and wave variability in coastal carbon budgets. iScience 24, 102382. https://doi.org/10.1016/j.isci.2021.102382

Brooks, K.L., Mossman, H.L., Chitty, J.L., Grant, A., 2015. Limited Vegetation Development on a Created Salt Marsh Associated with Over-Consolidated Sediments and Lack of Topographic Heterogeneity. Estuaries and Coasts 38, 325–336. https://doi.org/10.1007/s12237-014-9824-3

Burden, A., Austin, W., Fitton, R., Garbutt, A., Gupta, S., Hipkiss, A., Mahon, C., McGrath, T., Pontee, N., Reed, M., 2023. Feasibility study of VCS VM0033 (NEIRF1072 Saltmarsh Carbon Code), Report to the Natural Environment Investment Readiness Fund (NEIRF). UK Centre for Ecology & Hydrology, Bangor.

Burden, A., Garbutt, A., Evans, C.D., 2019. Effect of restoration on saltmarsh carbon accumulation in Eastern England. Biology Letters 15, 20180773. https://doi.org/10.1098/rsbl.2018.0773

Correa, R.E., Xiao, K., Conrad, S.R., Wadnerkar, P.D., Wilson, A.M., Sanders, C.J., Santos, I.R., 2022. Groundwater Carbon Exports Exceed Sediment Carbon Burial in a Salt Marsh. Estuaries and Coasts 45, 1545–1561. https://doi.org/10.1007/s12237-021-01021-1

Derby, R.K., Needelman, B.A., Roden, A.A., Megonigal, J.P., 2022. Vegetation and hydrology stratification as proxies to estimate methane emission from tidal marshes. Biogeochemistry 157, 227–243. https://doi.org/10.1007/s10533-021-00870-z

Duarte, C.M., Losada, I.J., Hendriks, I.E., Mazarrasa, I., Marbà, N., 2013. The role of coastal plant communities for climate change mitigation and adaptation. Nature Clim Change 3, 961–968. https://doi.org/10.1038/nclimate1970

Ganju, N.K., 2019. Marshes Are the New Beaches: Integrating Sediment Transport into Restoration Planning. Estuaries and Coasts 42, 917–926. https://doi.org/10.1007/s12237-019-00531-3

Kelleway, J.J., Saintilan, N., Macreadie, P.I., Ralph, P.J., 2016. Sedimentary Factors are Key Predictors of Carbon Storage in SE Australian Saltmarshes. Ecosystems 19, 865–880. https://doi.org/10.1007/s10021-016-9972-3

Kirwan, M.L., Guntenspergen, G.R., Langley, J.A., 2014. Temperature sensitivity of organic-matter decay in tidal marshes. Biogeosciences 11, 4801–4808. https://doi.org/10.5194/bg-11-4801-2014

Ladd, C.J.T., Duggan-Edwards, M.F., Bouma, T.J., Pagès, J.F., Skov, M.W., 2019. Sediment Supply Explains Long-Term and Large-Scale Patterns in Salt Marsh Lateral Expansion and Erosion. Geophysical Research Letters 46, 11178–11187. https://doi.org/10.1029/2019GL083315

Lovelock, C.E., Fourqurean, J.W., Morris, J.T., 2017. Modeled CO2 Emissions from Coastal Wetland Transitions to Other Land Uses: Tidal Marshes, Mangrove Forests, and Seagrass Beds. Frontiers in Marine Science 4.

Nolte, S., Koppenaal, E.C., Esselink, P., Dijkema, K.S., Schuerch, M., De Groot, A.V., Bakker, J.P., Temmerman, S., 2013. Measuring sedimentation in tidal marshes: a review on methods and their applicability in biogeomorphological studies. J Coast Conserv 17, 301–325. https://doi.org/10.1007/s11852-013-0238-3

Rosentreter, J.A., Borges, A.V., Deemer, B.R., Holgerson, M.A., Liu, S., Song, C., Melack, J., Raymond, P.A., Duarte, C.M., Allen, G.H., Olefeldt, D., Poulter, B., Battin, T.I., Eyre, B.D., 2021. Half of global methane emissions come from highly

variable aquatic ecosystem sources. Nat. Geosci. https://doi.org/10.1038/s41561-021-00715-2

Seddon, N., Sengupta, S., Garcia-Espinosa, M., Hauler, I., Herr, D., Rizvi, A.R., 2019. Nature-based Solutions in Nationally Determined Contributions: Synthesis and recommendations for enhancing climate ambition and action by 2020. IUCN and University of Oxford, Gland, Switzerland and Oxford. https://doi.org/10.1163/9789004322714_cclc_2019-0019-102

Sousa, A.I., Lillebø, A.I., Pardal, M.A., Caçador, I., 2010. The influence of *Spartina maritima* on carbon retention capacity in salt marshes from warm-temperate estuaries. Marine Pollution Bulletin, Estuarine Ecosystems: Structure, Function and Management (ECSA-42 Symposium in Russia) 61, 215–223. https://doi.org/10.1016/j.marpolbul.2010.02.018

Temmerman, S., Bouma, T.J., Govers, G., Lauwaet, D., 2005. Flow paths of water and sediment in a tidal marsh: Relations with marsh developmental stage and tidal inundation height. Estuaries 28, 338–352. https://doi.org/10.1007/BF02693917

Temmerman, S., Moonen, P., Schoelynck, J., Govers, G., Bouma, T.J., 2012. Impact of vegetation die-off on spatial flow patterns over a tidal marsh. Geophysical Research Letters 39. https://doi.org/10.1029/2011GL050502

Van Putte, N., Temmerman, S., Verreydt, G., Seuntjens, P., Maris, T., Heyndrickx, M., Boone, M., Joris, I., Meire, P., 2020. Groundwater dynamics in a restored tidal marsh are limited by historical soil compaction. Estuarine, Coastal and Shelf Science 244, 106101. https://doi.org/10.1016/j.ecss.2019.02.006

Wang, F., Sanders, C.J., Santos, I.R., Tang, J., Schuerch, M., Kirwan, M.L., Kopp, R.E., Zhu, K., Li, X., Yuan, J., Liu, W., Li, Z., 2021. Global blue carbon accumulation in tidal wetlands increases with climate change. National Science Review 8, nwaa296. https://doi.org/10.1093/nsr/nwaa296

Wilson, A.M., Evans, T.B., Moore, W.S., Schutte, C.A., Joye, S.B., 2015. What time scales are important for monitoring tidally influenced submarine groundwater discharge? Insights from a salt marsh. Water Resources Research 51, 4198–4207. https://doi.org/10.1002/2014WR015984

Xiao, K., Wilson, A.M., Li, H., Santos, I.R., Tamborski, J., Smith, E., Lang, S.Q., Zheng, C., Luo, X., Lu, M., Correa, R.E., 2021. Large CO2 release and tidal flushing in salt marsh crab burrows reduce the potential for blue carbon sequestration. Limnology and Oceanography 66, 14–29. https://doi.org/10.1002/lno.11582

Xin, P., Wilson, A., Shen, C., Ge, Z., Moffett, K.B., Santos, I.R., Chen, X., Xu, X., Yau, Y.Y.Y., Moore, W., Li, L., Barry, D.A., 2022. Surface Water and Groundwater Interactions in Salt Marshes and Their Impact on Plant Ecology and Coastal Biogeochemistry. Reviews of Geophysics 60, e2021RG000740. https://doi.org/10.1029/2021RG000740

Appendix A
Supporting Information for Chapter 2 - Sediment to Atmosphere CO_2 Efflux Increases at Retreating Salt Marsh Edges

Contents of this file

Introduction

Generalized Linear Mixed Effects Model

A Linear Mixed Effects Model (LMM) cannot be used to model the relationship between CO_2 flux to tidal cycle, erosion condition and distance to cliff, as CO_2 flux does not follow a normal distribution. A Generalized Linear Mixed Effects Model with gamma distribution and logistic link function is being fitted instead. The model includes measurement site as a random factor (i.e., Site).

Linear Mixed Effects Model

The Linear Mixed Effects Model is used to determine how is CO_2 flux related to soil temperature, groundwater level and tidal cycle. Response variable of CO_2 efflux does not meet model assumption of normality and is transformed using the cube root transformation. Assumptions for Linear Mixed Effects Model are being tested on model with a) random intercept for factor Site and b) random intercept and variable slope for each measurement campaign (i.e., Visit).

Table A.1 Statistical summary of the predictor variables from the Generalized Linear Mixed Effects Model (GLMM) of CO_2 flux with "Sites" as random intercept. Interactions between main effects are shown with an "x".

Formula: CO2 ~ Tidal_cycle + Erosion + distance_cliff + Tidal_cycle : Erosion + Tidal_cycle : distance_cliff + (1 | Site)				
Predictor variable	**Estimate**	**SE**	**z-value**	**P-value**
Tidal cycle [spring]	-1.278619	0.202127	-6.326	<0.001
Erosion [prograding]	-0.170113	0.208220	-0.817	0.413937
Distance to cliff	0.001213	0.066402	0.018	0.985428
Tidal cycle [spring] x Erosion [prograding]	-0.821210	0.258953	-3.171	0.002
Tidal cycle [spring] x Distance to cliff	0.423920	0.109384	3.876	<0.001

Table A.2 Statistical summary of model fit of predictor variables from Generalized Linear Mixed Effects Model (GLMM) of CO_2 flux with "Sites" as random intercept.

Tidal cycle	**Erosion**	**Fit**	**SE**	**Lower**	**Upper**
Neap	Eroding	1.4452458	0.20897471	1.0859370	1.9234406
Spring	Eroding	0.6999267	0.11068427	0.5120226	0.9567886
Neap	Prograding	1.2191652	0.18303582	0.9060902	1.6404148
Spring	Prograding	0.2597327	0.05486458	0.1710715	0.3943442

Table A.3 Statistical summary of the predictor variables of CO_2 flux from the Linear Mixed Effects Model (LMM) with random slope (Visit) and random intercept (Site). Interactions between main effects are shown with an "x".

Formula: CO2_cubrt ~ soil_temp_1day + groundwater_level_1day + Tidal_cycle + soil_temp_1day : groundwater_level_1day + groundwater_level_1day : Tidal_cycle + (Visit | Site)				
Predictor variable	**Estimate**	**SE**	**z-value**	**P-value**
Soil temperature	0.10568	0.01170	9.032	<0.001
Groundwater level	-1.51311	0.22571	-6.704	<0.001
Tidal cycle [spring]	0.03783	0.33808	0.112	0.911
Soil temperature x Groundwater level	0.07457	0.01316	5.666	<0.001
Groundwater level x Tidal cycle [spring]	-0.09639	0.43084	-0.224	0.823

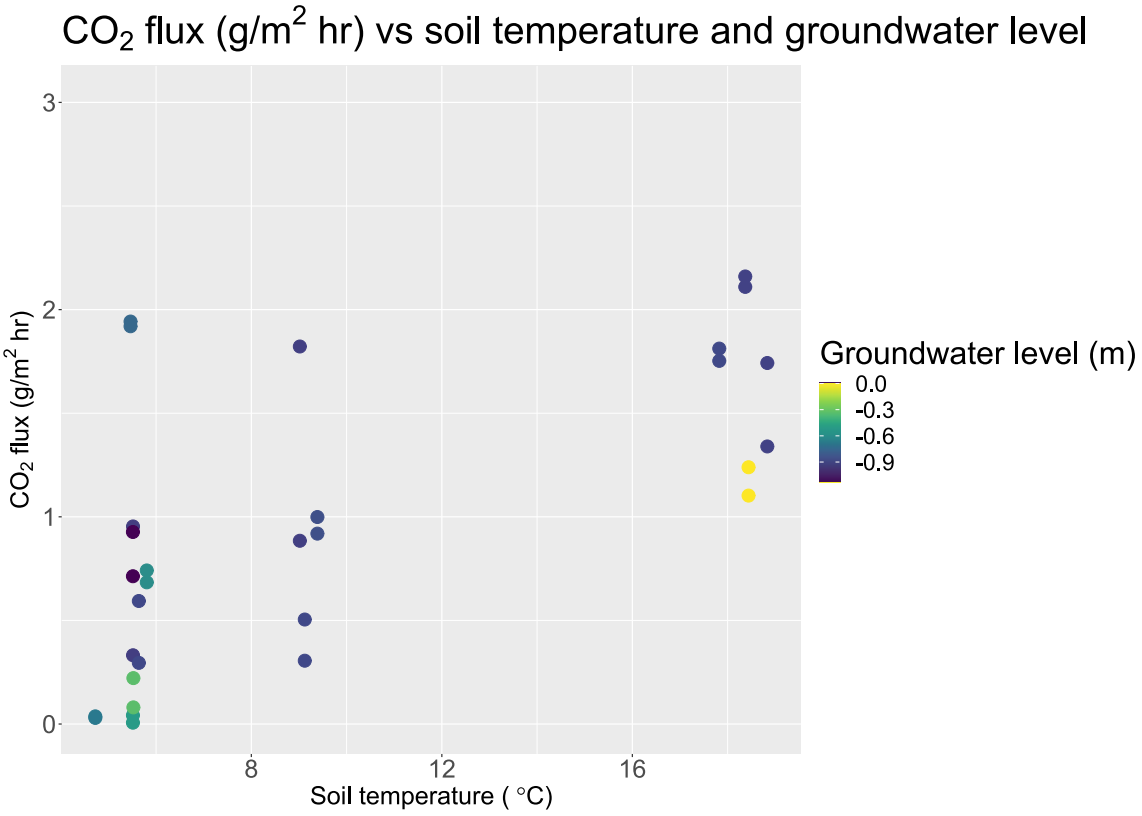

Figure A.1 Relationship between soil to atmosphere CO_2 flux (g/m^2 hr) to soil temperature and groundwater level (m), without random effects.

Table A.4 Kruskal-Wallis tests for comparison of groundwater level at low tide between sites during spring tidal cycles.

Spring tide	Chi-squared	Df	p-value
November 2021	35.981	3	<0.001
December 2021	35.575	3	<0.001
January 2022	59.248	3	<0.001
February 2022 [1. Spring Tide]	32.664	3	<0.001
February 2022 [2. Spring Tide]	40.628	3	<0.001
March 2022	33.797	3	<0.001

Table A.5 Kruskal-Wallis tests for comparison of groundwater level at low tide among spring tidal cycles within Sites.

Site	Chi-squared	df	p-value
ER1	29.384	5	<0.001
ER3	33.351	5	<0.001
PR5	2.9	5	0.715
PR7	20.561	5	<0.001

Table A.6 Site hydrodynamic and sampling structure.

ID	Condition	CO_2 flux	Ground water	Soil temperature	Soil core	Well elevation (m)	Average Inundation duration (hr)	Average (± St. Dev.) Groundwater level after high tide (m)
ER1	Eroding	Yes	Yes	Yes	Yes	4.495	109.90	-0.56 (± 0.05)
ER3	Eroding	Yes	Yes	Yes	Yes	4.549	91.23	-0.46 (± 0.10)
ER4	Eroding	Yes	Failed	Yes	Yes [not included]	NA	NA	NA
PR5	Prograding	Yes	Yes	Yes	Yes	4.62	82.93	-0.45 (± 0.10)
PR7	prograding	yes	Yes	Yes	Yes	4.123	159.89	-0.25 (± 0.11)
ER8	Eroding	Yes	No	Yes	No	NA	NA	NA
ER9	Eroding	Yes	No	Failed	No	NA	NA	NA
PR10	Prograding	Yes	No	Yes	No	NA	NA	NA
PR11	Prograding	Yes	No	Yes	No	NA	NA	NA
PR12	Prograding	yes	No	Yes	No	NA	NA	NA

Table A.7 CO_2 flux measurement distances to vegetation edge by measurement date.

ID	Date	Distance back/groundwater well (m)	Distance middle (m)	Distance front (m)
ER1	17.06.2021	NA	NA	0.3
	03.08.2021	3	1	0.3
	15.11.2021	2.4	0.4	NA
	25.01.2022	2.6	0.6	0.3
	09.03.2022	1.4	0.3	NA
ER3	03.08.2021	3	1	0.3
	15.11.2021	3	1	0.5
	25.01.2022	2.6	0.6	0.3
	09.03.2022	2.25	0.25	NA
ER4	04.08.2021	2.7	0.7	0.4
	15.11.2021	1.2	0.2	NA
	25.01.2022	0.8	NA	NA
	09.03.2022	0.68	NA	NA
PR5	03.08.2021	3	1	0.3
	15.11.2021	3	1	0.3
	25.01.2022	3	1	0.3
	09.03.2022	3	1	0.3
PR7	03.08.2021	3	1	0.3
	25.11.2021	3	1	0.3
	25.01.2022	3	1	0.3
	09.03.2022	3	1	0.3
ER8	04.08.2021	3	1	0.3
	17.11.2021	2.5	0.5	0.2
ER9	03.08.2021	3	1	0.3
	17.11.2021	2.8	0.8	0.2
PR10	04.08.2021	3	1	0.3
PR11	04.08.2021	3	1	0.3
PR12	04.08.2021	3	1	0.3

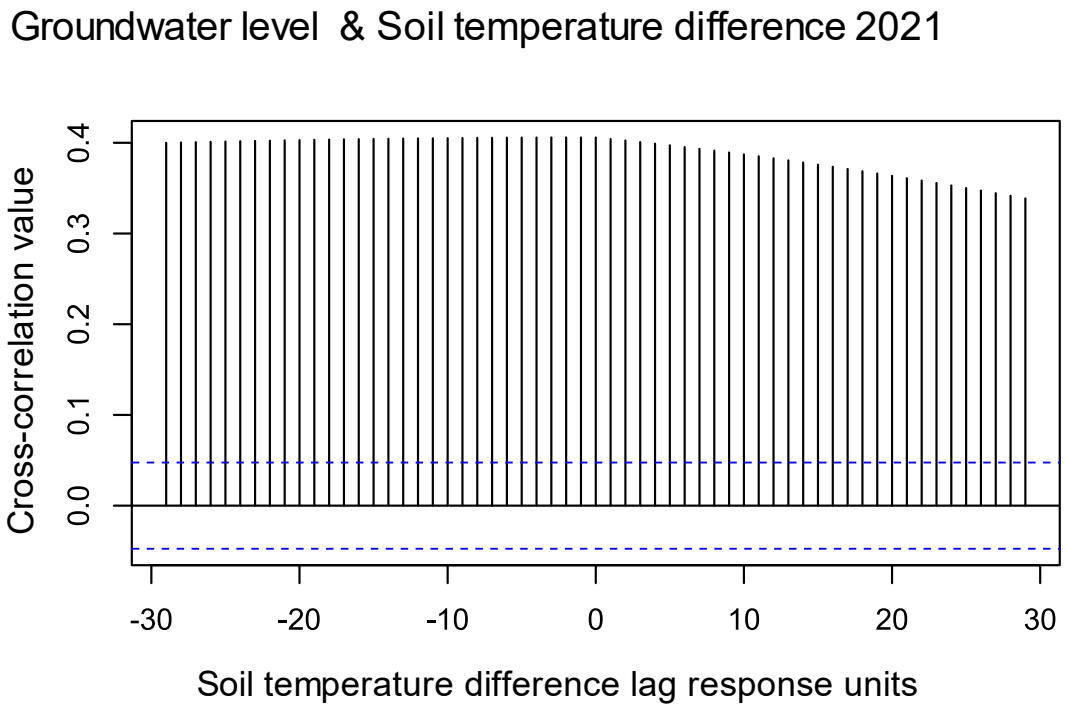

Figure A.2 Cross-correlation between groundwater level at site ER1 and soil temperature difference between site ER1 and PR5 during October and December 2021.

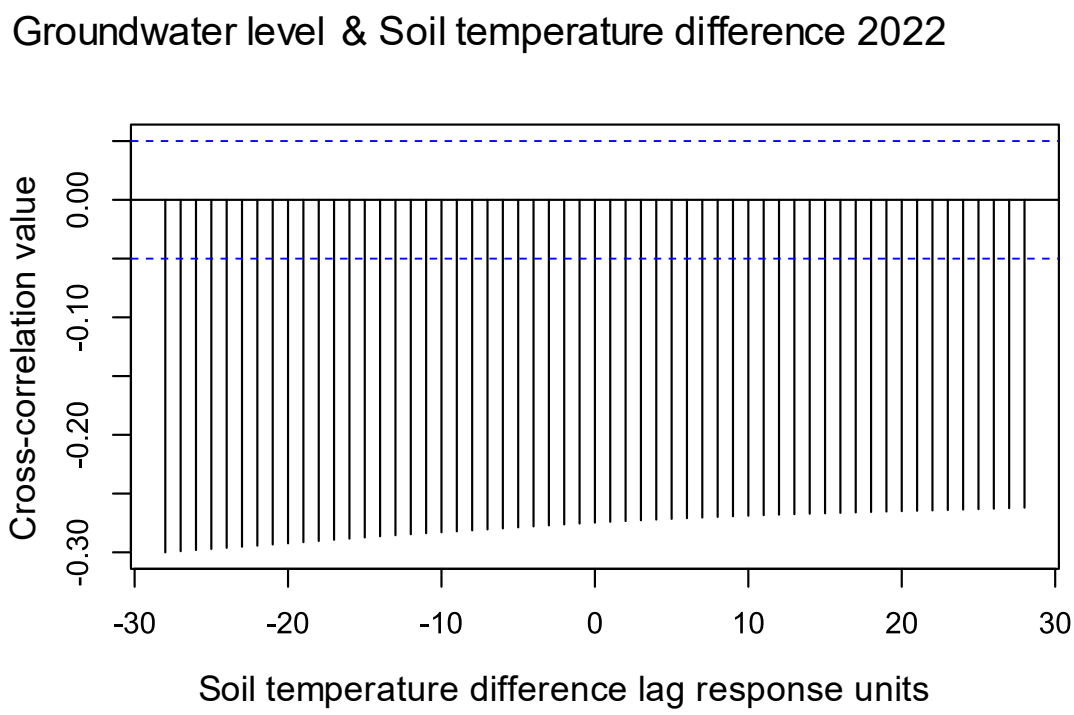

Figure A.3 Cross-correlation between groundwater level at site ER1 and soil temperature difference between site ER1 and PR5 during January and March 2022.

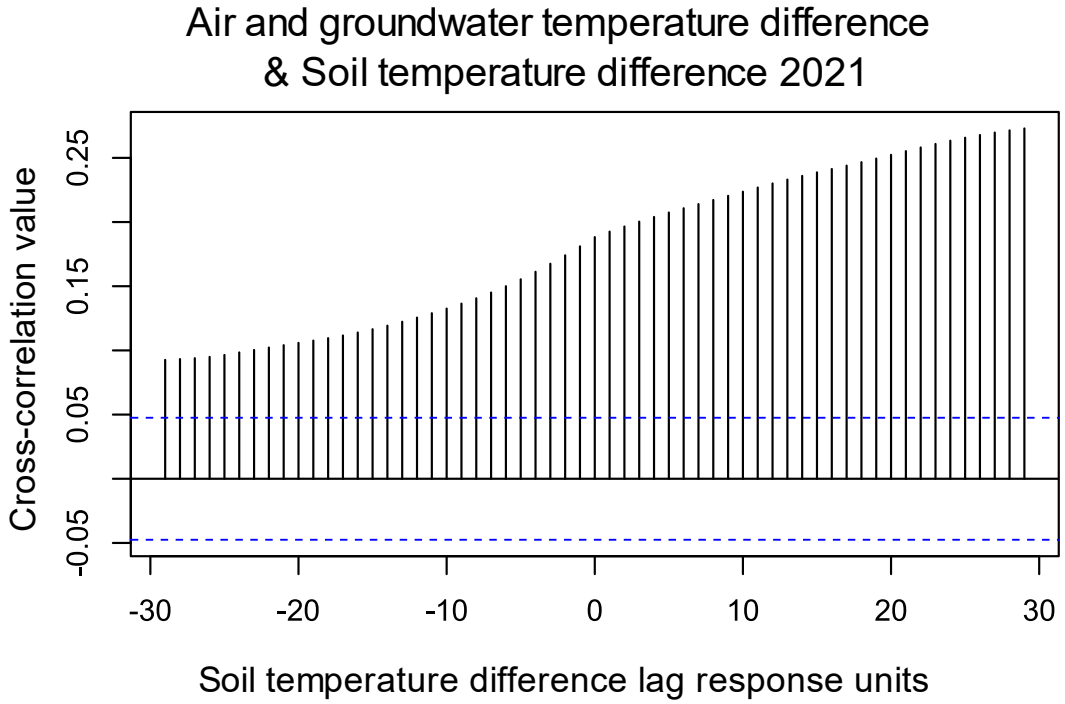

Figure A.4 Cross-correlation between air and groundwater temperature difference at site ER1 and soil temperature difference between site ER1 and PR5 during October to December 2021.

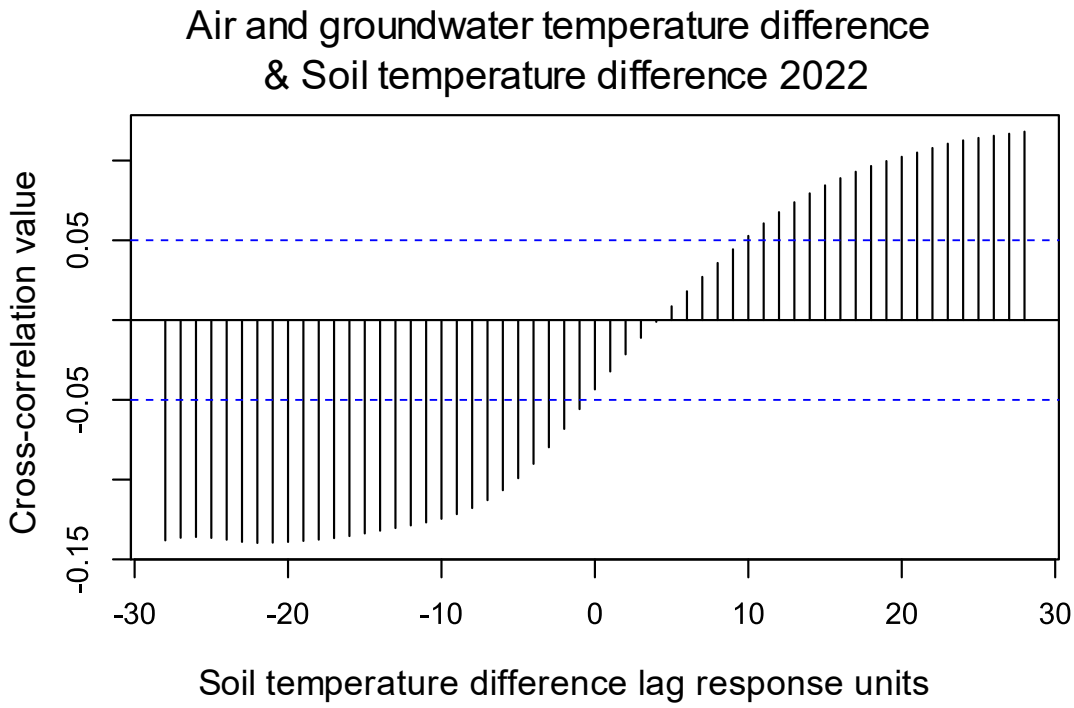

Figure A.5 Cross-correlation between air and groundwater temperature difference at site ER1 and soil temperature difference between site ER1 and PR5 during January and March 2022.

Table A.8 Statistical test summaries of Mixed Effects Models testing sediment characteristics by Condition (eroding vs prograding) and random effect of Site (ER1, ER3, PR5, PR7), i.e., Variable ~ Condition + (1|Site). Reporting for Condition [prograding].

Variable	**Transformation**	**Estimate**	**df**	**t value**	**P-value**
Median grain size	Square	1207.172	2.015	2.535	0.126
$\delta^{13}C$	NA	2.114	2.014	2.014	0.279
$\delta^{13}C_{org}$	Log+30.4	0.485	2.011	2.957	0.097
Clay percentage (<4µm)	Logit	-0.122	2.012	-0.677	0.568
			Site random effect		**0.023**
Silt percentage (4-63µm)	NA	-11.1	2.018	-3.152	0.087
Sand percentage (63-2000µm)	NA	11.826	2.017	2.475	0.131
Organic carbon percentage (%)	Gamma (log = "link")	-0.213		-0.79	0.43
			Site random effect		**0.03**
Inorganic carbon percentage (%)	Beta (link = "logit")	0.039		0.27	0.785

Appendix B

Supporting Information for Chapter 3 - Interactive Effects of Groundwater Level and Tidal Current Velocity Influence Salt Marsh Soil Temperature

Contents of this file

Introduction

The supporting information shows the relation between sites of different geomorphic conditions for measured variables, i.e., eroding (ER1 and ER3) and prograding (PR5 and PR7). Data is shown for the study period of August 2021 and February 2022.

Variables are groundwater level (Figure S1) and current velocity (Figure S2). As well as average groundwater and air temperature and average groundwater level by site and month. (Figure S3).

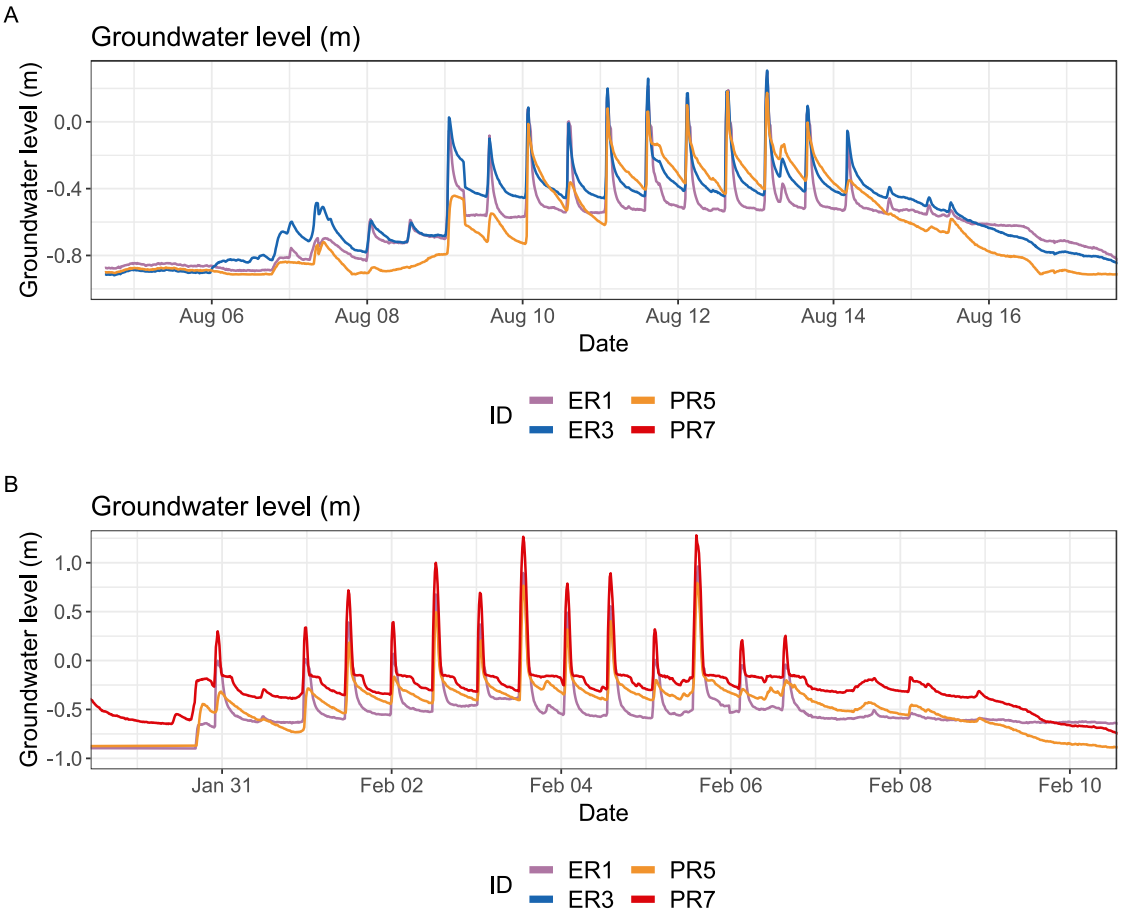

Figure B.1 Groundwater level (m) by site for August (A) and February (B).

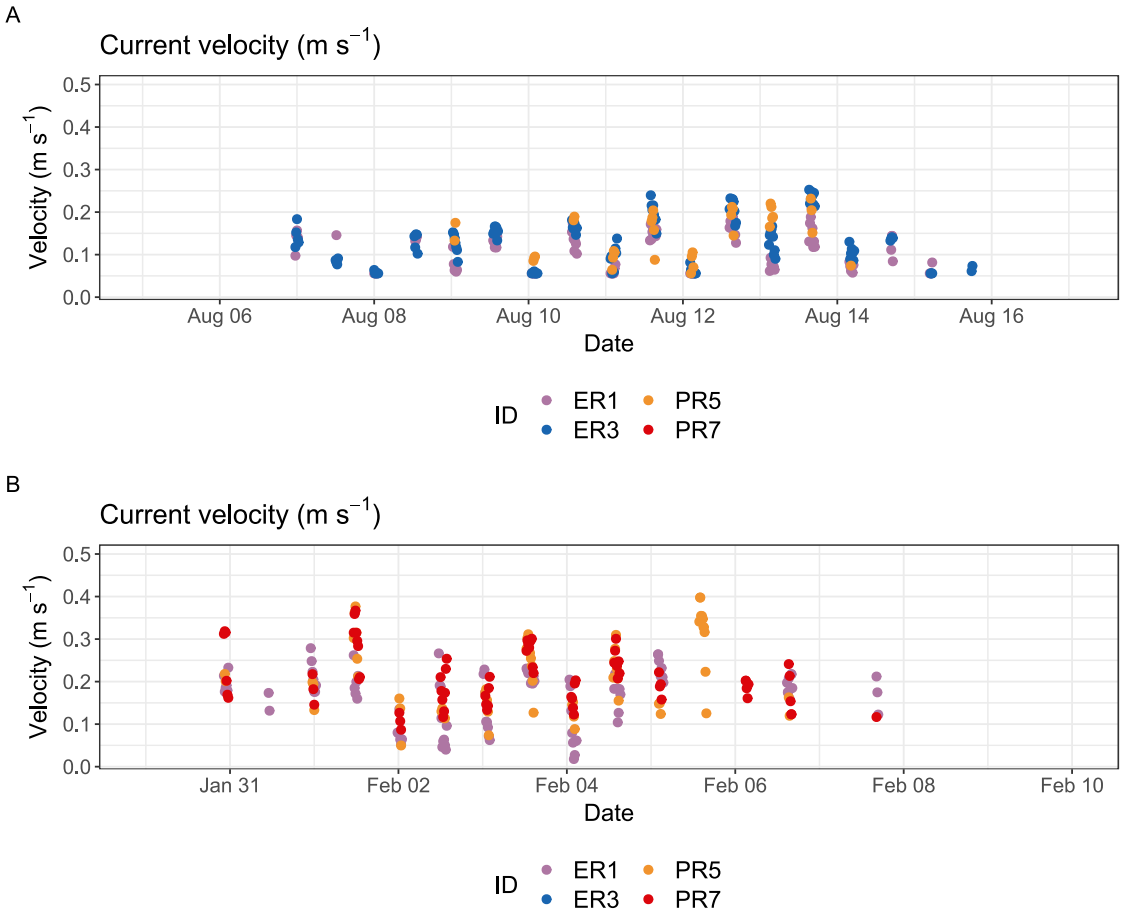

Figure B.2 Current velocity between site for August (A) and February (B).

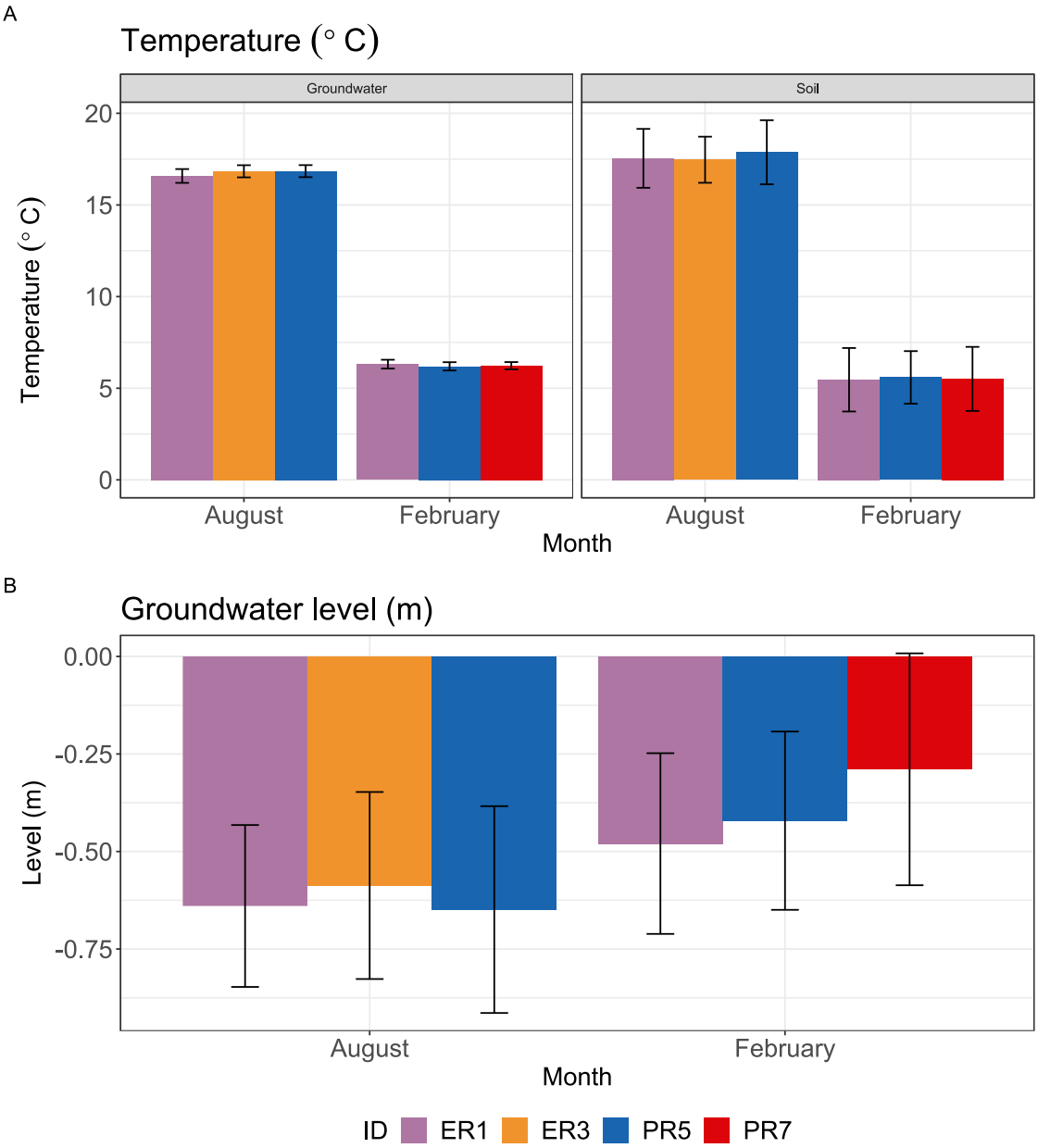

Figure B.3 Groundwater and air temperature (°C); B: Groundwater level (m) between sites (ER1, ER3, PR5, PR7) and months (August, February) during periods where groundwater logger were inundated. Mean ± Std.

Appendix C

Supporting Information for Chapter 4 – Differing soil carbon source depending on geomorphic condition at mangrove coastlines

Table C.1 Statistical summary of predictor variables from the Linear Mixed Effects Model (LMM) of sediment cores from Vietnam with Site/Condition/Transect as random intercept, i.e., Transect nested within Condition and Condition nested within Site (Variable ~ Condition + (1 | Site/Condition/Transect)); from Florida with Depth as random intercept, i.e., (Variable ~ Condition + (1 | Depth)), reporting for Condition [expanding].

Country	Variable ~ Condition [expanding]	Transformation	Estimate	t-value	p-value
Vietnam	Carbon concentration (mg)	Square root	-0.055	-0.706	0.553
	Carbon percentage	Arcsine	-0.016	-0.65	0.582
	Clay percentage	NA	-0.623	-0.065	0.954
	Silt percentage	NA	7.346	1.717	0.093
	Sand percentage	Logarithmic	0.306	0.612	0.604
	Carbon isotope ratio ($\delta^{13}C$)	Square root	0.788	1.834	0.142
	Median grain size (D50)	Reciprocal	-0.048	-0.453	0.695
	Loss on ignition percentage (LOI)	NA	-1.007	-0.366	0.75
Florida (US)	Carbon concentration (mg)	NA	-0.136	-2.056	0.056
	Carbon percentage	NA	-2.929	-1.661	0.115
	Clay percentage	**Logit**	**-0.43**	**-2.739**	**0.024**
	Silt percentage	**NA**	**-13.848**	**-2.947**	**0.017**
	Sand percentage	**NA**	**18.538**	**3.15**	**0.012**
	Carbon isotope ratio ($\delta^{13}C$)	NA	0.526	1.154	0.265
	Median grain size (D50)	**Square root**	**2.311**	**2.766**	**0.034**
	Loss on ignition percentage (LOI)	**NA**	**-7.214**	**-2.601**	**0.019**

Table C.2 Statistical summary of the Linear Mixed Effects Model (LMM) of sediment cores from Vietnam with Site/Depth as random intercept, i.e., Depth nested within Site, comparing $\delta^{13}C$ values between conditions at same depth ($\delta^{13}C$ ~ Condition + (1 | Site/Depth)), reporting for Condition [Expanding].

Between conditions at same depth - Vietnam				
Depth	**Transformation**	**Estimate**	**t-value**	**p-value**
Depth 0	NA	2.432	0.988	0.379
Depth 10	**Square root**	**41.541**	**3.451**	**0.024**
Depth 20	**NA**	**4.314**	**3.52**	**0.027**
Depth 30	Logarithmic	0.577	1.698	0.165
Depth 40	NA	2.897	1.558	0.18
Depth 50	NA	2.077	0.629	0.595

Table C.3 Statistical result of Linear Mixed Effects Model (LMM) of sediment cores from Vietnam with Site/Depth as random intercept, i.e., Depth nested within Site, comparing $\delta^{13}C$ values between Depths nested within Site ($\delta^{13}C$ ~ Depth + (1 | Site/Depth)), reporting for Depth [Depth = 50].

Between depth at same condition - Vietnam				
Data	**Transformation**	**Estimate**	**t-value**	**p-value**
Eroding site between Depth 0 and Depth 50	NA	1.668	0.452	0.695
Eroding site between Depth 10 and Depth 50	NA	3.196	1.221	0.35
Expanding site between Depth 0 and Depth 50	**NA**	**1.316**	**4.59**	**0.046**

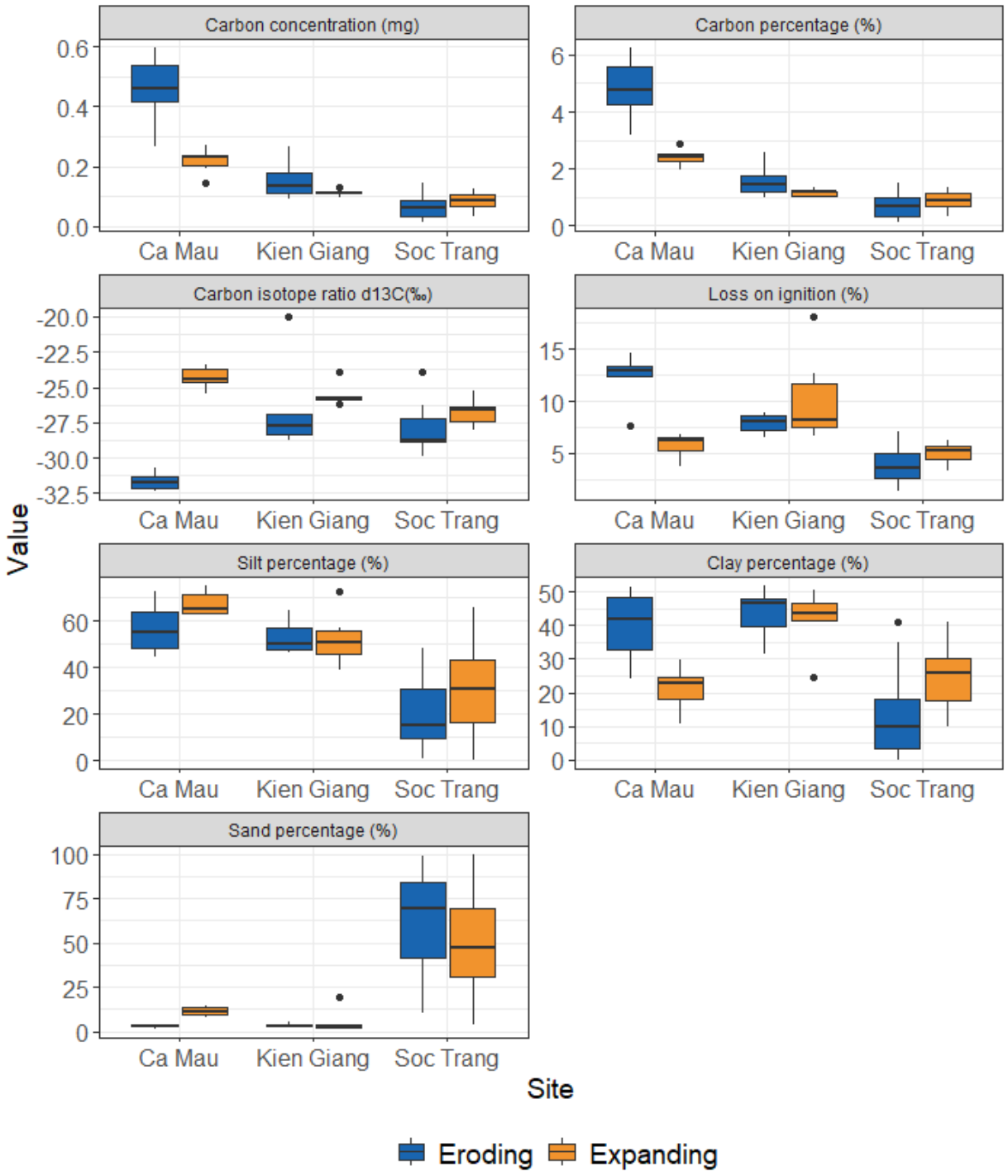

Figure C.1 Sediment properties of soil cores for sampling sites in Vietnam (Ca Mau, Kien Giang, Soc Trang) with eroding locations = blue; expanding locations = orange.

Table C.4 CO_2 flux literature review – Mekong Delta, Vietnam (Units =).

	sediment - air				**sediment - air Average of value converted**	**sediment - air StdDev of value converted**	**Total Average of value converted**	**Total StdDev of value converted**
	dry season		**wet season**					
Row Labels	**Average of value converted**	**StdDev of value converted**	**Average of value converted**	**StdDev of value converted**				
Vietnam	**211.11**	**122.47**	**302.75**	**153.46**	**256.93**	**139.52**	**256.93**	**139.52**
mangrove soil	**211.11**	**122.47**	**302.75**	**153.46**	**256.93**	**139.52**	**256.93**	**139.52**
Dusek et al., 2021	179.95	160.17			**179.95**	**160.17**	179.95	160.17
Vinh et al., 2019	257.84	37.44	302.75	153.46	**289.92**	**128.12**	289.92	128.12
Grand Total	**211.11**	**122.47**	**302.75**	**153.46**	**256.93**	**139.52**	**256.93**	**139.52**

Table C.5 Correlation matrix of sediment properties for eroding and expanding mangrove sites in Vietnam and Florida.

	LOI	$\delta^{13}C$	Carbon con.	Carbon %	Clay	Silt	Sand	D50	LRR
LOI	1	-0.39	0.76	0.89	-0.18	0.11	0.04	-0.21	-0.29
D13C	-0.39	1	-0.51	-0.4	0.09	0.15	-0.14	-0.05	0.67
Carbon con.	0.76	-0.51	1	0.83	-0.03	0.28	-0.14	-0.3	-0.27
Carbon %	0.89	-0.4	0.83	1	-0.37	-0.04	0.21	-0.04	-0.33
Clay	-0.18	0.09	-0.03	-0.37	1	0.5	-0.73	-0.73	0.21
Silt	0.11	0.15	0.28	-0.04	0.5	1	-0.93	-0.63	0.4
Sand	0.04	-0.14	-0.13	0.21	-0.73	-0.93	1	0.64	-0.31
D50	-0.21	-0.05	-0.3	-0.04	-0.74	-0.63	0.64	1	-0.37
LRR	-0.29	0.67	-0.27	-0.33	0.21	0.4	-0.31	-0.37	1

Table C.6 Principal component analysis (PCA) loadings for sediment properties of eroding and expanding mangrove sites in Vietnam and Florida.

	PC1	PC2
LOI	0.31	-0.4
$\delta^{13}C$	-0.31	0.22
Carbon con.	0.23	-0.48
Clay	-0.38	-0.22
Silt	-0.33	-0.37
Sand	0.39	0.33
Carbon %	0.37	-0.35
D50	0.29	0.39
LRR	-0.36	0.05